การย่อยสลายลินยูรอนด้วยแสงบนไทเทเนียและซิงค์ออกไซด์

นางสาวเสาวลักษณ์ สิทธิโชคธรรม

วิทยานิพนธ์นี้เป็นส่วนหนึ่งของการศึกษาตามหลักสูตรปริญญาวิศวกรรมศาสตรมหาบัณฑิต
สาขาวิชาวิศวกรรมเคมี   ภาควิชาวิศวกรรมเคมี
คณะวิศวกรรมศาสตร์   จุฬาลงกรณ์มหาวิทยาลัย
ปีการศึกษา 2554
ลิขสิทธิ์ของจุฬาลงกรณ์มหาวิทยาลัย

PHOTODEGRADATION OF LINURON ON TITANIA AND ZINC OXIDE

Miss Saowalux Sittichoktum

A Thesis Submitted in Partial Fulfillment of the Requirements

for the Degree of Master of Engineering Program in Chemical Engineering

Department of Chemical Engineering

Faculty of Engineering

Chulalongkorn University

Academic Year 2011

Thesis Title	PHOTODEGRADATION OF LINURON ON TITANIA AND ZINC OXIDE
By	Miss Saowalux Sittichoktum
Field of Study	Chemical Engineering
Thesis Advisor	Assistant Professor Varong Pavarajarn, Ph.D.

Accepted by the Faculty of Engineering, Chulalongkorn University in Partial Fulfillment of the Requirements for the Master's Degree

…………………………...…................Dean of the Faculty of Engineering

(Associate Professor Boonsom Lerdhirunwong, Dr.Ing.)

THESIS COMMITTEE

…………………………………………...Chairman

(Assistant Professor Anongnat Somwangthanaroj, Ph.D.)

………………………………………...Thesis Advisor

(Assistant Professor Varong Pavarajarn, Ph.D.)

………………………………………...Examiner

(Apinan Soottitantawat, D.Eng.)

…………......…………………………...External Examiner

(Associate Professor Puangrat Kajitvichyanukul, Ph.D.)

เสาวลักษณ์ สิทธิโชคธรรม: การย่อยสลายลินูรอนด้วยแสงบนไทเทเนียและซิงค์ออกไซด์.

(PHOTODEGRADATION OF LINURON ON TITANIA AND ZINC OXIDE) อ.ที่

ปรึกษาวิทยานิพนธ์หลัก: ผศ.ดร.วรงค์ ปวราจารย์, 116 หน้า.

การสลายตัวของลินูรอนซึ่งเป็นสารกำจัดวัชพืชชนิดหนึ่งในตระกูลฟีนิลยูเรียที่มักจะ
ปนเปื้อนในน้ำได้ถูกกระทำโดยใช้ปฏิกิริยาที่เร่งด้วยแสงบนไทเทเนียและซิงค์ออกไซด์ทั้งใน
รูปแบบที่มีในท้องตลาดและรูปแบบที่สังเคราะห์ขึ้น ตัวเร่งปฏิกิริยาขนาดนาโนได้ถูกสังเคราะห์ขึ้น
ด้วยวิธีการโซล-เจล ในกระบวนการย่อยสลายจะใช้ความเข้มข้นเริ่มต้นของลินูรอนที่ 10 ppm
และดำเนินการในเครื่องปฏิกรณ์แบบกะ ความเข้มข้นของลินูรอนถูกตรวจสอบเป็นระยะ โดยใช้
เครื่อง HPLC ที่ตรวจจับด้วยแสงยูวีที่ 254 นาโนเมตร นอกจากนั้นยังตรวจสอบการลดลงของ
ปริมาณสารอินทรีย์รวมที่ละลายอยู่ในน้ำซึ่งเป็นผลของการย่อยสลายลินูรอน พบว่าซิงค์ออกไซด์
มีประสิทธิภาพในการย่อยสลายและกำจัดลินูรอนได้ดีกว่าไทเทเนีย แม้ว่าซิงค์ออกไซด์จะมีพื้นที่
ผิวน้อยกว่าก็ตาม ซิงค์ออกไซด์สามารถย่อยสลายลินูรอนได้ 93% ภายใน 6 ชั่วโมงในขณะที่
ไทเทเนียทำการย่อยสลายลินูรอนได้เพียง 55% นอกจากนี้งานวิจัยนี้จะมุ่งเน้นในการศึกษาการ
เกิดขึ้นของสารตัวกลางของสารมลพิษในระหว่างการเกิดปฏิกิริยาซึ่งแตกต่างจากการศึกษาก่อน
หน้านี้ที่มุ่งเน้นไปที่การหายไปของสารมลพิษ สารตัวกลางหลายตัวที่ถูกพบจากการย่อยสลายได้ถูก
นำไปวิเคราะห์และระบุถึงสารตัวกลางที่เกิดขึ้นได้โดยใช้เครื่อง LC-MS การเปรียบเทียบสาร
ตัวกลางที่เกิดขึ้นเมื่อใช้ตัวเร่งปฏิกิริยาที่แตกต่างกันและ pH ที่แตกต่างกันพบว่ามีทั้งสารตัวกลางที่
เหมือนกันและสารตัวกลางที่แตกต่างกัน

ภาควิชา........วิศวกรรมเคมี........ลายมือชื่อนิสิต...

สาขาวิชา........วิศวกรรมเคมี........ลายมือชื่ออ.ที่ปรึกษาวิทยานิพนธ์หลัก.............................

ปีการศึกษา..............2554..............

5370518021: MAJOR CHEMICAL ENGINEERING
KEYWORDS: LINURON/ZINC OXIDE/TITANIA/PHOTOCATALYTIC
DEGRADATION/INTERMEDIATE

SAOWALUX SITTICHOKTUM: PHOTODEGRADATION OF LINURON ON
TITANIA AND ZINC OXIDE. ADVISOR: ASST. PROF. VARONG PAVARAJARN,
Ph.D., 116 pp.

Degradation of linuron (N-(3, 4-dichlorophenyl)-N'-methoxy-N'-methylurea), which is a
harmful phenylurea herbicide commonly found as residue in water, was conducted via
heterogeneous photocatalysis on commercial and synthesized titanium dioxide (TiO_2) and
commercial and synthesized zinc oxide (ZnO). Nanoparticles of the photocatalysts were
synthesized via the sol-gel method. The photocatalytic degradation of 10-ppm linuron
aqueous solution was conducted in a batch photo-reactor. Concentration of linuron was
periodically monitored using high performance liquid chromatography (HPLC) with 254-nm
UV detector. The decrease of total organic carbon as a result of mineralization of linuron was
also observed during the degradation process. It was found that zinc oxide shows higher
performance in degradation and mineralization of linuron than titanium dioxide, regardless of
much lower surface area. The degradation of linuron on zinc oxide was about 93% within 6
hours, while that achieved on titanium dioxide was only 55%. Unlike previous studies that
focused on the disappearance of the pollutant, this work also investigated intermediate
compounds formed during the reaction. Several intermediates were detected during the course
of the degradation. Attempts were made to identify the intermediate products through
analyses using liquid chromatography with mass spectrometry (LC-MS). Comparison of the
intermediates formed, when different photocatalysts and difference pH were used, revealed
intermediates that were observed from both catalysts as well as intermediates that were
specific to one particular catalyst.

Department: Chemical Engineering Student's Signature……………………………….
Field of Study: Chemical Engineering Advisor's Signature…………………………….
Academic Year: 2011

ACKNOWLEDGEMENTS

The author would like to express her gratitude to her advisor, Assistant Professor Dr.Varong Pavarajarn, for his extensive guidance, patience, support, and encouragement throughout the research.

I would also grateful to thank to Assistant Professor Anongnat Somwangthanaroj as the chairman, Dr. Apinan Sootitantawat, and Associate Professor Puangrat Kajitvichyanukul, members of the thesis committee for their kind cooperation, comment, and discussions.

I would also like to thank all my friends and all members of the Center of Excellent in Particle Technology who always provide the encouragement and cooperate along the research study.

This work was also partially by Centennial Fund of Chulalongkorn University for the partial financial support to this work.

Finally, I would like to dedicate this thesis to my parents and my families, who have always been the source of her support and encouragement.

CONTENTS

LIST OF TABLES

LIST OF FIGURES

CHAPTER I

INTRODUCTION

Thailand is a country with large agricultural area. The amount of herbicides used in Thailand is ranked 48th in the world. According to the survey of Food and Agriculture Organization (FAO), of the United Nations, the pesticide import of Thailand in 2007 was 79,239 tons, which had been increased by 56,286 tons within 5 years. The high import and use of herbicides and pesticides is one of the main environmental problems, especially for the phenyl herbicides that have been widely used in conventional production of corn, vegetables and fruits [1]. Example of herbicides in the phenyl urea family is linuron. It is also classified as harmful chemicals with great chemical stability and toxicity [2]. Linuron has been found as contaminant in soil and ground water.

Linuron can be degraded by photocatalytic degradation process [3, 4]. The photocatalytic degradation of linuron has been reported on oxide semiconductor photocatalysts. Among various oxide semiconductors, titania has been investigated and reported as one of the most suitable catalysts for widespread environmental applications. It has good physical and chemical properties, such as strong oxidizing power [5], and high catalytic and photocatalytic activity [6, 7]. Zinc oxide (ZnO) is another important oxide semiconductor photocatalyst that has been considered as an alternative to TiO_2 because its photocatalysis mechanism has been proven to be similar to that of TiO_2. TiO_2 and ZnO can be synthesized by many methods. One of the popular techniques is sol-gel method because of its low cost, reliability, reproducibility, simplicity and relative mild conditions of synthesis [8, 9].

Most studies about the degradation of pollutants focuses on the disappearance of the pollutants. However, the detailed investigations of intermediate compounds that occur during the decomposition process are not frequently reported. Nevertheless, intermediate compounds may occur with higher toxicity than the initial pollutants. Some intermediate compounds are more than several times more toxic than the initial pollutants.

In this research, the photocatalytic degradations of linuron on titania and zinc oxide with sol-gel method are investigated. This work not only investigates the degradation of

linuron, but also interests in identifying the formation of intermediates formed during the photocatalytic degradation.

Objectives of the research:

The objective of this research is to investigate the photocatalytic degradation and the formation of intermediates during the photodegradation of linuron solution, using TiO_2 and ZnO as catalyst, as well as to investigate mechanism of photodegradation of linuron.

The present thesis is arranged as follows:

Chapter I is the introduction of this work.

Chapter II describes the basic theory about photocatalysts such as chemical properties of zinc oxide and titanium dioxide, photocatalyst synthesis and about linuron such as chemical and properties of linuron, photocatalytic process, adsorption of linuron, and kinetics of photodegradation of linuron. Furthermore, previous works relating to this research is also presented in this chapter.

Chapter III shows materials, the experimental equipments, the preparation of zinc oxide and titanium dioxide by the sol-gel process and characterizations of products.

Chapter IV describes the results and discussion of the research.

In the last chapter, the overall conclusions of this research and future work are given.

CHAPTER II
THEORY AND LITERATURE REVIEWS

2.1 Photocatalysts

Photocatalyst is a substance that can release free radicals that are susceptible to reaction when activated by light. Various types of materials have been investigated as a potential photocatalyst to degrade organic matters. In this research, TiO_2 and ZnO, which are inexpensive and non-toxic yet effective catalysts, are used.

2.1.1 Physical and Chemical Properties of Titanium Dioxide

Titanium dioxide, also known as titanium (IV) oxide or titania, has great potential for many industrial applications such as filter materials, anti-reflection films, sensors, dye-sensitive solar cells and photocatalysts. Titanium dioxide has wide band gap of 3.2 eV. Charge carriers, i.e. electrons and holes, are produced when titania is excited. Consequently, highly reactive radicals are generated and oxidation-reduction reaction of species adsorbed on the surface of titania can occur [10]. Basic thermochemical data of titania are shown in Table 2.1.

Table 2.1 Thermochemical data for formation of titania compound.

Compound	State	Heat of formation ΔH°_f, kJ/mol		Free energy of formation ΔG°_f, kJ/mol		Entropy S, J/mol.K	
		298 K	1300 K	298 K	1300 K	298 K	1300 K
TiO_2							
-Anatase	Crystal	-933.0	-930.0	-877.6	-697.4	49.9	150.6
-Rutile	Crystal	-944.7	-942.4	-889.5	-707.9	50.3	149.0

Titanium dioxide occurs in three different crystalline polymorphic forms: rutile (tetragonal), anatase (tetragonal) and brookite (orthorhombic). The crystallographic characteristic of these varieties are shown in Table 2.2 and Figure 2.1. Anatase usually occurs in near-regular octahedral form, while rutile forms slender prismatic crystals that are frequently twinned. Nevertheless, both anatase and rutile are anisotropic of which physical properties vary according to direction relative to the crystal axes. However, in most applications using these substances, the distinction between crystallographic directions is lost

because of the random orientation from large number of small particles or grains in the particle.

Table 2.2 Cystallographic characteristic of anatase, rutile and brookite [11].

	Crystal Structure	Density, kg/m^3	Lattice parameter, nm		
			a	b	c
Anatase	Tetragonal	3830	0.3733	-	0.937
Rutile	Tetragonal	4240	0.4584	-	0.2953
Brookite	Orthorhombic	4170	0.5436	0.9166	0.5135

Three allotropic forms of titania have been prepared artificially, but only rutile has been obtained in the form of transparent large single crystal. The transformation from anatase to rutile is accompanied by evolution of ca. 12.6 kJ/mol (3.01 kcal/mol). The rate of phase transformation is greatly affected by temperature and by presence of other substances which may either catalyze or inhibit the transformation. The lowest temperature at which the conversion from anatase to rutile takes place at a measurable rate is approximately 500-550°C [12]. This is consistent with the research of Cheng et al, which investigated that the phase transformation from anatase to rutile did not take place when powder was calcined at temperatures below 600°C [13].

(a)   (b)   (c)
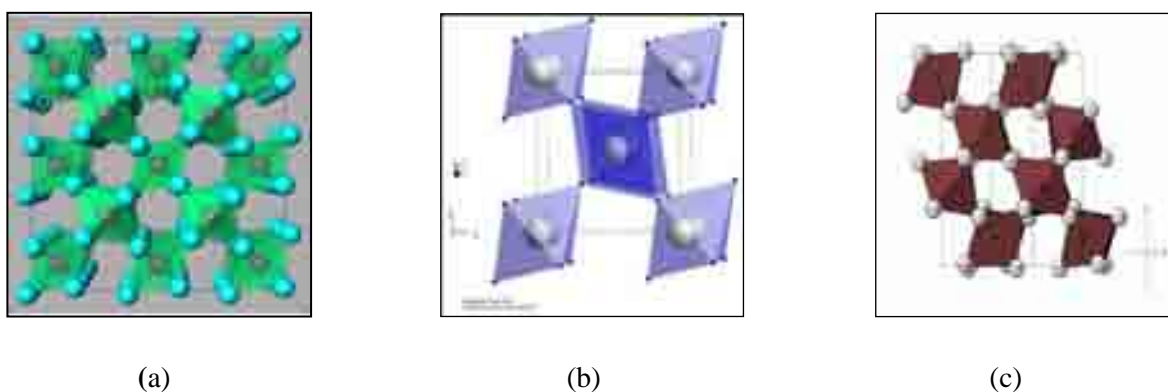
Figure 2.1 Crystal structure of TiO_2; (a) Anatase, (b) Rutile, (c) Brookite.

Titanium dioxide generally exhibits the highest photocatalytic activity among all photocatalysts. The anatase phase usually exhibits the best photocatalytic behavior, while the rutile phase is the most stable phase. The use of TiO_2 as a photocatalyst has been of great interest due to its high activity, photochemical inertness, non-toxicity, efficiency, and low cost.

2.1.2 Physical and Chemical Properties of Zinc Oxide

Zinc oxide is an inorganic compound with the formula ZnO. Zinc oxide is a white or yellowish powder. The crystal structures shared by zinc oxide are wurtzite, zinc blende, and rocksalt, as schematically shown in Figure 2.2. At ambient conditions, the thermodynamically stable phase is wurtzite. The zinc-blende structure can be formed only by the growth of ZnO on cubic substrate. The rocksalt structure may be obtained at relatively high pressure.
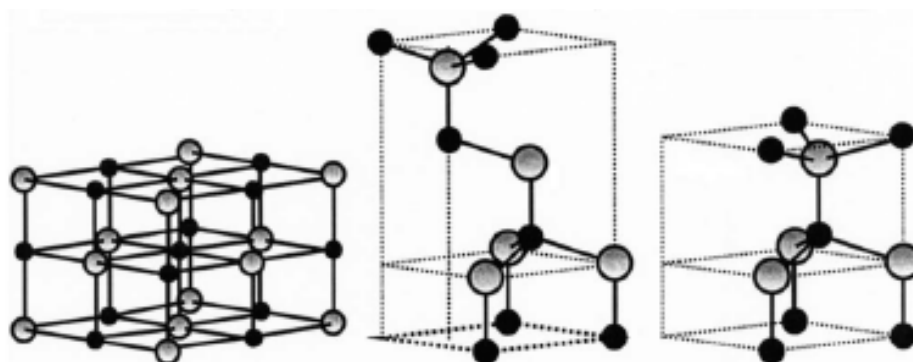
Figure 2.2 Stick and ball representation of zinc oxide crystal structures: (a) cubic rocksalt, (b) cubic zinc blende, and (c) hexagonal wurtzite. The shaded gray and black spheres denote Zn and O atoms, respectively.

Zinc oxide is an n-type semiconductor with a band gap of 3.20 eV and the free excitation energy of 60 meV, which makes it very high potential for room temperature light emission. This also gives zinc oxide strong resistance to high temperature electronic degradation during operation. Therefore, it is attractive for many opto-electronic applications in the range of blue and violet light as well as UV devices for wide range of technological applications. Zinc oxide also exhibits dual semiconducting and piezoelectric properties. The other properties are given in Table 2.3.

Table 2.3 Properties of wurtzite zinc oxide.

Molecular formula	ZnO
Molecular weight	81.38 g/mole
Lattice parameters at 300 K	
a	0.32495 nm
c	0.52069 nm
a/c	1.602 (ideal hexagonal structure is 1.633)
Density	5.606 g/cm^3
Melting point	1970 – 1975 °C (decomposes)
Thermal conductivity	130 W/m.K
Linear expansion coefficient	a: 6.5 x 10^{-6}
(/^{o}C)	c: 3.0 x 10^{-6}
Static dielectric constant	8.656
Energy gap	3.2 eV, direct
Excitation binding energy	60 meV
Appearance	White solid
Synonyms	Zinc white; Zinc flowers; Calamine; C.I. pigment white 4
Solubility	Insoluble in water and alcohols. Soluble in acids and bases.
Physicochemical stability	Stable under normal conditions of handling and storage.

Although zinc oxide has the same band gap as titania, which is the most widely used photocatalyst, the use of zinc oxide as photocatalyst has not been thoroughly investigated. Nevertheless, some researchers have reported that the activity of zinc oxide is higher than titania. [14].

2.1.3 Synthesis of Photocatalyst

In general, titanium dioxide and zinc oxide particles have been prepared by several methods such as thermal decomposition method [15, 16], precipitation method [17] and sol–gel method [9, 18]. Previous researches have revealed that different photocatalyst synthesis methods result in different surface properties, which consequently affect the interaction between catalyst surface and the compound to be degraded. For this work the photocatalysts were prepare by sol-gel method because of its low cost, reliability, reproducibility, high purity, good microstructure, simplicity and relative mild conditions of synthesis [8, 9].

The sol–gel process is a versatile solution process for making ceramic and glass materials. The sol–gel process, as the name implies, involves the evolution of inorganic networks through the formation of a colloidal suspension (sol) and gelation of the sol to form a network in a continuous liquid phase (gel). A sol is a dispersion of the solid particles, with diameter of 1–1000 nm, in a liquid where only the Brownian motions kept particles in suspension. While a gel is a state where both liquid and solid are dispersed in each other, which presents a solid network filled with liquid components. The precursors for synthesizing these colloids consist of a metal or metalloid element surrounded by various reactive ligands. Metal alkoxides are most popular because they react readily with water. The alkoxides are hydrolyzed giving the oxide as a colloidal product. The sol is then either treated or simply left to form gel. To obtain a final product, the gel is heated. This heating serves several purposes. It removes the solvent, decomposes anions such as alkoxides or carbonates to give oxides, allows rearrangement of the structure of the solid and allows crystallization.

The parameters affecting reaction rate of the sol-gel process include pH, molar ratio of reactants, aging time and temperature. The reaction of sol-gel process follows Equation (1)-(3).

Hydrolysis:

$$M\text{-}O\text{-}R + H_2O \longrightarrow M\text{-}OH + R\text{-}OH \tag{1}$$

Condensation:

$$M\text{-}OH + HO\text{-}M \longrightarrow M\text{-}O\text{-}M + H_2O \tag{2}$$

$$M\text{-}O\text{-}R + HO\text{-}M \longrightarrow M\text{-}O\text{-}R + R\text{-}OH \tag{3}$$

Whereas, M is Metal and OR is Alkoxyl group
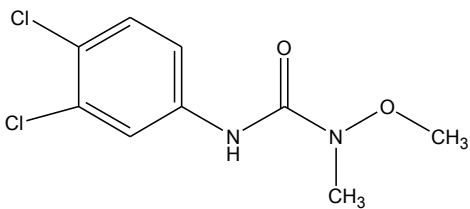
In this research, the sol-gel method is selected for the synthesis of the photocatalysts because it is a method that can easily produce nanoparticles. Moreover, properties of the catalysts such as surface area, pore size and perfection of crystals can be easily customized by adjusting the synthesis parameters such as solution pH, calcination temperature, concentration of reactants and aging time. In addition, the sol-gel method can be applied to synthesize composite that is uniformly at the molecular level. In this work TiO_2 and

ZnO that were prepared by the sol-gel method were used as photocatalyst for photocatalytic degradation of linuron.

2.2 Linuron

Linuron [1-methoxy-1-methyl-3-(3,4-dichlorophenyl)urea], is one of the most important commercial ureas. It has good contact activity and it may kill emergent weed seedlings. Linuron was used to control annual and perennial broadleaf and grassy weeds on crop and non-crop sites. It is used as a pre- and a post-emergent herbicide. It works by inhibiting photosynthesis in plants. It is labeled for use in soybean, cotton, potato, corn, bean, pea, winter wheat, asparagus, carrot, and fruit crops. It is also used on crops stored in warehouses and storerooms. Half-life of linuron in soil ranges from 3 – 4 months. Therefore, this compound has been found as contaminant in surface and ground waters. The rapid and simple wastewater treatment of linuron is urgently required. Its properties are shown in Table 2.4.

Table 2.4 Physicochemical properties of linuron.

Structure formula	
Molecular weight	249.17 g/mol
Molecular formula	$C_9H_{10}Cl_2N_2O_2$
Melting point	85 – 94°C
Vapor pressure	0.0020 Pa at 24°C
Appearance	White crystalline solid
Synonyms	Afalon; Alafon; Cephalon; Garnitan; Linex; Linurex; Premalin; Rotalin; Sarclex; etc.
Solubility	75 ppm in water at 25°C
Toxicity	Excessive exposure to linuron may affect blood, and may cause cancer. Its effect to aquatic organism vary and likely to be harmful to other wildlife. It is considered as low toxicity herbicide.
Half -life	3-4 months in most soils

2.3 Photocatalytic Process

Photocatalytic process is a technology for oxidation/degradation of organic contaminants in environmental control. It can use sunlight, which is available in abundance, as the energy source to initiate the photodecomposition of pollutants. The end products of this treatment process are usually harmless compounds such as carbon dioxide, water and inorganic ions such as chloride and nitrate. It has been widely used as an alternative physical-chemical process for the elimination of toxic and hazardous organic substances in wastewater, drinking water, and air. In this process, a semi-conductor activated by ultra-violet (UV) radiation is used as a catalyst to destroy organic contaminants.

The heterogeneous photocatalytic process used in pollutant degradation involves the adsorption of pollutants on the surface sites, and the chemical reaction to convert pollutant into carbon dioxide and water [19]. Photocatalysis in a form of semiconductors has been extensively investigated. Titanium dioxide and zinc oxide are semiconductor often used as a photocatalyst in the photocatalysis process. TiO_2 and ZnO have attracted great interest as promising photocatalysts in areas of environmental and energy, due to their high photocatalytic activity, resistance to photocorrosion, photo-stability, low cost and non-toxicity [20].

Photocatalysis can be defined as the acceleration of photoreaction by presence of catalyst. The photocatalysis over an oxide semiconductor is initiated by the absorption of photon with energy equal to or greater than the band gap of the semiconductor, producing electron-hole (e^-/h^+). The generations of electron-hole pairs are represented in Eq. (4). The photo-generated holes and electrons give rise to oxidation and reduction processes, respectively. In an aqueous solution, water molecules adsorb onto surface of the catalyst. They are oxidized giving rise to $OH^\bullet$ radicals. As the process is usually carried out in aerobic conditions, the species to be reduced is oxygen, generating the superoxide radical as following Eq. (5) to (7). Organic pollutants adsorbed onto the surface of the catalyst are subsequently oxidized by $OH^\bullet$ radicals.

$$Semiconductor \ + \ h\nu \ \longrightarrow \ h^+ \ + \ e^- \qquad (4)$$

$$h^+ \ + \ H_2O_{ads} \ \longrightarrow \ OH^\bullet \ + \ H^+ \qquad (5)$$

$$h^+ \ + \ OH^-_{ads} \ \longrightarrow \ OH^\bullet \qquad (6)$$

$$e^- \ + \ O_2 \ \longrightarrow \ O_2^- \qquad (7)$$
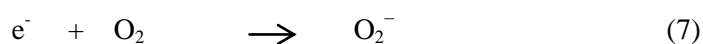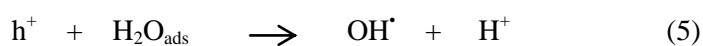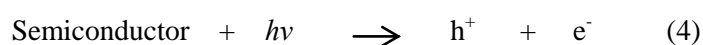
Support of the OH$^{\bullet}$ radical as the main reactive oxidant derives from the observation that intermediates detected during the photocatalytic degradation of halogenated aromatic compounds are typically hydroxyl structures, as those found when similar aromatics react with a known source of OH$^{\bullet}$ radicals.

The mechanism of the photocatalytic degradation of aqueous organic compound on anatase titania can be expressed by a series of advanced oxidation process of Haque et al. as following [21]:

1) Absorption of efficient photons ($h\nu \geq E_G = 3.2$ eV) by titania

$$(\text{TiO}_2) + h\nu \rightarrow e_{CB}^- + h_{VB}^+ \tag{8}$$
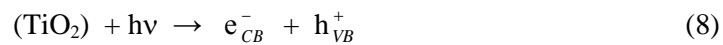
2) Oxygen ionosorption (first step of oxygen reduction)

$$(\text{O}_2)_{\text{ads}} + e_{CB}^- \rightarrow \text{O}_2^{\bullet -} \tag{9}$$
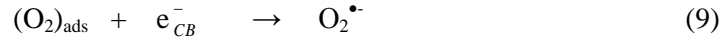
3) Neutralization of OH$^-$ groups by photoexcited holes

$$(\text{H}_2\text{O} \Leftrightarrow \text{H}^+ + \text{OH}^-)_{\text{ads}} + h_{VB}^+ \rightarrow \text{H}^+ + \text{OH}^{\bullet} \tag{10}$$
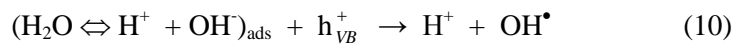
4) Neutralization of O$_2^{\bullet -}$ by protons

$$\text{O}_2^{\bullet -} + \text{H}^+ \rightarrow \text{HO}_2^{\bullet} \tag{11}$$

5) Transient hydrogen peroxide formation

$$2\,\text{HO}_2^{\bullet} \rightarrow \text{H}_2\text{O}_2 + \text{O}_2 \tag{12}$$

6) Decomposition of H$_2$O$_2$ and second reduction of oxygen

$$\text{H}_2\text{O}_2 + e^- \rightarrow \text{OH}^{\bullet} + \text{OH}^- \tag{13}$$

7) Oxidation of the organic reactant via successive attack by $OH^{\bullet}$ radical

$$R \; + \; OH^{\bullet} \; \rightarrow \; R'^{\bullet} \; + \; H_2O \qquad\qquad (14)$$

8) Direct oxidation by reaction with holes

$$R \; + \; h^+ \; \rightarrow \; R^{+\bullet} \rightarrow \text{degradation products} \qquad (15)$$
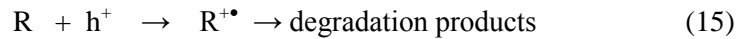
The mechanism of photocatalytic degradation of organic matter on zinc oxide can be expressed by applying the research of Daneshvar et al.[2]. The photocatalytic degradation of organic matter in the solution is initiated by photoexcitation of the semiconductor, followed by the formation of electron-hole pairs on the surface of the zinc oxide particles upon the illumination by light with energy higher than the band gap energy, as following in (Eq.16).

$$ZnO \; + \; h\nu \; \rightarrow \; e_{CB}^{-} \; + \; h_{VB}^{+} \qquad\qquad (16)$$
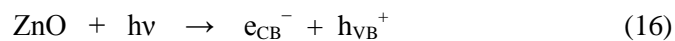
The high oxidative potential of the hole (h_{VB}^{+}) in the catalyst permits the direct oxidation of herbicide into the reactive intermediates (Eq.17).

$$h_{VB}^{+} \; + \; \text{herbicide} \; \rightarrow \; \text{oxidative products of the herbicide} \qquad (17)$$
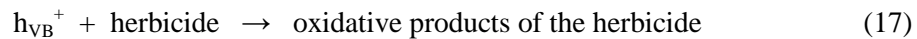
Very reactive hydroxyl radicals can also be formed either by the decomposition of water (Eq.18) or by the reaction of the hole with OH^{-} (Eq.19).

$$h_{VB}^{+} \; + \; H_2O \; \rightarrow \; H^+ + \; OH^{\bullet} \qquad\qquad (18)$$
$$h_{VB}^{+} \; + \; OH^{-} \; \rightarrow \; OH^{\bullet} \qquad\qquad (19)$$
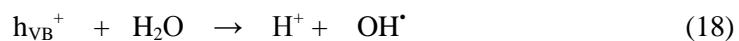
Electrons in the conduction band ($e_{CB}-$) on the catalyst surface can reduce molecular oxygen to superoxide anion (Eq.20). This radical, in the presence of organic scavengers, may form organic peroxides (Eq.21) or hydrogen peroxide (Eq.22).

$$e_{CB}^{-} \; + \; O_2 \qquad\qquad \rightarrow \; O_2^{\bullet -} \qquad\qquad (20)$$
$$O_2^{\bullet -} \; + \; \text{herbicide} \qquad \rightarrow \; \text{herbicide} - OO^{\bullet} \qquad (21)$$
$$O_2^{\bullet -} \; + \; HO_2^{\bullet} \; + \; H^+ \; \rightarrow \; H_2O_2 \; + \; O_2 \qquad\qquad (22)$$
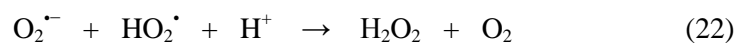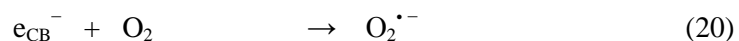
Electrons in the conduction band are also responsible for the production of hydroxyl radicals, which have been indicated as the primary cause of organic matter mineralization (Eq.23) [22, 23].

$$OH^{\bullet} \; + \; herbicide \qquad \rightarrow \; degradation \; of \; the \; herbicide \qquad (23)$$

In recent years, photocatalytic processes have been presented on several papers [2, 24-27]. These papers offer extensive details on the photocatalytic degradation of various non-biodegradable organic pollutants such as insecticides, herbicides, and wastewater from textile and some other industries contain residual dyes. The common photocatalytic degradation processes employs either semiconductor/UV or UV/Fenton processes. According to these papers, the photocatalytic processes are able to degrade non-biodegradable organic pollutants.

2.4 Photocatalytic Degradation of Linuron

2.4.1 Kinetics of Photocatalytic Degradation of Linuron

According to many papers on photocatalytic processes that have been reported in the recent years, the degradation rate depends on parameters influencing the oxidation such as pH value, initial concentration, catalyst loading and temperature [28-30]. They have also found that the kinetic model suitable for representing photocatalytic reaction is the Langmuir – Hinshelwood model [31]. In this model, it is assumed that the reaction occurs on the heterogeneous catalyst surface and the rate of reaction (r) is proportional to the fraction of surface covered by the substrate (θ):

$$r = -\frac{dC}{dt} = k_r\theta = k_r\frac{KC}{1+KC} \qquad (24)$$

where C is the concentration of the substance being degraded, t is the irradiation time, k_r is true rate constant and K is the constant of adsorption equilibrium.

When the solution is highly diluted, the term KC can be neglected. Most of researchers approximated Langmuir – Hinshelwood kinetics to first order kinetics for the

condition KC<<1[8, 21, 32]. In this case the reaction is essentially an apparent first order reaction. After integration, Eq. (24) can be simplified to Eq. (25):

$$\ln \frac{C_0}{C} = k_{app} t \qquad (25)$$

where k_{app} is the apparent rate constant of a pseudo first-order reaction.

Kinetic studies were assessed by monitoring the change in the concentration of linuron at certain interval of time. Apparent first order rate constants (k_{app}) were determined employing Eq. 25 from plot of ln C_o/C versus irradiation time. The k_{app} was determined by calculating the slope of the line obtained. The resulting first order rate constants have been used to calculate degradation rate for the degradation of linuron on TiO$_2$ [33].

2.4.2 Adsorption of Linuron on Photocatalyst

The adsorption models were used to describe the adsorption of linuron surface of the photocatalyst. The adsorption isotherm defines the equilibrium state of the process. Several equations representing the isotherm are available. Two important isotherms were selected for this study: the Langmuir and Freundlich isotherm models. The Langmuir adsorption isotherm assumes that adsorption takes place at specific sites within the adsorbent, and it has been used successfully for many adsorption processes of monolayer adsorption. The linearized from of the Langmuir isotherm model is [34, 35]:

$$\frac{1}{q_e} = \frac{1}{q_{max}} + \frac{1}{bq_{max}} \frac{1}{C_e} \qquad (26)$$

where q_e is amount of adsorbate on adsorbent at equilibrium (mg/g), q_{max} is maximum adsorption capacity (mg/g), C_e is equilibrium concentration (mg/l), and b is constant related to energy of the sorption system (l/mg).

The essential features of the Langmuir isotherm can be expressed in terms of a dimensionless constant separation factor *(r)*, which was calculated by the following relationship:

$$r = \frac{1}{1+bC_0} \qquad (27)$$

The values $r > 1$ indicates the isotherm shape that unfavorable adsorption condition. The values $0 < r < 1$ indicates favorable adsorption conditions [36]. In the special cases where $r = 1$ and $r = 0$ the adsorption is linear and irreversible, respectively.

For the Freundlich isotherm is an emprical equation used to describe heterogeneous systems. The Freundlich isotherm is represented in logaritmic form as follows [29, 35, 36]:

$$\ln q_e = \ln K_f + \frac{1}{n} \ln C_e \qquad (28)$$

where $\frac{1}{n}$ is adsorption intensity and K_f is Freundlich constant related to adsorption capacity $(\text{mg/g(mg/l)}^{-1/n})$.

Freundlich's parameter relates to the mean energy of adsorption. A very weak adsorbent/adsorbate interaction occurs at values of n lower than 1, while values higher than 1 suggest a strong adsorbent/adsorbate interaction. At value of n equal to 1 it is assumed that all sites are energetically similar [35].

In this work, the Langmuir and Freundlich isotherm models were used to describe the adsorption process of linuron on TiO_2 and ZnO. Studying the adsorbability of linuron on TiO_2 and ZnO allows one to predict the mechanism and kinetics that promote the linuron's photooxidation.

2.4.3. Degradation Products

Most studies about the degradation of pollutants focuses on the disappearance of the pollutants. However, the detailed investigations of intermediate compounds that occur during the decomposition process are not frequently reported. Nevertheless, intermediate compounds may occur with higher toxicity than the initial pollutants. Some intermediate compounds are more than several times more toxic than the initial pollutants.

In the study of intermediate compounds resulting from the degradation of herbicides, many researchers have proposed degradation pathway of various herbicides. It was found that the differences in the intermediate compounds and degradation pathway have been reported, depending on the degradation process.
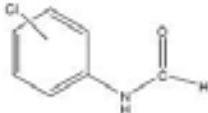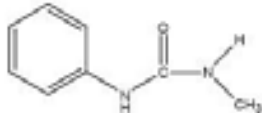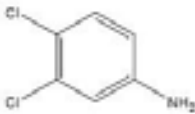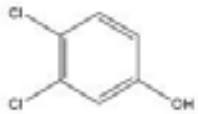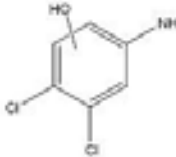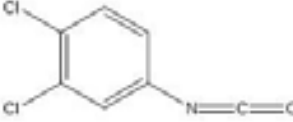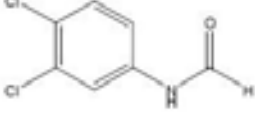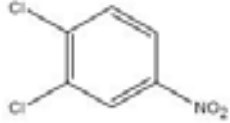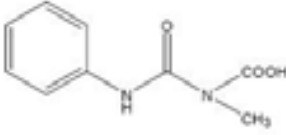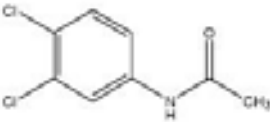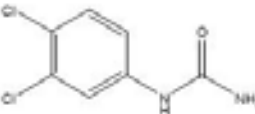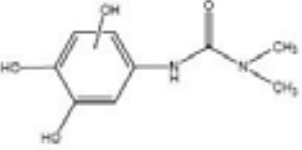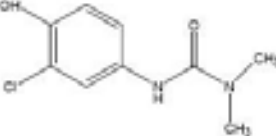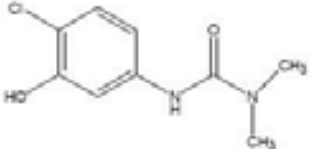
The degradation reaction catalyzed by using light on TiO_2 has been reported by several researchers and found that different conditions of degradation produce different intermediate products. For example, Katsumata et al. studied the degradation of diuron [3-(3,4-dichlorophenyl)-1,1-dimethylurea] in aqueous solution by photocatalyzed oxidation, using synthesized titania as catalyst. In this study, photodegradation of diuron gave four kinds of intermediate products. The structures of the four photoproducts are represented as follows:

Compound 1 or

Compound 2

Compound 3
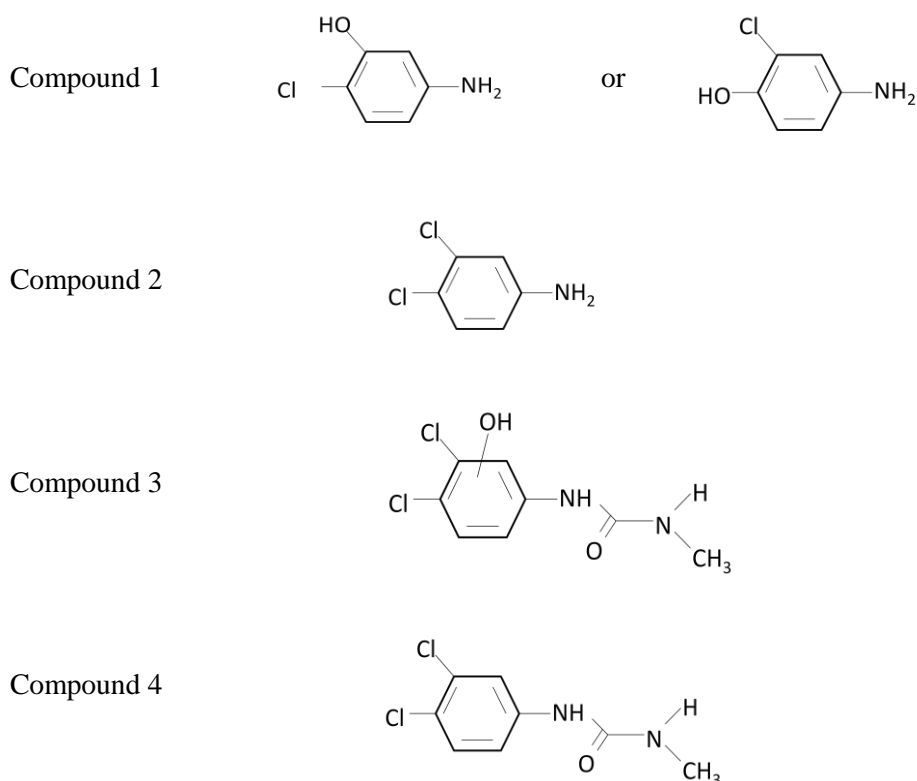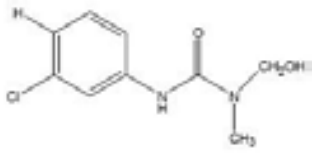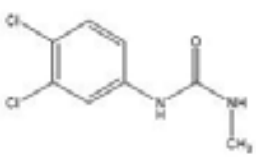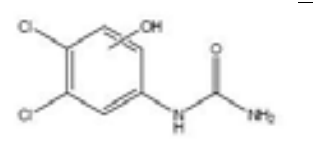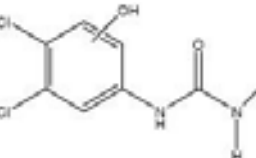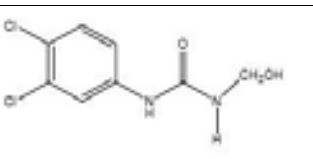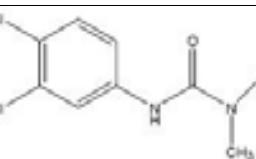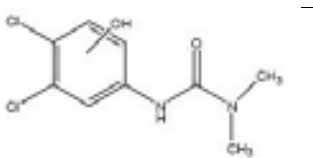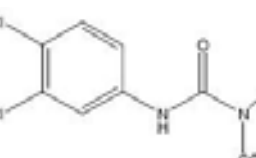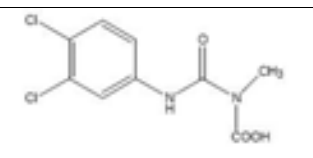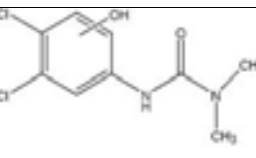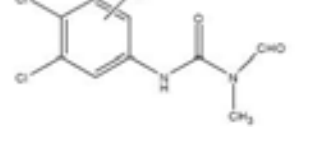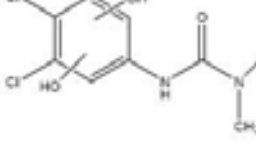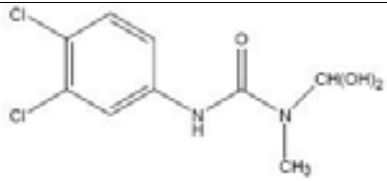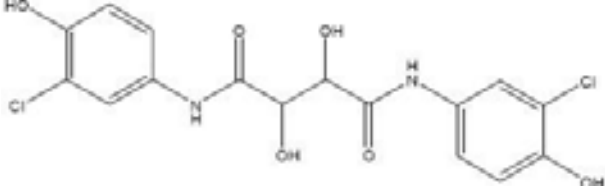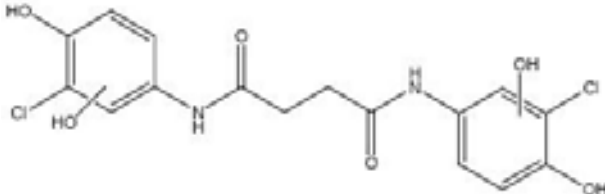
Compound 4

These compounds occurred even after the degradation of diuron had reached about 97% under UV irradiation after 8 hours [37]. Carrier et al. investigated the removal of diuron and thermal degradation products under catalytic wet air oxidation condition, using Ru/TiO_2 as catalyst at 140 °C and 180 °C. During the thermal degradation of diuron, three main intermediate compounds were formed, namely 3,4-dichloroaniline (DCA), dimethylamine (DMA), and 3-(3,4-dichlorophenyl)-1,1-methylurea [38]. Moreover,

Pradittakan et al. investigated the comparison of the intermediates formed from the reaction using different photocatalysts, i.e. titania and zinc oxide and revealed common intermediates as well as different intermediates. The results confirmed that the degradation of diuron generates lots of intermediates. The structures of all intermediates detected were proposed in Table 2.5 [39].

Table 2.5 Possible intermediates generated from photodegradation of diuron on zinc oxide and titania.

Structure	ZnO	TiO$_2$	Structure	ZnO	TiO$_2$
	◆	◆		◆	◆
	◆	◆		◆	◆
		◆			◆
		◆		◆	
		◆		◆	◆
	◆	◆			◆
	◆	◆		◆	◆

Structure	ZnO	TiO$_2$	Structure	ZnO	TiO$_2$
	◆	◆		◆	◆
	◆	◆		◆	
	◆			◆	◆
	◆	◆		◆	◆
	◆			◆	
	◆			◆	

Structure	ZnO	TiO$_2$
	◆	
	◆	
	◆	
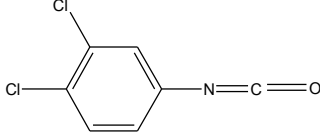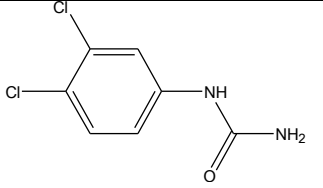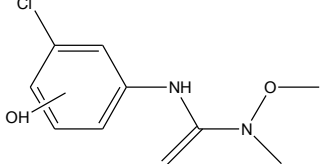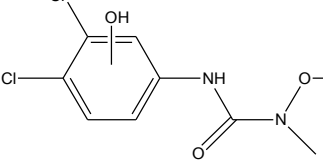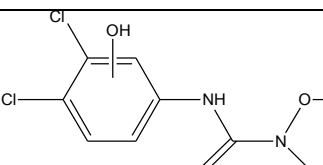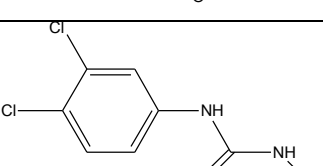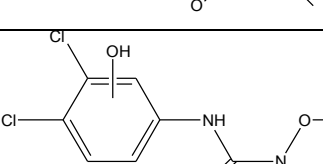
The difference in intermediate products may results from the difference in properties of the catalyst and the different conditions of the reaction. Nevertheless most research has reported that intermediate compounds are formed by dehalogenation reaction of the aromatic ring, hydroxylation reaction of the aromatic ring and molecular chain attached to the aromatic ring and demethylation reaction.

The degradation of diuron, which has slightly different structure comparing with the linuron, has proved to generate several intermediate. For the photocatalytic degradation of the linuron, Katsumata et al. studied photodegradation of linuron in aqueous solution by the photo-Fenton reaction. The degradation rate was strongly influenced by the pH and initial concentrations of H_2O_2 and Fe (II). An initial linuron concentration of 10 mg L^{-1} was completely degraded after 20 min under the optimum conditions. The degree of linuron mineralization was about 90% under UV irradiation after 25 h. The overall reaction can be estimated as follows:

$$2C_9H_{10}C_{12}N_2O_2 + 25O_2 \rightarrow 4HNO_3 + 4HCl + 18CO_2 + 6H_2O$$

Linuron gave eight kinds of intermediate products. The structures of the photoproducts are represented in Table 2.6.

Table 2.6 Photoproducts obtained by degradation of linuron.

Product no.	Retention time (min)	Molecular weight (m/z)	Photoproduct
1	14.4	187	
2	17.2	204	
3	28.9	230	
5	32	264	
6	32.9	264	
7	33.2	218	
8	33.6	264	

The product number 3 and 4 were formed from linuron due to the replacement of hydroxyl group to one chlorine atom. Similarly, the product number 5, 6 and 8 were found to be the products in which hydroxyl group added to the benzene ring of linuron. The product number 1, 2 and 7 were identified as the compounds of which the alkyl groups were

eliminated. Therefore the possible degradation pathway for linuron based on the intermediate products was proposed in Figure 2.3 [3].
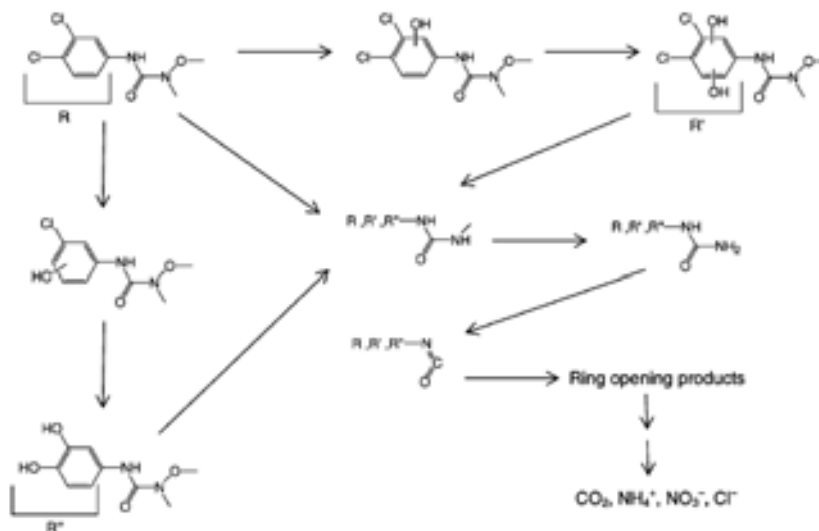
Figure 2.3. Proposed degradation mechanism of linuron by use of the photo-Fenton process [3].

As mentioned earlier, different condition of degradation and different properties of the photocatalyst yielded different intermediate products [39]. Yet, such systematic investigations on the degradation of linuron has not been conducted. It is therefore one of the objectives of this study to investigate degradation pathways with respect to the reaction conditions.

CHAPTER III

EXPERIMENTAL

This chapter describes the experimental procedures for catalyst preparation and photodegradation of linuron. It is divided into four parts: materials used, preparation of TiO_2 and ZnO, adsorption studies and photocatalytic degradation process.

3.1 Materials

List of the chemicals employed in this work and their structures are illustrated in Table 3.1

Table 3.1 List of chemical agents used in the research.

Chemical agents	Using for	Manufacturer / Grade
1. Zinc acetate $(CH_3COO)_2Zn.2H_2O$	Synthesis of ZnO	Ajax Finechem, 99.5%
2. Diethanolamine $(HOCH_2CH_2)_2NH$	Synthesis of ZnO	Ajax Finechem, 98.5%
3.Titanium (IV) butoxide $C_{16}H_{36}O_4Ti$	Synthesis of TiO_2	Fluka, 97%
4. Acetic Acid Glacial CH_3COOH	Synthesis of TiO_2	Quality Reagent Chemical Product, 99.8%
5. Ethanol C_2H_6O	Synthesis of ZnO and TiO_2	VWR Internation, 99.9%
6. Water H_2O	Synthesis of ZnO and TiO_2	
7. Hydrochloric acid HCl	Synthesis of ZnO and TiO_2, Adjust pH	J. T. Baker, 37.7%
8. Sodium hydroxide NaOH	Adjust pH	Ajax Finechem, 98%
9. Linuron (3-[3,4-(dichlorophenyl)-1-methoxy-1-methylurea])	substrate of degradation	Sigma-Aldrich Laborchemikalien GmbH, 99.9%
10. Dichloroaniline $C_6H_5C_{l2}N$	substrate of degradation	Aldrich Chemistry

Chemical agents	Using for	Manufacturer / Grade
11. Acetonitrile CH$_3$CN	mobile phase for HPLC analysis	Duksan Pure Chemicals, 99.9%
12. DI-water H$_2$O	mobile phase for HPLC analysis	

3.2 Preparation of TiO$_2$ and ZnO

3.2.1 Synthesis of Photocatalyst

In the present study, TiO$_2$ and ZnO were prepared via the sol-gel process. Tetrabutyltitanate (TBT) was used to prepare transparent TiO$_2$ sol. Firstly, 5 ml of TBT was dissolved in 20 ml ethanol and stirred for 30 minutes to get the precursor solution. A mixture of 0.26 ml distilled water, 3.4 ml glacial acetic acid, 0.18 ml hydrochloric acid and 5 ml ethanol was added to the precursor solution under vigorous stirring. After that, the solution was continuously stirred for 1 h to achieve a transparent yellow TiO$_2$ sol. On the other hand, zinc acetate was used as a precursor to prepare ZnO sol. At first, 3.29 g of zinc acetate was dissolved in 20 ml ethanol and stirred for 5 min at 50°C to get the precursor solution. A mixture of 0.26 ml distilled water, 0.18 ml hydrochloric acid, 1.58 ml diethanolamine, and 5 ml ethanol was then dropped into the precursor solution under a strong stirring. After that, the solution was continuously stirred for 2 h to achieve a transparent ZnO sol. The TiO$_2$ sol and ZnO sol were gelled at room temperature about 24 hours and dried at 80°C for 12 hours in an oven. After that, the obtained products were calcined at 500°C for 2 hours in a box furnace with the heating rate of 10°C/min

3.2.2 Characterizations of Photocatalysts

The synthesized photocatalysts were characterized by various techniques, as following:

Phase identification of the synthesized photocatalyst were carried out from X-ray diffraction analysis (XRD), by a SIEMENS D5000 X-ray diffractometer using Ni-filtered CuKa radiation. The measurements were carried out in the 2θ range of 20-80 degree at the scan step of 0.04 degree. The crystallite size of prepared ZnO nanopowder and TiO$_2$

nanopowder were determined from the half-height width of the diffraction peak of XRD pattern, according to the Debye-Scherrer equation:

$$D = \frac{k\lambda}{\beta \cos\theta} \qquad (29)$$

Where k is a constant equal to 0.9, λ is the X-ray wavelength, β is the full width at half maximum, θ is the half diffraction angle.

The specific surface area, pore volume and pore size distribution were determined through nitrogen adsorption-desorption analysis. The specific surface area were calculated using the Brunauer-Emmett-Teller model (BET) and the pore size distributions were obtained from desorption branches of the isotherms using the Barret, Joyner, Halenda method (BJH), by Belsorp mini II BEL, Japan at the Center of Excellence on Particle Technology, Chulalongkorn University. The operating conditions are as follows:

Sample weight	~ 0.1- 0.2 g
Degas temperature	200°C
Vacuum pressure	< 10 mmHg

The thermal behavior was analyzed by using thermogravimetric analysis on a Mettler-Toledo TGA/DSC1 STARe System at Center of Excellence in Particle and Technology Engineering laboratory, Chulalongkorn University. The samples were analyzed using heating rate of 10°C/min in 40 ml/min flow of oxygen from temperature of 25 to 1000°C.

Finally, the band gap of the synthesized photocatalysts were measurement by UV-VIS spectrophotometer analysis on PerkinElmer Lambda 650, wavelength between 220 and 800 nm and step size 1 nm at a research laboratory collaborated between Mektec Manufacturing Corporation (Thailand) Ltd. and Chulalongkorn University. The spectra recorded at wavenumber 400-800 cm^{-1}.

3.3 Adsorption Studies

All experiments about adsorption of linuron onto the surface of TiO_2 and ZnO were carried out in batches. Studies were conducted with suspensions prepared by mixing the photocatalyst with 550 ml of linuron solution. The concentration of linuron was varied from 1, 5, 10, 15, to 20 ppm, respectively, while the content of the photocatalyst was kept at 10 mg/10 ml of the linuron solution. The mixture was stirred at room temperature for 3 h in the dark. The final concentration of linuron was measured by high performance liquid chromatography (HPLC). The HPLC system included Hyper clone column (150×8 mm inner diameter; 5 μm particle size) (Phenomenex, USA) with a mobile phase of 70% acetonitrile and 30% DI water; a flow rate of 1.5 ml/min and a UV detector at 254 nm.

3.4 Photocatalytic Degradation Process

3.4.1 Photodegradation Apparatus

The schematic of the protodegradation apparatus used in this work is shown in Figure 3.1. The components of the apparatus and their functions are described as the follows.
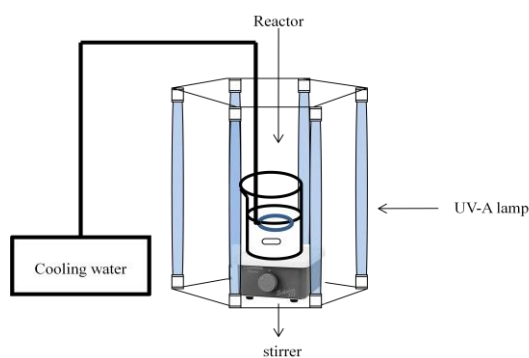
Figure 3.1 Diagram of the equipment setup for the photocatalytic degradation.

The system is consisting of:
- Cooling coil used to control temperature during the experiment to be 30 ± 2 °C.
- 6 UV-A lamps (Phillips TLD 15W/05) used as a light source of the photocatalytic reaction.
- A magnetic stirrer used to generate turbulent conditions in mixture during the experiment to keep mixture homogeneous.

3.4.2 Photocatalytic Degradation Procedure

The photocatalytic activities of the synthesized photocatalysts were determined from the photodegradation of linuron under UV irradiation. The photodegradation was conducted in a 600-ml pyrex reactor, in which the mixture of 550-ml linuron solution and the photocatalysts was contained. The content of the photocatalyst was kept at 1 mg of the catalyst per 10 ml of the solution. The mixture was kept in dark for 30 min to allow complete adsorption of linuron on the surface of catalysts, prior to the reaction. After that, the solution was irradiated by six UV-A lamps (Phillips TLC 15w/05). During the irradiation, agitation was maintained by a magnetic stirrer to keep the catalyst uniformly dispersed within the solution.

3.4.3 Characterization of Product during Photocatalytic Degradation

The linuron solution was periodically sampled to monitor the concentration of linuron via HPLC. The HPLC system included Hyper clone column (150×8 mm inner diameter; 5 µm particle size) (Phenomenex, USA) with a mobile phase of 70% acetonitrile and 30% DI water; a flow rate of 1.5 ml/min and a UV detector at 254 nm. Attempts were made to identify the intermediate products formed in the photocatalytic degradation of linuron in aqueous suspension of photocatalysts through LC-MS analysis. LC-MS identification was carried out using an Agilent 1100 Series in positive and negative modes under the following condition: Nebulizer pressure 45 psig, Drying gas temperature 275 $^{\circ}$C, Drying gas flow 12 Lmin^{-1}, Capillary voltage 4000 V and Fragment voltage 120 V.

CHAPTER IV

RESULTS AND DISCUSSION

The photocatalytic reaction on photocatalysts can be applied to remove many organic compounds from wastewater. In this research, the photocatalytic degradations of linuron on titania and zinc oxide synthesized by sol-gel method were investigated. Properties of the photocatalysts were characterized by many techniques. Then, they were compared in the photocatalytic degradation of linuron. This work not only investigates the degradation of linuron, but also interests in identifying the formation of intermediates formed during the photocatalytic degradation because the intermediate compounds formed could be more toxic than the parent herbicides.

4.1 Properties of Synthesized Photocatalysts

In this research, photocatalysts were synthesized by sol-gel method and calcined at 500°C for 2 hours. Physical properties of photocatalysts were investigated by many techniques such as XRD, BET and TGA. Then, they were compared in the photocatalytic degradation of linuron.

4.1.1 Synthesized Titania

The powder obtained from the sol-gel method was confirmed to be titania. The crystalline phases of titania was analyzed by XRD. The XRD measurement on this powder was conducted and the result was show in Figure. 4.1. The result confirms that titania was formed in anatase phase without contamination from other crystalline phases. The crystallite size of synthesized titania was calculated from the half-height width of the diffraction peak of XRD pattern, using the Debye-Scherrer equation:

$$D = \frac{k\lambda}{\beta \cos\theta} \tag{29}$$

where k is a constant equal to 0.9, λ is the X-ray wavelength (1.5418A°), β is the full width at half maximum, θ is the diffraction angle. The calculated results are shown in Table 4.1.
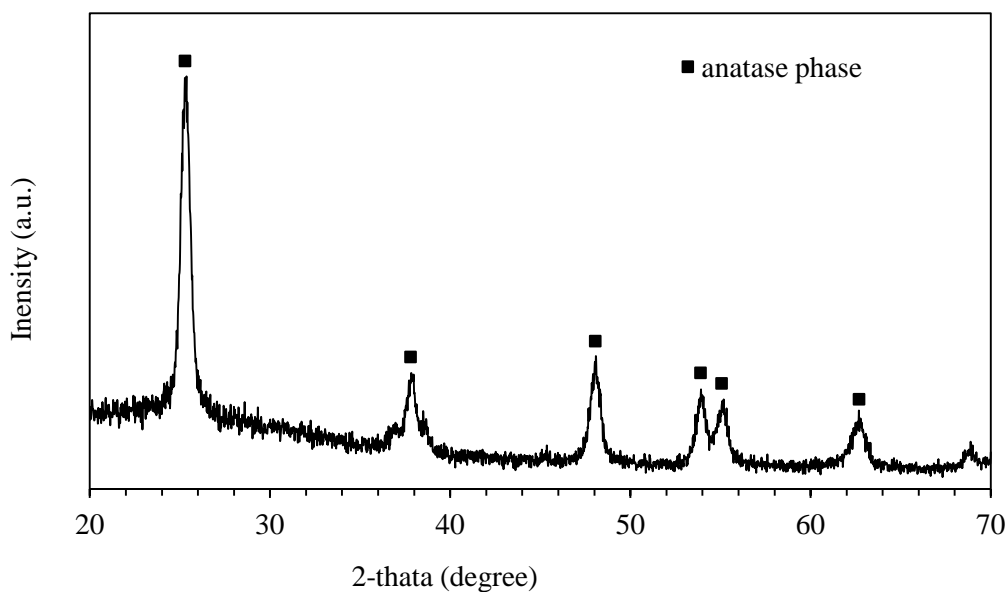
Figure 4.1 XRD patterns of the synthesized titania powder.

Table 4.1 Crystallite size and surface area of titania.

Type of titania	Crystallite size, (nm)	Specific surface area, S_{BET}, (m^2/g)	Average pore diameter (nm)	Band gap energy (eV)
Commercial titania	NA	40.00	26.97	3.53
Synthesized titania	7.49	42.65	26.74	3.20

The specific surface areas for both synthesized and commercial titania measured by nitrogen adsorption-desorption are also shown in Table 4.1. The results show that the synthesized titania revealed type-IV adsorption-desorption isotherm with a hysteresis loop, which indicates the presence of mesopores, as shown in Figure 4.2. The calculated specific surface area of the synthesized and commercial titania based on BET model was found to be 42.65 and 40.00 m^2/g, respectively.
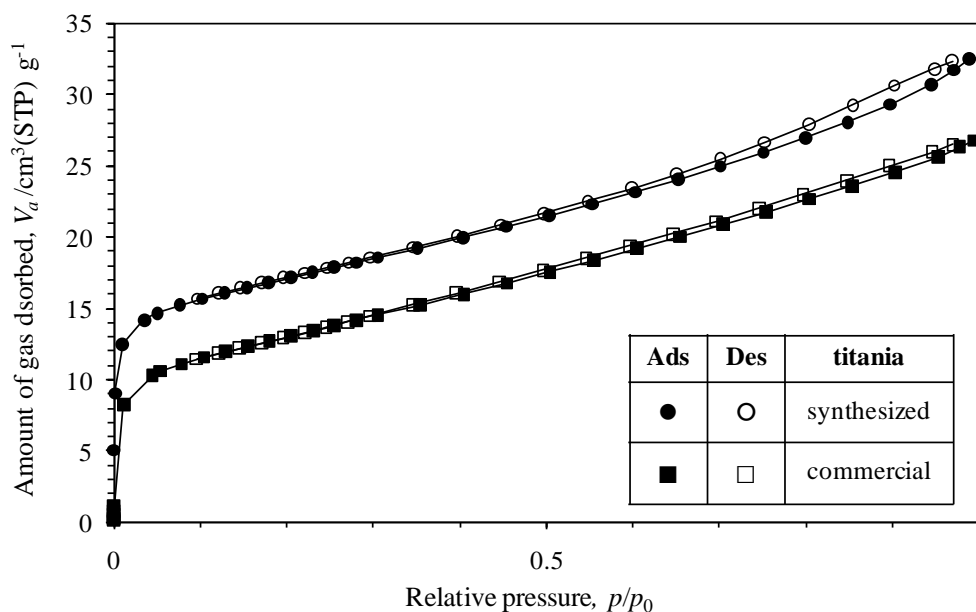
Figure 4.2 Adsorption/desorption isotherm of synthesized titania and commercial titania.

The band gap energy of synthesized and commercial titania were calculated on data measured by UV/ visible spectroscopy by using the relation $v_0 = E_g/h$ where v_0 is frequency at absorption edge , h is Planck constant $(4.135\times10^{-15}$ eV.s) and E_g is the band gap energy. The frequency is related to the wavelength by the relation $v_0 = c/\lambda_{1/2}$ where c is the speed of light $(3\times10^8$ m/s) and $\lambda_{1/2}$ is wavelength at absorption edge (nm). The band gap energy of synthesized and commercial titania are shown in Table 4.1.

The thermogravimetric result for the obtained titania powder, after calcined at 500°C for 2 hours (heating rate of 10°C/min), heated from 0-1000°C in flowing O_2 is shown in Figure 4.3. According to the TGA analysis results, it is clearly seen that the TGA curve indicates no weight loss. Therefore, it can be assumed that calcination temperature of 500°C is high enough for complete combustion of organic residue in the catalyst. The results confirm that this synthesized titania had no residual organics compound within the powder.
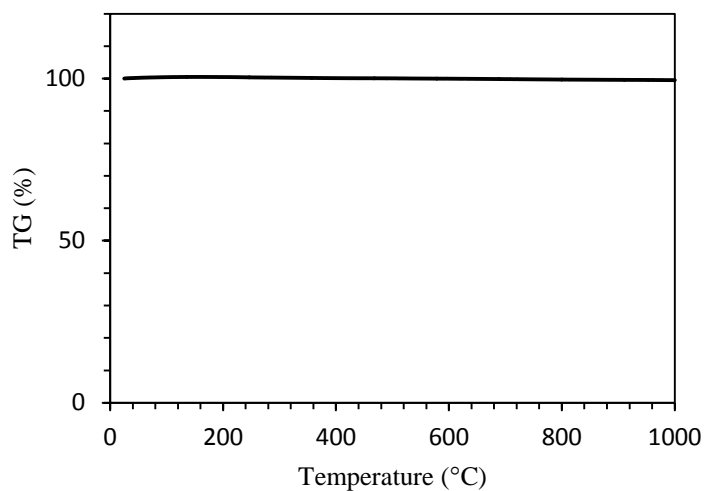
Figure 4.3 TGA curve of the synthesized titania powder after calcined at 500°C for 2 h.

4.1.2 Synthesized Zinc Oxide

The particles were synthesized by sol-gel method. This powder after calcination was analyzed by XRD. The XRD analysis result is shown in Figure 4.4. It is comfirmed that the powder obtained is zinc oxide in wurtzite phase. No diffraction peaks corresponding to other phases are detected in this catalyst. The crystallite size of the synthesized zinc oxide calculated by the Debye-Scherrer equation are shown in Table 4.2
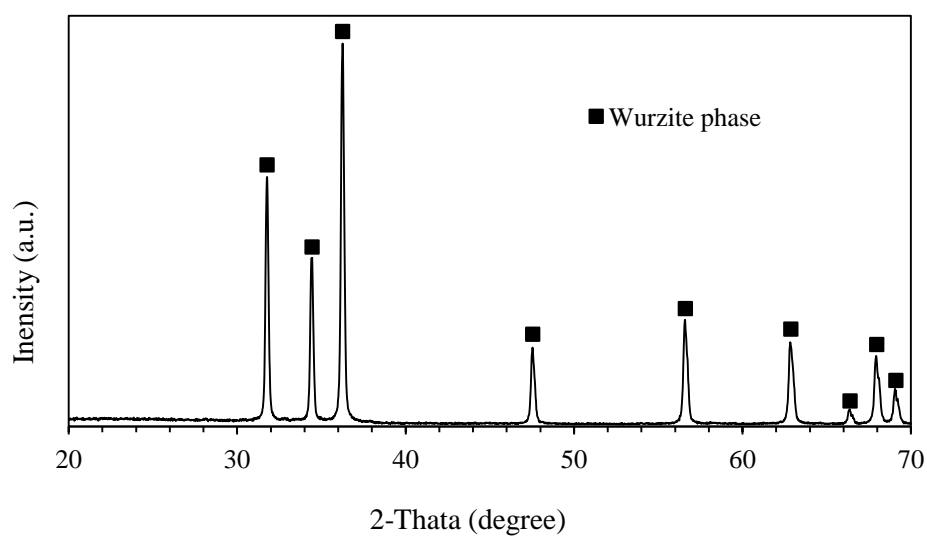
Figure 4.4 XRD patterns of the synthesized zinc oxide powder.

Table 4.2 Crystallite size and surface area of zinc oxide.

Type of zinc oxide	Crystallite size, (nm)	Specific surface area, S_{BET}, (m^2/g)	Average pore diameter (nm)	Band gap energy (eV)
Commercial zinc oxide	NA	4.35	3.0526	3.265
Synthesized zinc oxide	9.58	4.00	6.0979	3.230

The band gap energy for both synthesized and commercial zinc oxide were studied from adsorption wavelength data measured from UV-Visible spectroscopy. The results are shown in Table 4.2. The nitrogen adsorption-desorption isotherms of zinc oxide are shown in Figure 4.5. Isotherms of the synthesized and commercial zinc oxide are type-II which indicates non-porousity. Using the BET method, the surface area of the synthesized and commercial zinc oxide are shown in Table 4.2.

Ads	Des	zinc oxide
●	○	synthesized
■	□	commercial
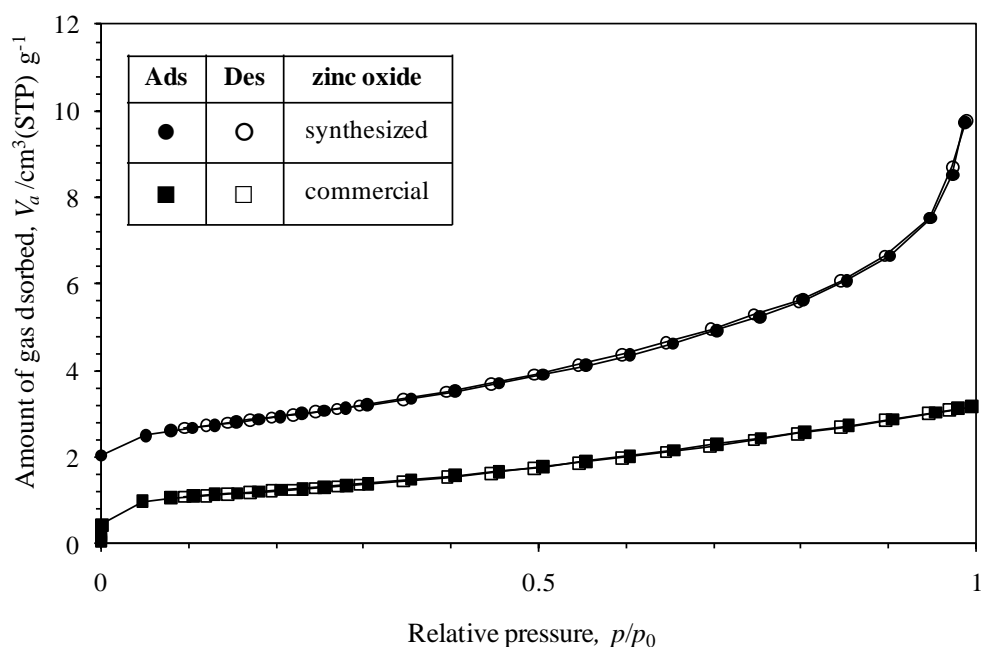
Figure 4.5 Adsorption/desorption isotherm of synthesized zinc oxide and commercial zinc oxide.

The TGA result for the obtained zinc oxide powder, after calcined at 500°C for 2 hours (heating rate of 10°C/min), heated from 0-1000°C in flowing O_2 is shown in Figure 4.6. According to the TGA analysis results, it is clearly seen that the TGA curve indicates no weight loss. It can be assumed that calcination temperature of 500°C is high enough for complete combustion of organic residue. The results confirm that the synthesized zinc oxide had no residual organics compound within the powder.
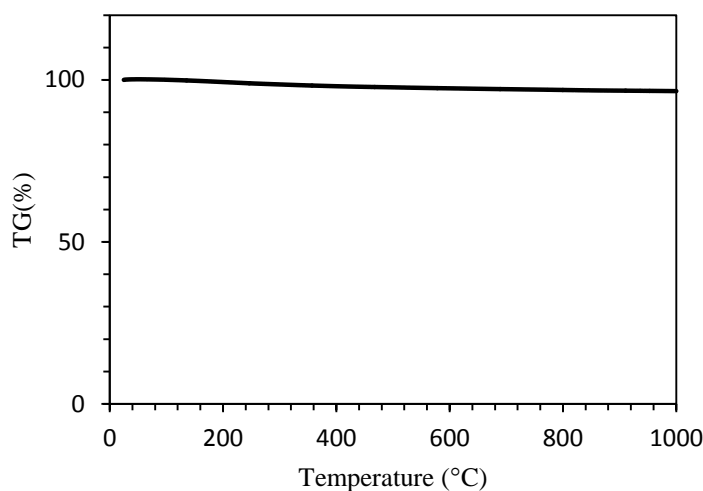
Figure 4.6 TGA curve of the synthesized zinc oxide powder after calcined at 500°C for 2 h.

4.2 Adsorption Studies

4.2.1 Adsorption Isotherm of Linuron on Catalyst

In this section, linuron was adsorbed onto the surface of the catalysts. The adsorption experiments were carried out in batches. The initial concentration of linuron was varied from 1, 5, 10, 15 and 20 ppm while the content of the photocatalyst was kept at 10 mg/10 ml of the linuron solution. The mixture was stirred at room temperature for 3 h in the dark. The final concentration of linuron was measured by high performance liquid chromatography (HPLC). Figure 4.7 – Figure 4.10 show results of the adsorption of linuron on commercial titania, synthesized titania, commercial zinc oxide and synthesized zinc oxide, respectively, as a function of the contact time at room temperature. The results show that the adsorption on titania takes place rather fast at low concentration of 1, 5, and 10 ppm. The adsorption equilibrium was reached within 30 min. On the other hand, at the high

concentration of 15 and 20 ppm, the adsorption equilibrium was reached at 80 min. Similar results were observed for the adsorption of linuron on zinc oxide except that the adsorption equilibrium was reached after 100 min when the concentration of linuron was 15 and 20 ppm.
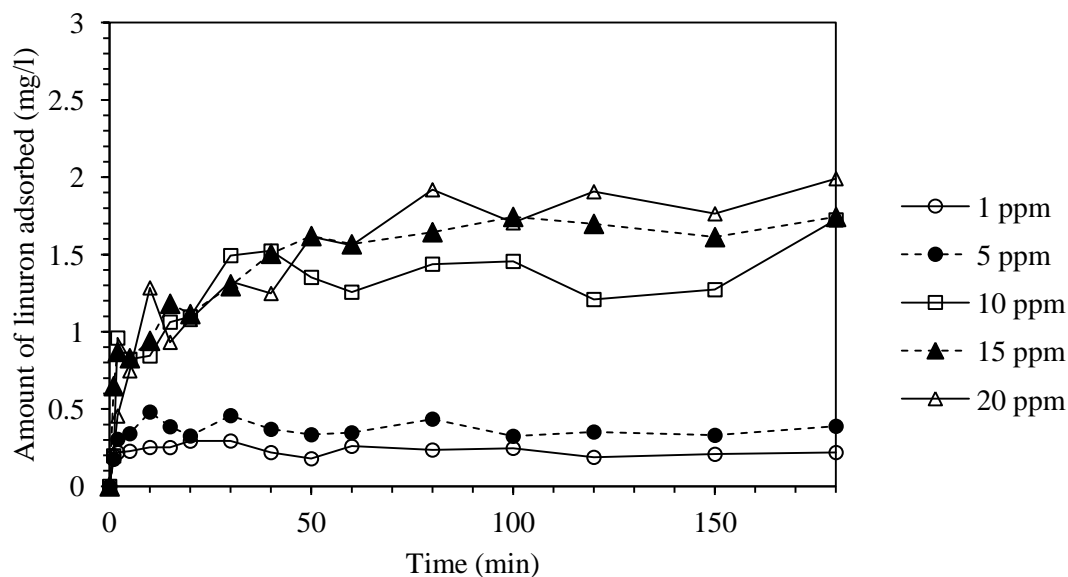
Figure 4.7 Adsorption of linuron on the surface of commercial titania when the initial concentration was 1, 5, 10, 15 and 20 ppm.
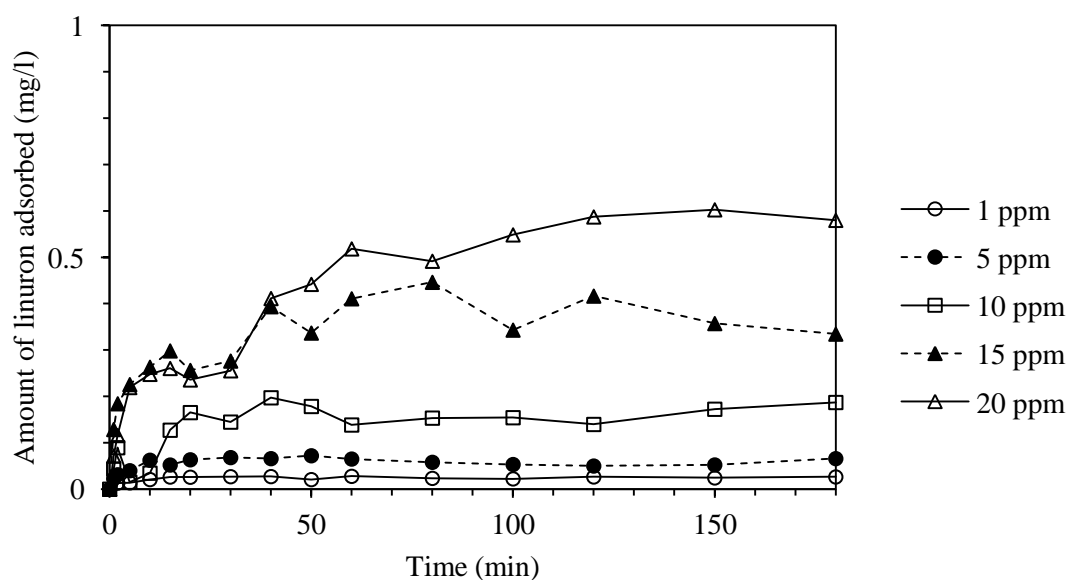
Figure 4.8 Adsorption of linuron on the surface of synthesized titania when the initial concentration was 1, 5, 10, 15 and 20 ppm.
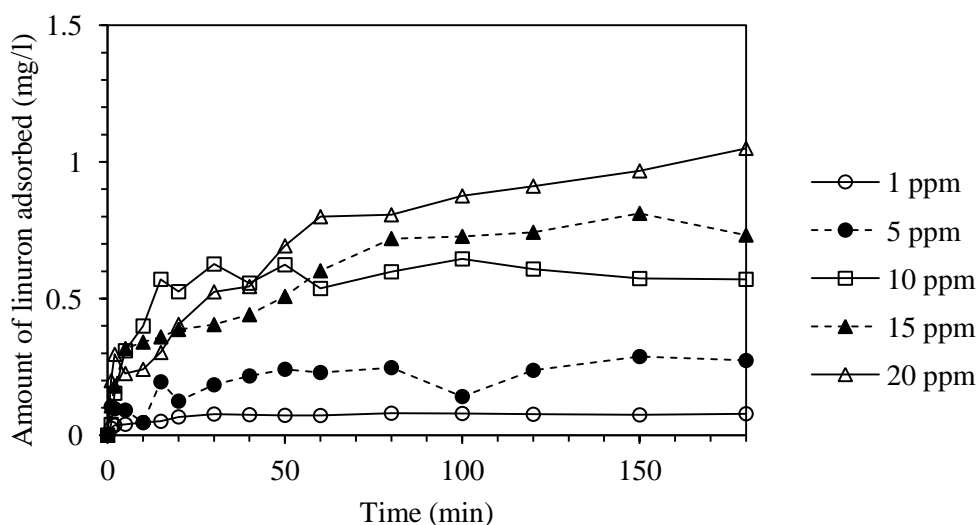
Figure 4.9 Adsorption of linuron on the surface of commercial zinc oxide when the initial concentration was 1, 5, 10, 15 and 20 ppm.
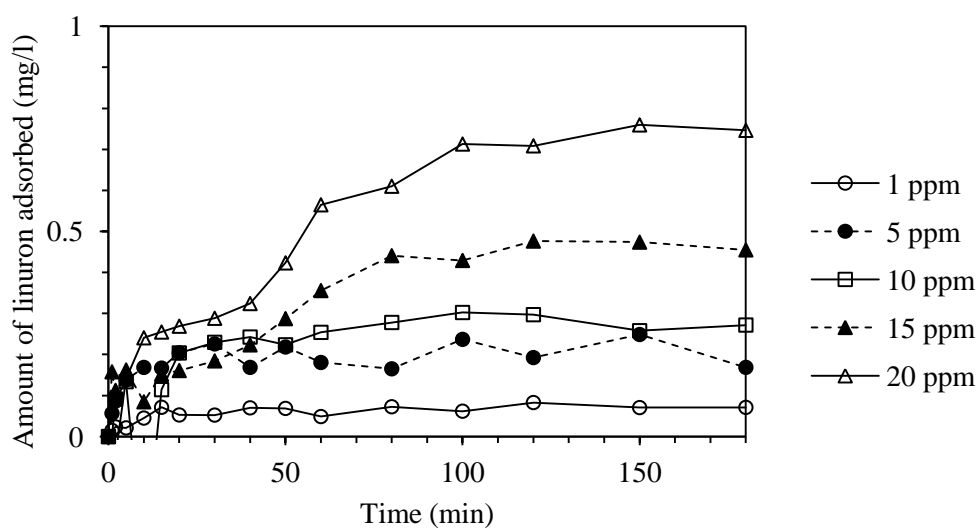
Figure 4.10 Adsorption of linuron on the surface of synthesized zinc oxide when the initial concentration was 1, 5, 10, 15 and 20 ppm.

The sorption ability of titania and zinc oxide can be investigated from the adsorption isotherm. Figure 4.11 shows the adsorption isotherm of linuron on commercial titania, synthesized titania, commercial zinc oxide and synthesized zinc oxide at room temperature. It is found that the equilibrium isotherms obtained for commercial zinc oxide and synthesized zinc oxide, appear as linear curve which describes strong chemical interection between linuron and ZnO. On the other hand, commercial titania and synthesized

titania show nonlinear curves. The non-linear curve might express surface unsaturation, which would further lead to an linuron-TiO$_2$ interaction.
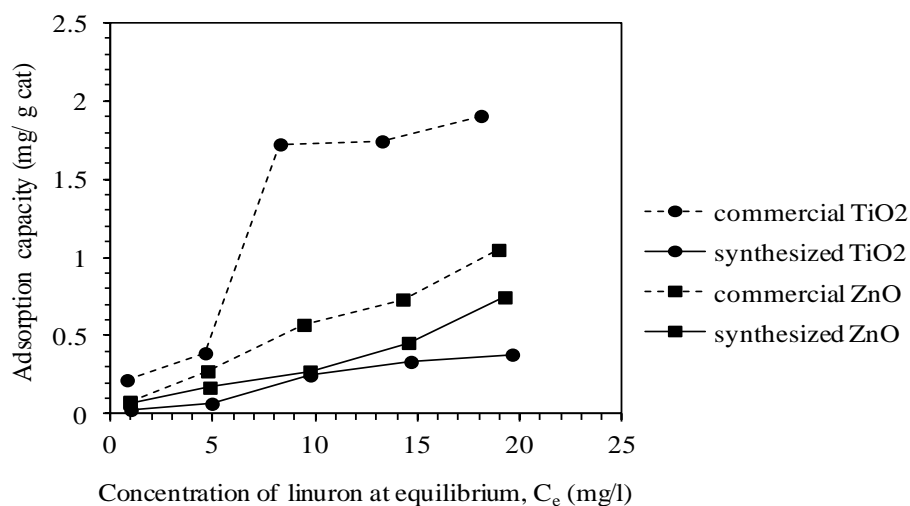
Figure 4.11 Adsorption isotherm of linuron onto the surface of commercial titania, synthesized titania, commercial zinc oxide and synthesized zinc oxide at room temperature.

The adsorption models were used to describe the adsorption process. The adsorption isotherm defines the equilibrium state of the process. In this studty, the adsorption effects of linuron on the catalyst surfaces are decribed with either the Langmuir or Freundlich isotherm models. The Langmuir adsorption isotherm has been used successfully for many adsorption processes of monolayer adsorption. According to the linearized form of the Langmuir isotherm model [34, 35]:

$$\frac{1}{q_e} = \frac{1}{q_{\max}} + \frac{1}{bq_{\max}} \frac{1}{C_e} \qquad (30)$$

where q_e is amount of adsorbate on adsorbent at equilibrium (mg/g), q_{max} is maximum adsorption capacity (mg/g), C_e is equilibrium concentration (mg/l), and b is constant relating to energy of the sorption system (l/mg).

For the Freundlich isotherm, it is an emprical equation used to describe of multilayer adsorption. The Freundlich isotherm is represented in logaritmic form as follows [29, 35, 36]:

$$ln\, q_e = lnK_f + \frac{1}{n}lnC_e \qquad (31)$$

where $\frac{1}{n}$ is adsorption intensity and K_f is Freundlich constant relating to adsorption capacity $(mg/g(mg/l)^{-1/n})$.

Figure 4.12 and Figure 4.13 show the data fitted to Langmuir isotherm and Freundlich isotherm model and the fitted parameters are shown in Table 4.3. It was found that the Freundlich adsorption model fitted the experimental data better than the Langmuir model, as observed from the R^2 values. It is comfirm that the adsorption of linuron onto the surface of the catalyst can be multilayer. By comparing the Freundlich adsorption constants obtained from the commercial and synthesized titania, it is found that the commercial titania has much higher adsorption capacity than the synthesized titania and both kinds of the ZnO. Nevertheless, the synthesized TiO_2 has lower adsorption capacity than the commercial and synthesized ZnO.

Table 4.3 Parameters for Langmuir and Freundlich isotherm models for adsorption of linuron on commercial titania, synthesized titania, commercial zinc oxide and synthesized zinc oxide.

Model	Parameters	Values			
		commercial titania	synthesized titania	commercial zinc oxide	Synthesized zinc oxide
Langmuir isotherm model	q_{max} (mg/g)	1.5295	0.4411	1.4813	0.5025
	b (ppm^{-1})	0.2037	0.0640	0.0601	0.1734
	R^2	0.407	0.597	0.872	0.494
Freundlich isotherm model	K_f (ppm^{-1})	0.2244	0.0231	0.0806	0.0651
	n	1.32	1.06	1.17	1.37
	R^2	0.810	0.949	0.987	0.857

Figure 4.12 Parameters fitting for the Langmuir model for adsorption of linuron on: (a) commercial titania, (b) synthesized titania, (c) commercial zinc oxide and (d) synthesized zinc oxide.

K_f is a Freundlich constant that shows the adsorption capacity of an adsorbent, while n is a constant which shows the strength of the interaction between adsorbate and adsorbent [36]. A very weak adsorbent/adsorbate interaction occurs at values of n lower than 1, while values higher than 1 suggest a strong adsorbent/adsorbate interaction. At value of n equal to 1 it is assumed that all sites are energetically similar [35]. In this case, n value are 1.32, 1.06, 1.17 and 1.37 for adsorption of linuron on commercial TiO_2, synthesized TiO_2, commercial ZnO and synthesized ZnO, respectively, indicating strong interaction between linuron and all kinds of catalyst.
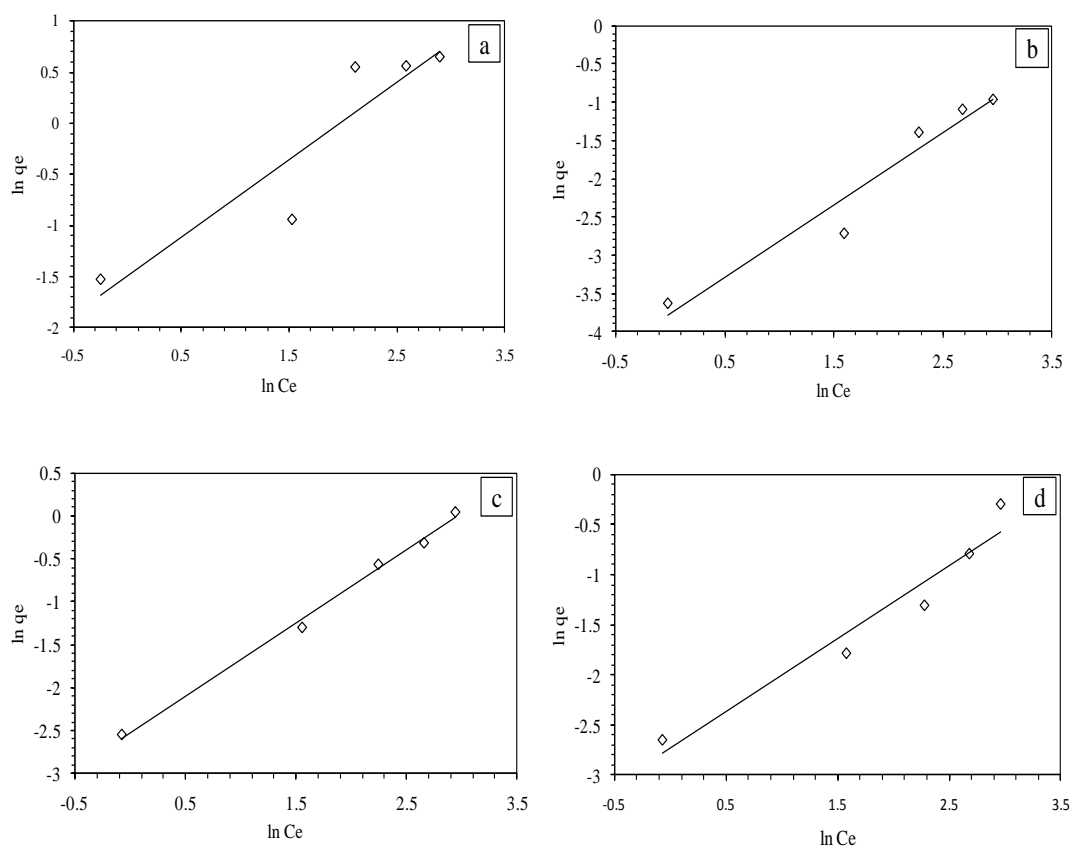
Figure 4.13 Parameters fitting for the Freundlich model for adsorption of linuron on: (a) commercial titania, (b) synthesized titania, (c) commercial zinc oxide and (d) synthesized zinc oxide.

4.2.2 Adsorption Isotherm of Dichloroaniline

The structure of dichloroaniline is consisted of an aromatic ring attached with two chlorine group and one amino group. It has a structure similar to one side of linuron. It is therefore believed at the adsorption behavior of dichloroaniline on the surface of catalysts should be beneficial to understand the position of adsorption of linuron on catalyst surface, while we could not study other compound because we could not find a compound with the same structure as the aliphatic side of linuron for comparison. The adsorption experiments of dichloroaniline were carried out in batches under the same adsorption condition as the adsorption of linuron. Figure 4.14 - Figure 4.15 show results of the adsorption of dichloroaniline on commercial titania and commercial zinc oxide, respectively, as a function of the contact time at room temperature. The results show that the adsorption on titania takes place rather fast at low concentration of 1,5, and 10 ppm. The adsorption equilibrium was reached within 30 min. On the other hand, at the high concentration of 15 and 20 ppm, the

adsorption equilibrium was reached at 50 min. Similar results were observed for the adsorption of dicloroaniline on zinc oxide except that the adsorption equilibrium was reached after 80 min when the concentration of linuron was 15 and 20 ppm.
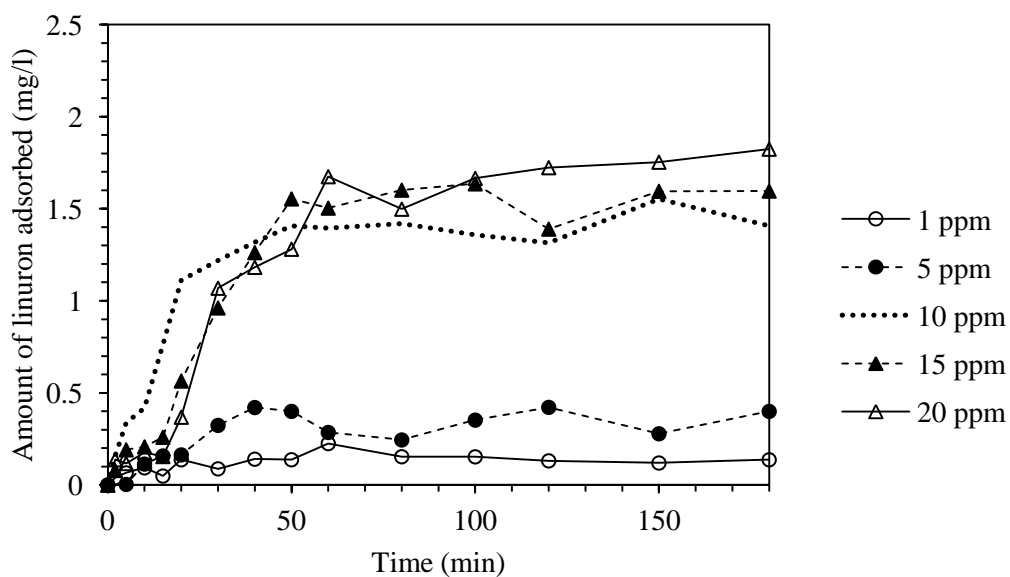
Figure 4.14 Adsorption of dichloroaniline on the surface of commercial titania when the initial concentration was 1, 5, 10, 15 and 20 ppm.
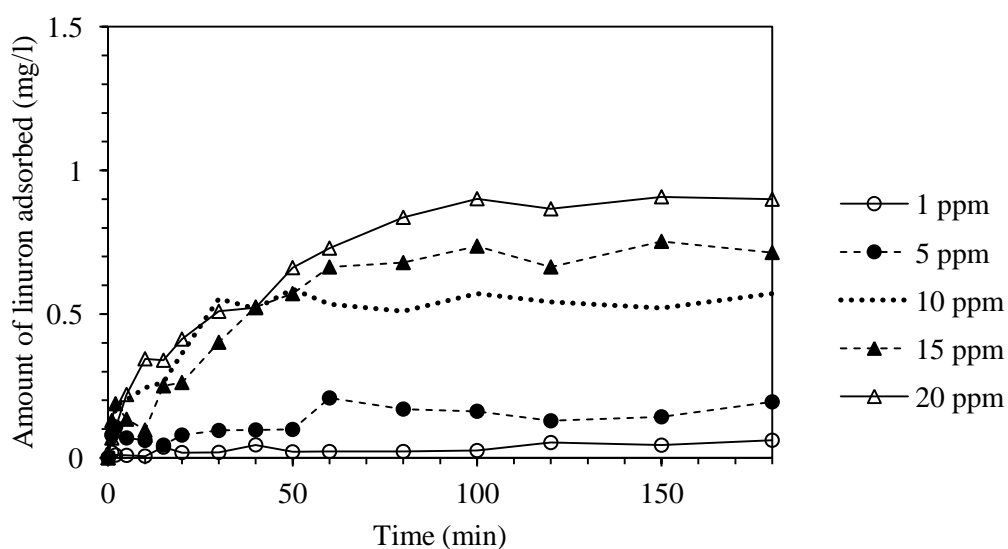
Figure 4.15 Adsorption of dichloroaniline on the surface of commercial zinc oxide when the initial concentration was 1, 5, 10, 15 and 20 ppm.
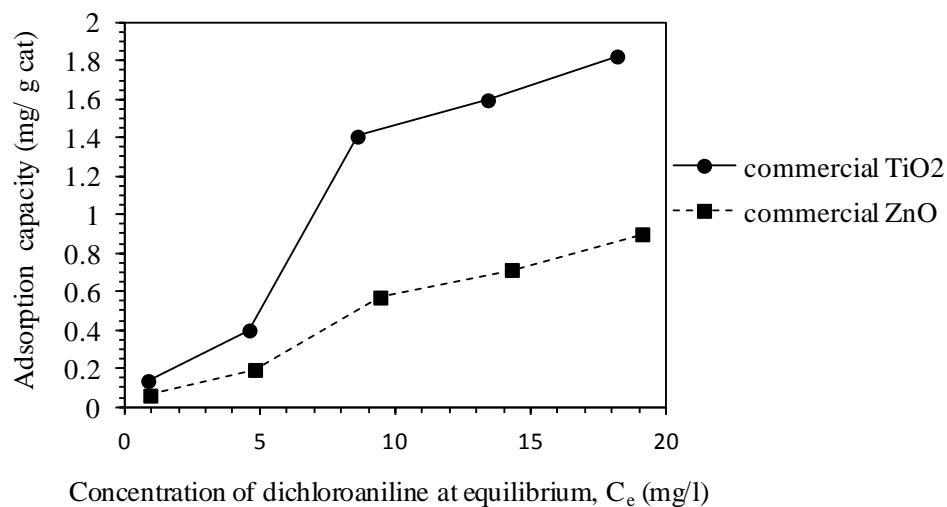
Figure 4.16 Adsorption isotherm of dichloroaniline onto the surface of commercial titania and commercial zinc oxide at room temperature.

Figure 4.17 and Figure 4.18 show parameters fitting for the Langmuir and Freundlich models. The fitted parameters are shown in Table 4.4. It is found that the Freundlich adsorption model fits the experimental data better than the Langmuir model. It is confirmed that the adsorption of dichloroaniline onto all catalysts studied can be in form of multilayer. Comparing the Freundlich adsorption constants obtained from the commercial TiO_2 and commercial ZnO, it is found that the commercial has indicating higher adsorption capacity than the commercial ZnO. The *n* value are 1.10 and 1.08 for the adsorption of dichloroaniline on the commercial titania and commercial zinc oxide, respectively, which indicates strong interaction between dichloroaniline and the catalysts.

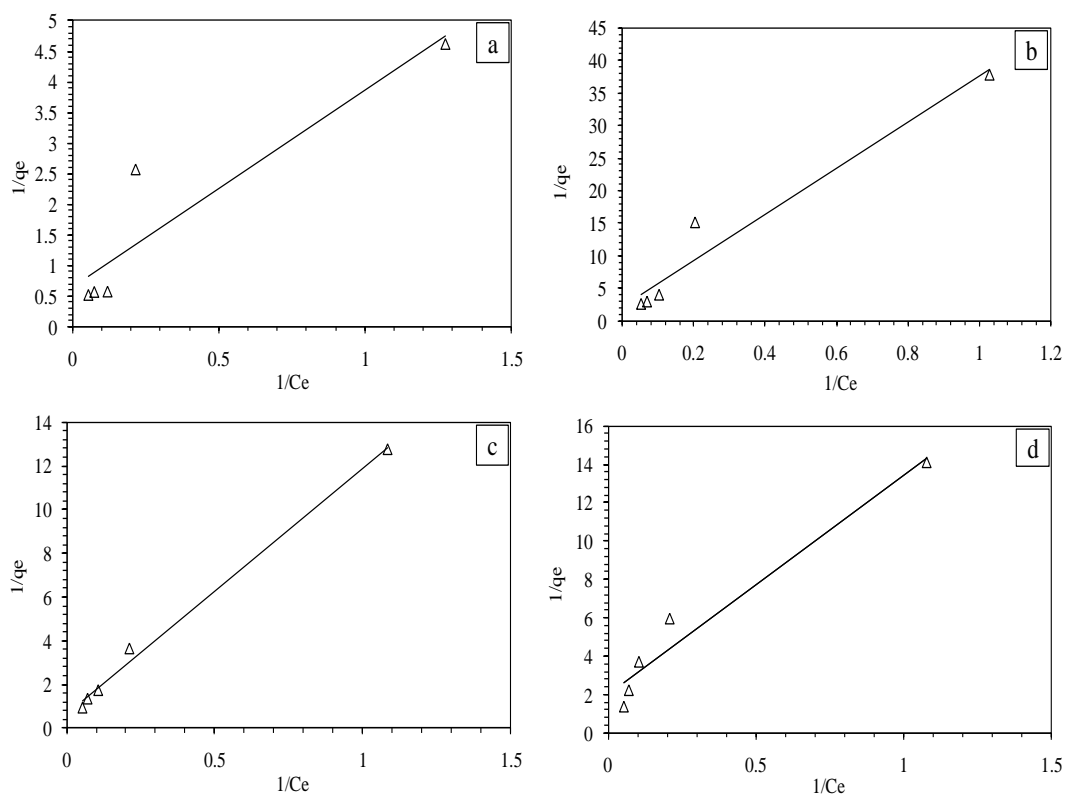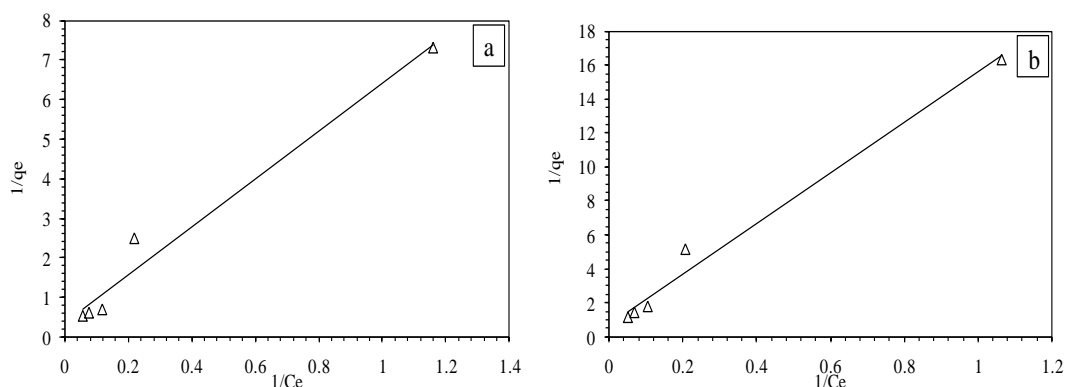**Figure 4.17** Parameters fitting for the Langmuir model for adsorption of dichloroanline on: (a) commercial titania, (b) commercial zinc oxide.

Figure 4.18 Parameters fitting for the Freundlich model for adsorption of dichloroaniline on: (a) commercial titania, (b) commercial zinc oxide.

As mentioned earlier, the structure of dichloroaniline is consisted of an aromatic ring attached with two chlorine group and one amino group which it is similar to the one side of linuron. However, according to the adsorption results on TiO_2 and ZnO, the Freundlich parameters of the adsorption and adsorption isotherm of dichloroaniline are similar to when compared with the adsorption of linuron as shown in Figure 4.19. So, it can be suggested that the position of aromatic ring attached with two chlorine group on linuron was adsorbed to the surface of catalyst.

Table 4.4 Parameters for Langmuir and Freundlich isotherm model for adsorption of dichloroaniline on commercial titania, synthesized titania, commercial zinc oxide and synthesized zinc oxide.

Model	Parameters	Values	
		commercial titania	commercial zinc oxide
Langmuir isotherm model	q_{max} (mg/g)	2.7019	1.4678
	b (ppm^{-1})	0.0610	0.0457
	R^2	0.749	0.827
Freundlich isotherm model	K_f (ppm^{-1})	0.1446	0.0599
	n	1.10	1.08
	R^2	0.902	0.973

(a)   (b)
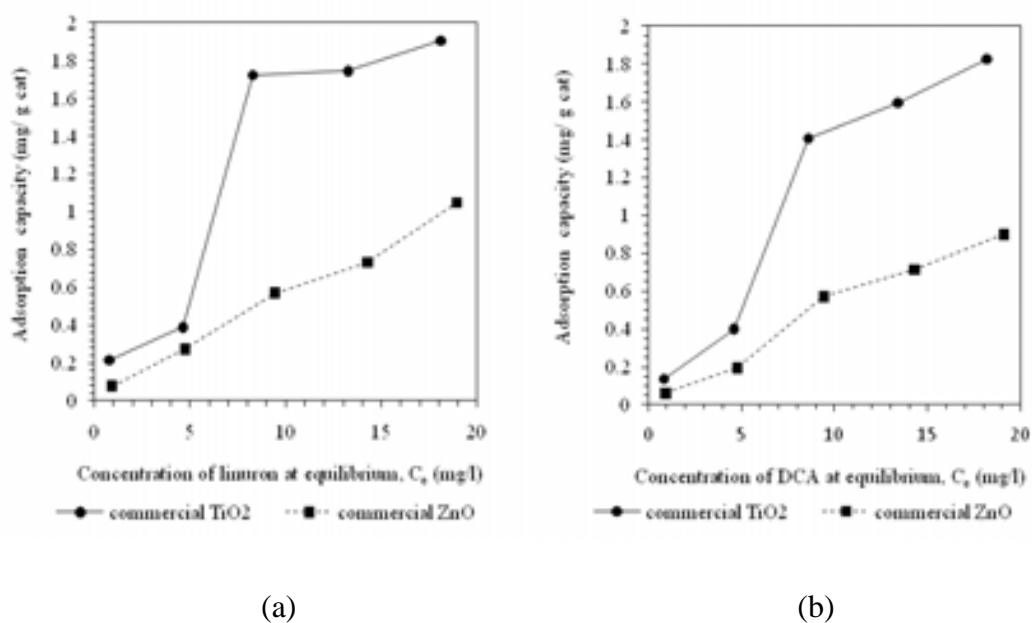
Figure 4.19 Comparison between adsorption isotherms of: (a) linuron and (b) dichloroaniline.

4.3 Photodegradation of Linuron

It has been reported that the photocatalytic systems are generally based on the generation of hydroxyl radicals [37]. Very reactive hydroxyl radicals can be formed by the decomposition of water or by the reaction of the hole with hydroxyl ion. The radical is a strong oxidizing agent leading to degradation of organic pollutants, following by the complete mineralization of organic pollutants. Degradation of linuron can be expressed by the following equation.

$$\text{Linuron} \longrightarrow \text{Intermediates} \longrightarrow CO_2 + H_2O + HNO_3$$

The total mineralization is expressed by the following equation:

$$C_9H_{10}C_{12}N_2O_2 + 12.5O_2 \longrightarrow 2HNO_3 + 2HCl + 9CO_2 + 3H_2O$$

In this work, photocatalytic degradation of linuron in an aqueous solution using titania and zinc oxide as the catalyst was investigated for 6 hours of UV-A irradiation. The photocatalytic activities of titania and zinc oxide were determined from the photodegradation of linuron conducting in a 600-ml pyrex reactor, in which it contained 550 ml of linuron solution. The content of the photocatalyst was kept at 1 mg of the catalyst per 10 ml of the solution. The initial linuron concentration was fixed at 10 ppm. The mixture was kept in dark for 30 min to allow complete adsorption of linuron on the surface of the catalysts. In the absence of the photocatalyst, linuron concentration remained nearly constant with time of reaction as shown in Figure 4.20. The results show that the degradation of linuron is less than 7% after 6 hours of UV irradiation without the catalyst, which is much slower than the photocatalytic degradation of linuron on the catalyst.

4.3.1 Photodegradation of Linuron on Titania

Concentrations of linuron during the photocatalytic degradation with respect to the initial linuron concentration (C/C_0) when the synthesized and commercial titania were used as catalyst are shown in Figure 4.20. The results report that the commercial titania has higher activity in degrading linuron than the synthesized titania. The degradation of linuron on the commercial titania is about 99% within 6 hours of UV-A irradiation, while that achieved on synthesized titania is only 55%. The reason for this result could not be explained in this study.

According to many researchers, kinetic of the photodegradation of many organic pollutants is described by the pseudo-first order kinetics.

$$r = -\frac{dC}{dt} = k_{app}C \qquad (33)$$

where r is the rate of linuron degradation, C is the concentration of the linuron being degraded, k_{app} is the apparent rate constant of a pseudo first order model, t is the irradiation time. For batch operation, Eq. (33) can be integrated to Eq. (34) when C_0 is initial concentration of linuron.

$$\ln\frac{C_0}{C} = k_{app}t \qquad (34)$$

Kinetics studies were assessed by monitoring the change in the concentration of linuron at certain interval of time. The resulting first-order rate constants have been used to calculate degradation rate for the degradation of linuron on synthesized and commercial titania. The results are shown in Figure 4.21. This figure presents $\ln(C_0/C)$ versus irradiation time (t) at natural pH. The apparent rate constant (k_{app}) can be determined from the slope of the curve obtained. The apparent rate constants for synthesized and commercial titania are shown in Table 4.5. The R^2 values are 0.9261 and 0.8818, respectively.

Figure 4.20 Concentration of linuron with respect to the initial linuron concentration (C/C_0) during the photocatalytic degradation on titania: ($\square$) synthesized titania, ($\bigcirc$) commercial titania and ($\triangle$) without catalyst.

—
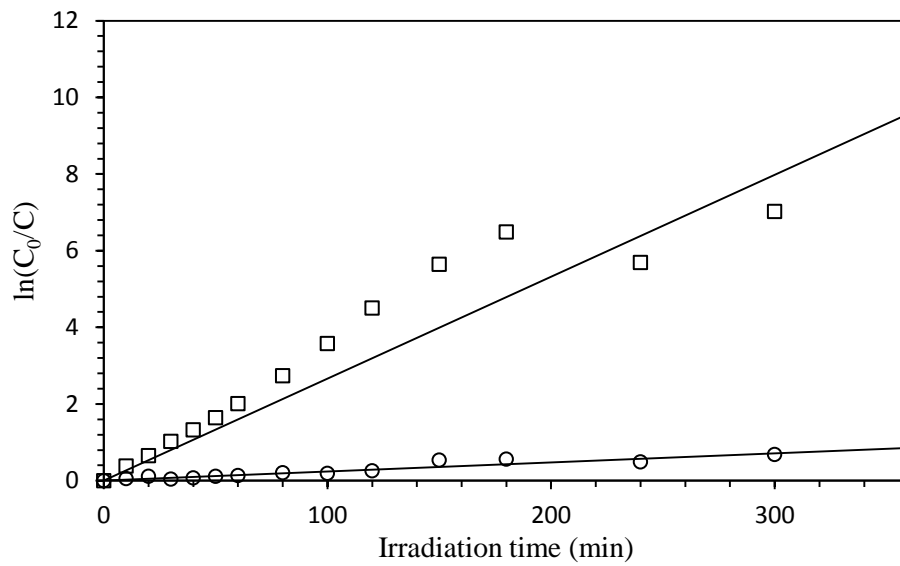
Figure 4.21 First-order linear transforms plot of the photocatalytic degradation on titania: (□) synthesized titania and (○) commercial titania.

From the degradation data, it was observed that the first-order kinetics does not provide a good fit to the experimental data when the synthesized and the commercial titania were used as the catalyst because the conversion of this reaction does not reach 100%. Therefore, the data shown in Figure 4.20 were also fitted against the Langmuir-Hinshelwood kinetic model. In this model, it is assumed that the reaction occurs on the heterogeneous catalyst surface and the rate of reaction (r) is proportional to the fraction of surface covered by the substrate (θ):

$$r = -\frac{dC}{dt} = k_r \theta = k_r \frac{KC}{1 + KC} \tag{35}$$

where C is the concentration of the substance being degraded, t is the irradiation time, k is true rate constant and K is the constant of adsorption equilibrium.

The constants k_r and K can be calculated from the corresponding integrated expression in Equation (36).

$$\ln\left(\frac{C_0}{C}\right) + K(C_0 - C) = k_r K t \tag{36}$$

The fitted parameters, i.e. the reaction rate constants (k_r), and the adsorption constants (K) are shown in Table 4.5. This assumes that the photodegradation reaction of linuron by using titania as the catalyst follows the Langmuir-Hinshelwood model.

Table 4.5 The apparent rate constant (k_{app}), reaction rate constants (k_r), and the adsorption constant (K) for the photocatalytic degradation of linuron using synthesized and commercial titania as catalyst.

catalyst	Pseudo first-order model		Langmuir-Hinshelwood model		
	k_{app}(min^{-1})	R^2	k_r(ppm/min)	K (ppm^{-1})	R^2
Commercial titania	0.0266	0.8818	0.6086	0.0534	0.9676
Synthesized titania	0.0024	0.9261	0.2333	0.0126	0.9553

From values of parameters in the Langmuir-Hinshelwood model, the rate-limiting step can not be defined because there is not enough data to confirm. However, it was found that the commercial TiO_2 has higher value of both the adsorption constant and the reaction rate constant than the synthesized TiO_2. Therefore, linuron can adsorb onto the surface of the commercial titania better than the synthesized titania. Similarly, the reaction occurs on commercial titania surface better than synthesized titania surface. It should be noted that the value of Langmuir-Hinshelwood constant is consistent with the results from the adsorption study.

Figure 4.22 show the changes of TOC (Total organic carbon) as a function of time during the photocatalytic degradation of linuron by using commercial and synthesized titania as the catalyst. It is found that TOC/TOC_0 of the commercial titania decreases clearly with prolonged irradiation time. For the synthesized titania, the TOC decreases gradually. The TOC/TOC_0 in the photocatalytic degradation for the commercial and synthesized titania is decreased by 68.8 and 8.5 %, respectively, within 6 h of irradiation time. The TOC does not reach zero at the end of the degradation of linuron, although the concentration of linuron has reached zero, which confirms that the photodegradation process decomposes linuron and generates reaction intermediates.

Figure 4.22 Total organic carbon (TOC) with respect to the initial TOC of linuron solution (TOC/TOC$_0$) during the photocatalytic degradation on: ($\square$) commercial titania, ($\lozenge$) synthesized titania.

4.3.2 Photodegradation of Linuron on Zinc Oxide

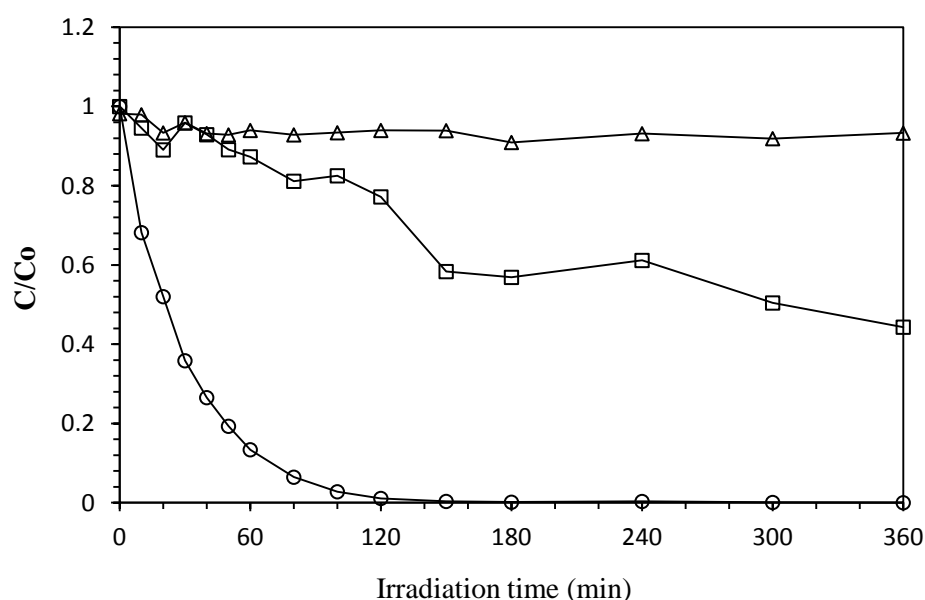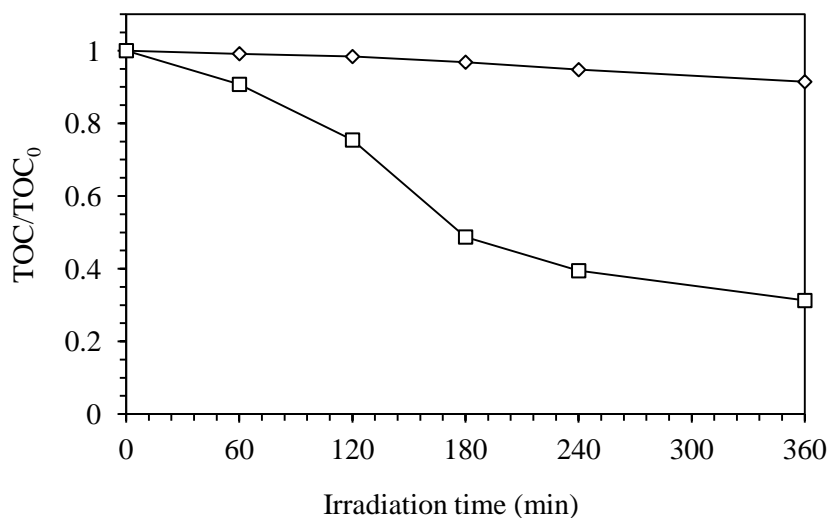Figure 4.23 shows the disappearance of linuron by photocatalytic degradation, i.e., concentration of linuron with respect to the initial linuron concentration (C/C$_0$) during the photocatalytic degradation, using the synthesized and commercial zinc oxide as the catalyst. The commercial zinc oxide shows higher performance in degrading linuron than the synthesized zinc oxide. The degradation of linuron on the commercial zinc oxide was about 99% within 6 hours of UV-A irradiation, while that achieved on synthesized zinc oxide was 93%. From the degradation data, the first-order transformation were plotted as shown in Figure 4.24. The apparent rate constants (k_{app}) were determined from the slopes of curves and presented in Table 4.6. It was observed that the first-order kinetics does not provide a good fit to the experimental data when the commercial zinc oxide was used as the catalyst. Therefore, the data shown in Figure 4.23 were also fitted against the Langmuir-Hinshelwood kinetic model. The fitted parameters, i.e. the reaction rate constants (k_r), and the adsorption constants (K), are shown in Table 4.6. Experiment data show that the photodegradation of linuron on zinc oxide is consistent with the Langmuir-Hinshelwood model.
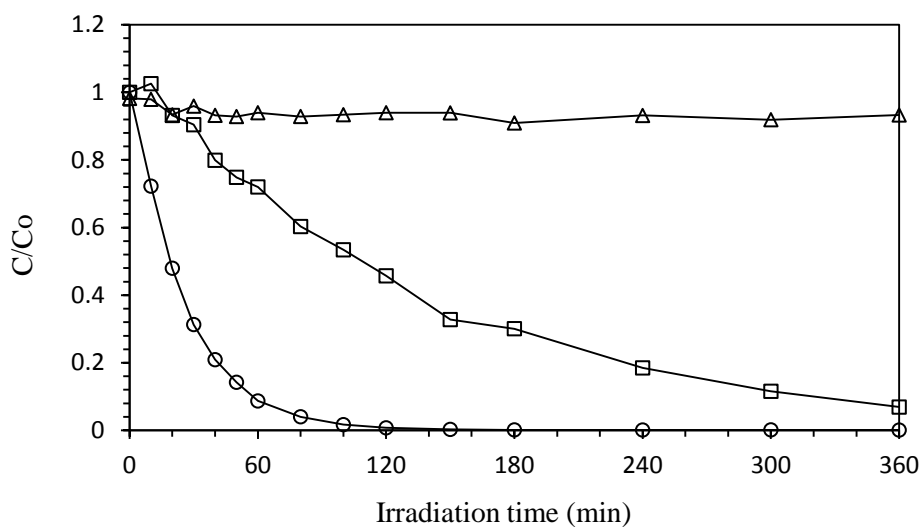
Figure 4.23 Concentration of linuron with respect to the initial linuron concentration (C/C_0) during the photocatalytic degradation on zinc oxide: ($\square$) synthesized zinc oxide, ($\bigcirc$) commercial zinc oxide and ($\triangle$) without catalyst.
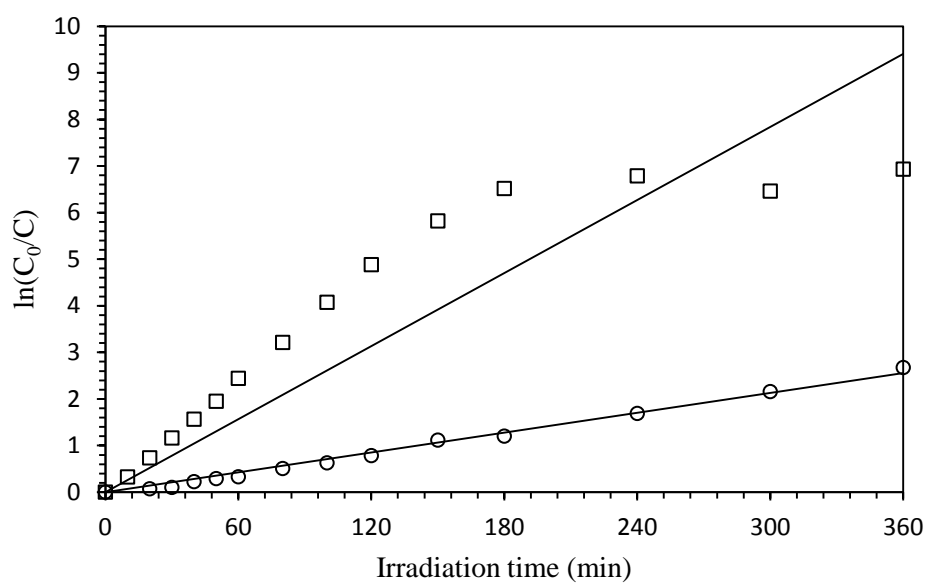

Figure 4.24 First-order linear transforms plot of the photocatalytic degradation on zinc oxide: ($\square$) synthesized zinc oxide and ($\bigcirc$) commercial zinc oxide.

Table 4.6 The apparent rate constant (k_{app}), reaction rate constants (k_r), and the adsorption constant (K) for the photocatalytic degradation of linuron using synthesized and commercial zinc oxide as catalyst.

catalyst	Pseudo first-order model		Langmuir-Hinshelwood model		
	k_{app}(min^{-1})	R^2	k_r (ppm/min)	K (ppm^{-1})	R^2
Commercial zinc oxide	0.0261	0.7439	0.7118	0.0454	0.9394
Synthesized zinc oxide	0.0071	0.9914	0.5955	0.0132	0.9974

Figure 4.25 shows the changes in TOC as a function of time during the photocatalytic degradation of linuron by using commercial and synthesized zinc oxide as the catalyst. It is found that the TOC/TOC$_0$ in the photocatalytic degradation using the commercial and synthesized zinc oxide decrease by 68.7 and 21.4 %, respectively, within 6 h of irradiation time. The TOC value is reduced rapidly within 5 h and slows down afterward. Similar to that observed in the photodegradation of linuron on titania, the TOC value does not reach zero even after all linuron has been degraded. This indicates that photodegradation process decomposes linuron and generates reaction intermediates.
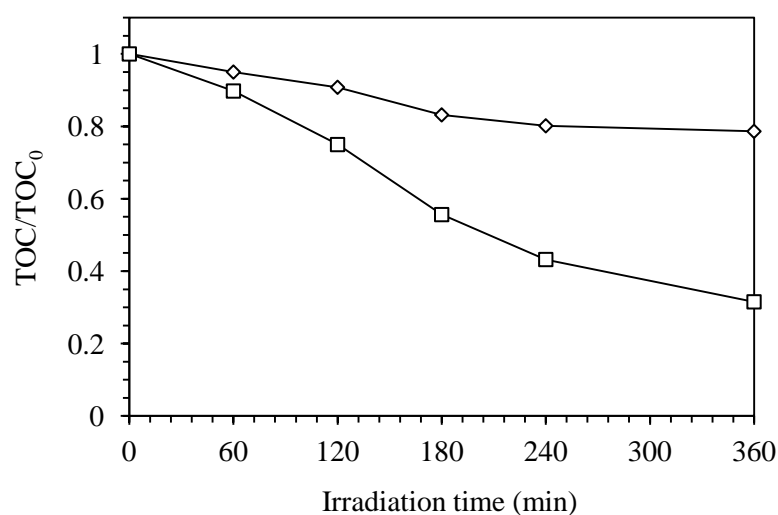

Figure 4.25 Total organic carbon (TOC) with respect to the initial TOC of linuron solution (TOC/TOC$_0$) during the photocatalytic degradation on zinc oxide: (□) commercial zinc oxide, (◊) synthesized zinc oxide.

By comparing the adsorption constant and the reaction rate constant between the commercial and synthesized zinc oxide, it is found that commercial zinc oxide has higher value of the adsorption constant and the reaction rate constant than the synthesized zinc oxide. Therefore, linuron can adsorb on the commercial zinc oxide surface better than the synthesized zinc oxide surface. Similarly, the reaction occurs on the commercial zinc oxide surface is faster than the synthesized zinc oxide surface.

Normally, it is expected that the adsorption constant (K) from the Langmuir-Hinshelwood model should be egual to (K_f) value obtained by the adsorption experiment. However, the adsorption constants from the Langmuir-Hinshelwood model and the Freundlich adsorption isotherm are quite different from each other. In this study, it was found that the Freundlich adsorption constant (K_f) is higher than the value of (K) value from the Langmuir-Hinshelwood model.

Both tiatania and zinc oxide have been known to be capable of producing of radicals upon the exposure with UV light. However, comparison of the catalytic activities of titania and zinc oxide in degrading linuron clearly indicates that the synthesized zinc oxide exhibits higher photocatalytic activity than synthesized titania, regardless of much lower surface area. It can be indicated that the surface area is not the major factor affecting the extent of decomposition. For particle size, when the particle size decreases, the amount of the dispersion particles per volume in the solution will increase, resulting the enhancement of the photon absorbance. The particle size may have higher adsorption affinity towards linuron molecules filled in the pores and can play a role in enhancing the photocatalytic activity. The results of adsorption study show that the amount of linuron adsorbed at equilibrium an zinc oxide is higher than that on titania. Furthermore, according to the Freundlich adsorption constant (K), it was found that ZnO has higher adsorption capacity than TiO_2. This may be the reason for faster degradation rate observed on ZnO. The energy band structure is one reason for greater activity of zinc oxide. The band position of TiO_2 and ZnO are shown in Table 4.7 [40]. The valance band (VB) energy for ZnO is lower than that for TiO_2. Therefore, the VB holes for ZnO (and the hydroxyl radicals) should have great oxidizing power ($2H_2O \longrightarrow O_2 + 4 H^+ + 4 e^-$: E^o=1.23 V)[33]. The conducting band (CB) energy for TiO_2 is close to the potential required to electrolytically reduce water to hydrogen gas ($2H_2O + 2 e- \longrightarrow H_2 + 2OH^-$: E^o= 0 V), but that for ZnO is higher in the energy, which means that ZnO has higher reducing power. Therefore, ZnO can drive the very important reaction involving the

electrolytic reduction of molecular oxygen (O_2) to superoxide (O_2^-). Superoxide is found to be almost as important as the holes and hydroxyl radicals in breaking down organic compounds.

Table 4.7 Band position of TiO_2 and ZnO in aqueous solution.

semiconductor	Valenceband (V)	Conduction band (V)
TiO_2	+3.1	-0.1
ZnO	+3.0	-0.2

4.4 Photodegradation of Dichloroaniline

In the photodegradation of linuron, 3, 4-dichloroaniline is one of the intermediate compounds. So, in this context, the degradation of 3, 4-dichloroaniline is presented. It should lead to better understanding of the degradation of linuron. The degradation of 3, 4-dichloroaniline was carried out under the same degradation condition as the degradation of linuron.

4.4.1 Photodegradation of Dichloroaniline on Titania

Figure 4.26 shows the disappearance of dichloroaniline by the photocatalytic degradation, using the synthesized and commercial titania as the catalyst. The results indicate that the commercial titania has higher activity in degrading dichloroaniline than the synthesized titania. The degradation of dichloroaniline on the commercial titania was about 99% within 6 hours of UV-A irradiation, while that achieved on the synthesized titania was 44%. From the degradation data, the Langmuir-Hinshelwood kinetic model were fitted, The fitted parameters, i.e. the reaction rate constants (k_r), and the adsorption constants (K), are shown in Table 4.8.
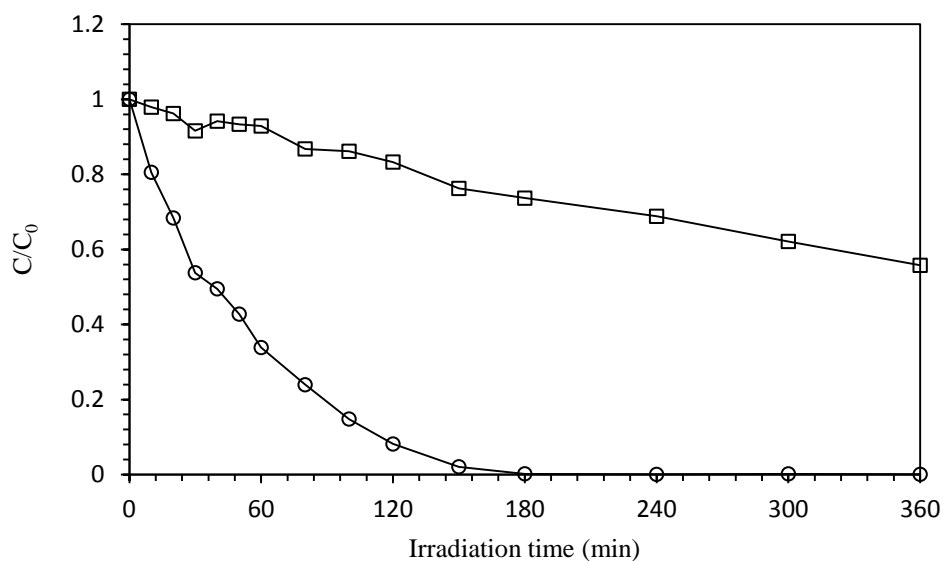
Figure 4.26 Concentration of dichloroaniline with respect to the initial dichloroaniline concentration (C/C_0) during the photocatalytic degradation on tiatania: (□) synthesized titania and (○) commercial titania.

Table 4.8 The reaction rate constants (k_r), and the adsorption constant (K) for the photocatalytic degradation of dichloroaniline using synthesized and commercial titania as catalyst.

catalyst	Langmuir-Hinshelwood model		
	k_r (ppm/min)	K (ppm^{-1})	R^2
Commercial titania	0.2387	0.1208	0.9568
Synthesized titania	0.0453	0.0437	0.9836

From the Langmuir-Hinshelwood model parameters of photodegradation of dichloroaniline, it was found that the commercial TiO_2 has higher value of the adsorption constant and the reaction rate constant than the synthesized TiO_2. Therefore, dichloroaniline can adsorb on the commercial titania surface better than the synthesized titania surface. Similarly, the reaction occurs on the commercial titania surface is faster than the synthesized titania surface.

4.4.2 Photodegradation of Dichloroaniline on Zinc Oxide

Figure 4.27 shows the disappearance of dichloroaniline by photocatalytic degradation, i.e., concentration of dichloroaniline with respect to the initial dichloroaniline concentration (C/C_0) during the photocatalytic degradation using the synthesized and commercial zinc oxide as the catalyst. The results indicate that the commercial zinc oxide has higher performance in degrading dichloroaniline than the synthesized zinc oxide. The degradation of dichloroaniline on commercial zinc oxide was about 99% within 6 hours of UV-A irradiation, while that achieved on synthesized zinc oxide was 80%. From the degradation data, the Langmuir-Hinshelwood kinetic model was fitted. The fitted parameters, i.e. the reaction rate constants (k_r), and the adsorption constants (K), are shown in Table 4.9.
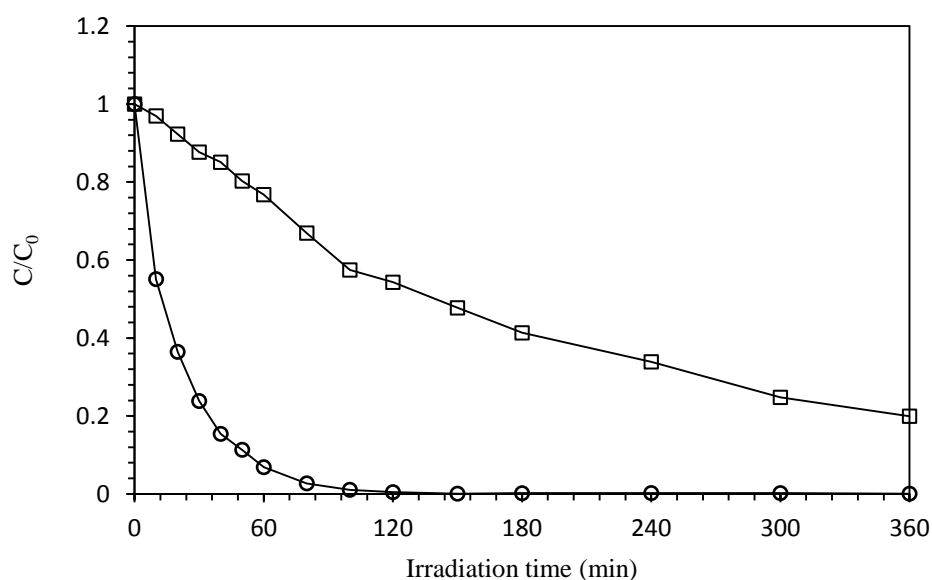

Figure 4.27 Concentration of dichloroaniline with respect to the initial dichloroaniline concentration (C/C_0) during the photocatalytic degradation on zinc oxide: ($\square$) synthesized zinc oxide and ($\bigcirc$) commercial zinc oxide.

Table 4.9 The apparent rate constant (k_{app}), reaction rate constants (k_r), and the adsorption constant (K) for the photocatalytic degradation of dichloroaniline using synthesized zinc oxide and commercial zinc oxide as catalyst.

catalyst	Langmuir-Hinshelwood model		
	k_r (ppm/min)	K (ppm^{-1})	R^2
Commercial zinc oxide	0.3130	0.1132	0.9173
Synthesized zinc oxide	0.0722	0.0980	0.9748

The result of the adsorption constant and the reaction rate constant of zinc oxide is similar to the adsorption constant and the reaction rate constant of titania. The commercial zinc oxide surface can adsorb dichloroaniline better than the synthesized zinc surface. Similarly, the reaction occurs on the commercial zinc oxide surface is faster than the synthesized zinc oxide surface.

By comparing the adsorption constants from the photodegradation of linuron and dichloroaniline, it was found that the adsorption constant of dichloroaniline is higher than the adsorption constant of linuron for all catalysts. It can be indicated that dichloroaniline can adsorb onto all catalysts better than linuron. On the contrary, the reaction rate constant of linuron is greater than the reaction rate constant of dichloroaniline. Therefore, the reaction of linuron occurs on all catalysts is faster than the reaction of dichloroaniline.

4.5 Intermediate Products of the Photodegradation of Linuron

4.5.1 Effect of Type of Photocatalysts

The focus here is the identification of intermediate compounds formed from the photocatalytic degradation of linuon using different photocatalyst. Several intermediates were detected during the photocatalytic degradation process. It has been hypothesized that the intermediates are formed from the reaction between radicals formed from photocatalyst and linuron. Linuron could be attacked by the radicals on two main sites, i.e. the aromatic ring

attached with two chlorine groups and the alkoxy alkyl urea group. Molecular structure of linuron is shown in Figure 4.28.
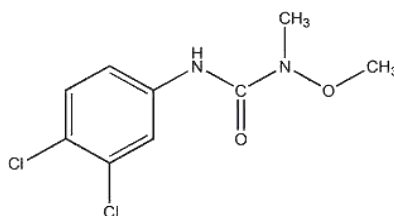

Figure 4.28 Chemical structure of linuron.

When the commercial and the synthesized titania were employed as the catalyst, HPLC analysis shows 13 and 15 kinds of intermediate, respectively. On the other hand 13 intermediates and 14 intermediates were detected when the commercial and the synthesized zinc oxide were used as the catalyst, respectively. Concentrations of the intermediates generated in the process change during the course of the degradation as shown in Figure 4.29 - Figure 4.32. It should be noted that the actual concentrations of the intermediates were not determined because of the lack of the standard samples. Nevertheless, these results indicated the complexity of the degradation of linuron.
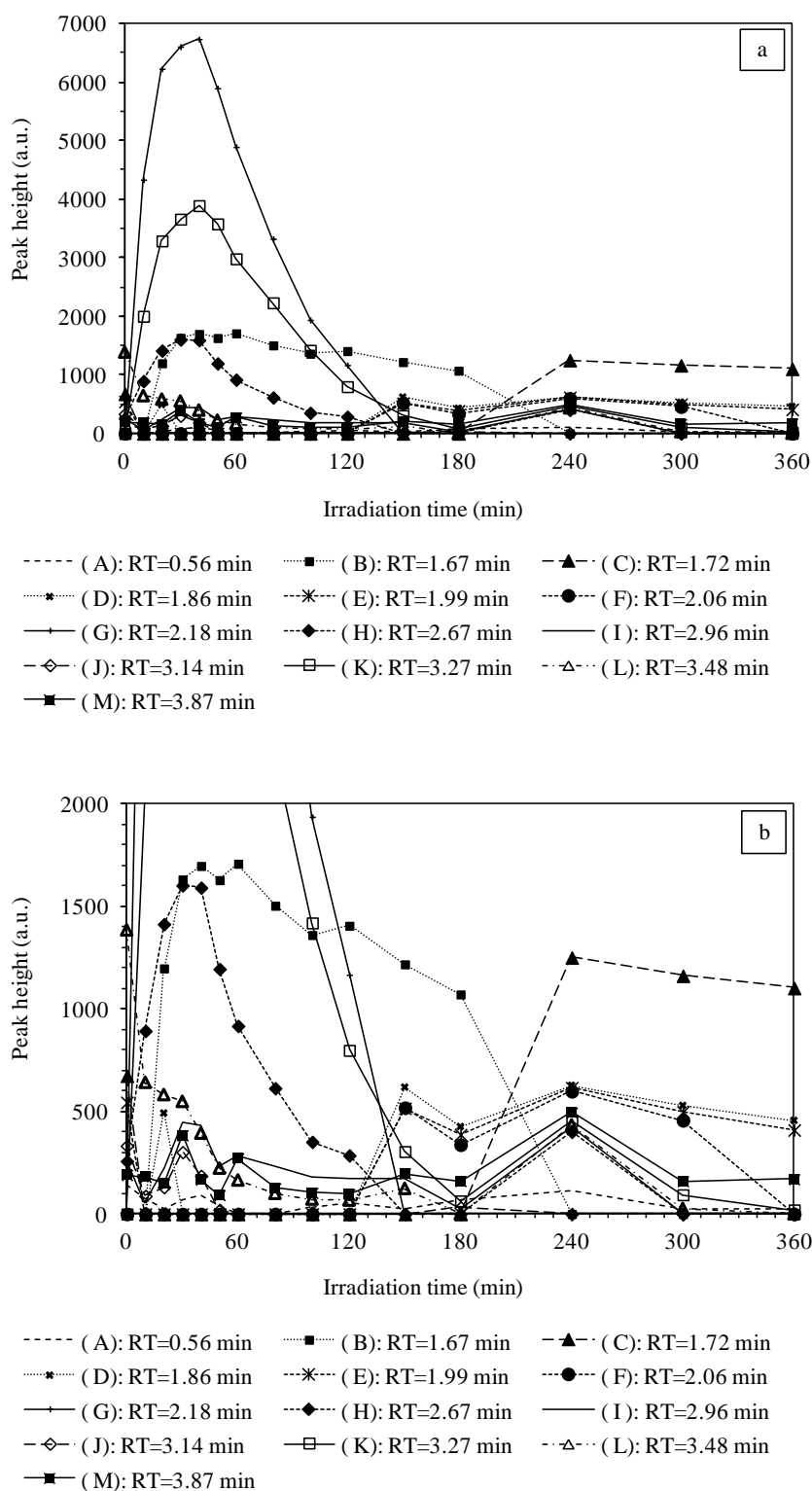
Figure 4.29 (a) HPLC peak height of intermediates generated during photocatalytic
degradation of linuron on commercial titania and (b) enlargement of (a).
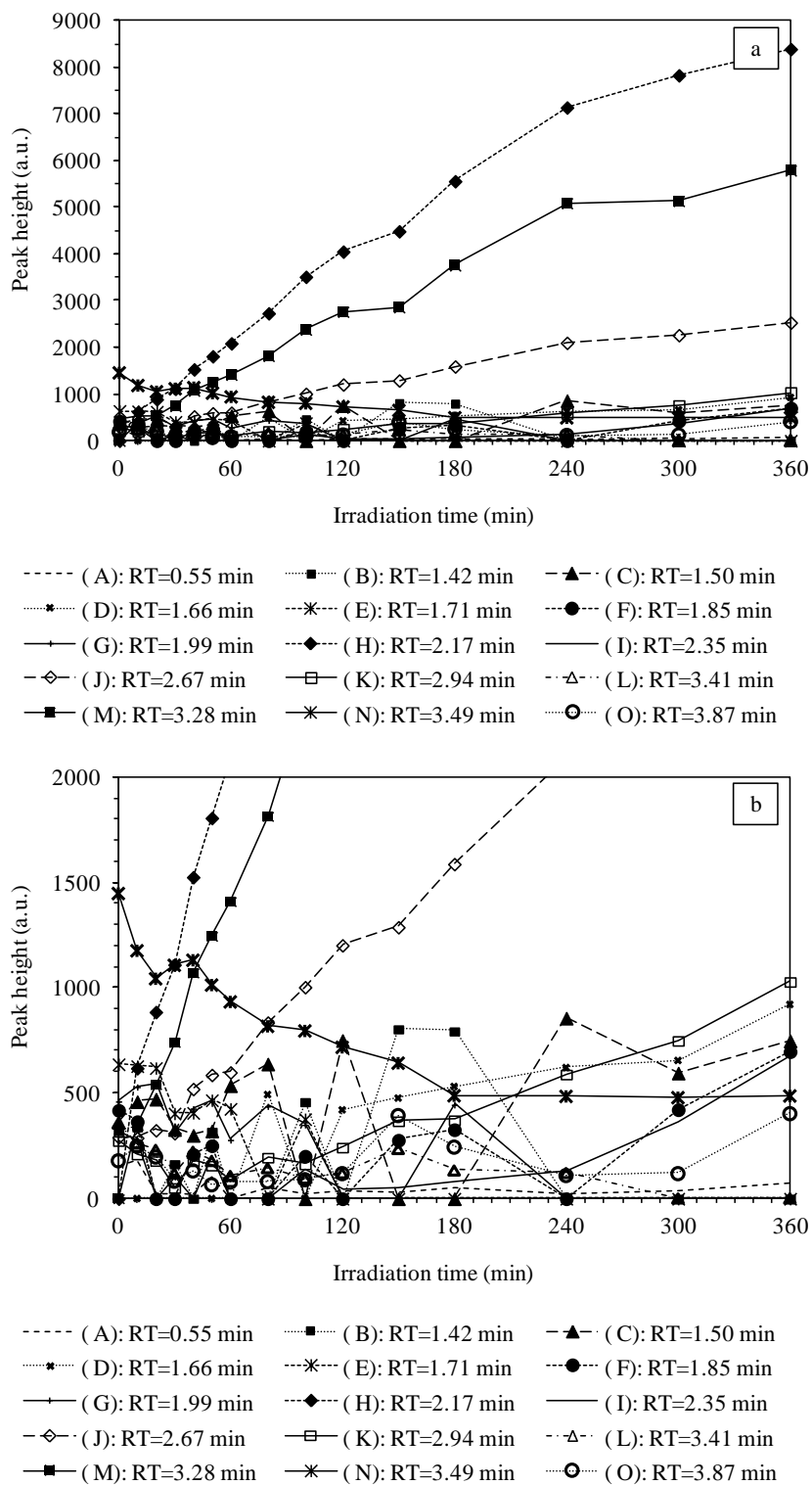
Figure 4.30 (a) HPLC peak height of intermediates generated during photocatalytic degradation of linuron on synthesized titania and (b) enlargement of (a)**.**
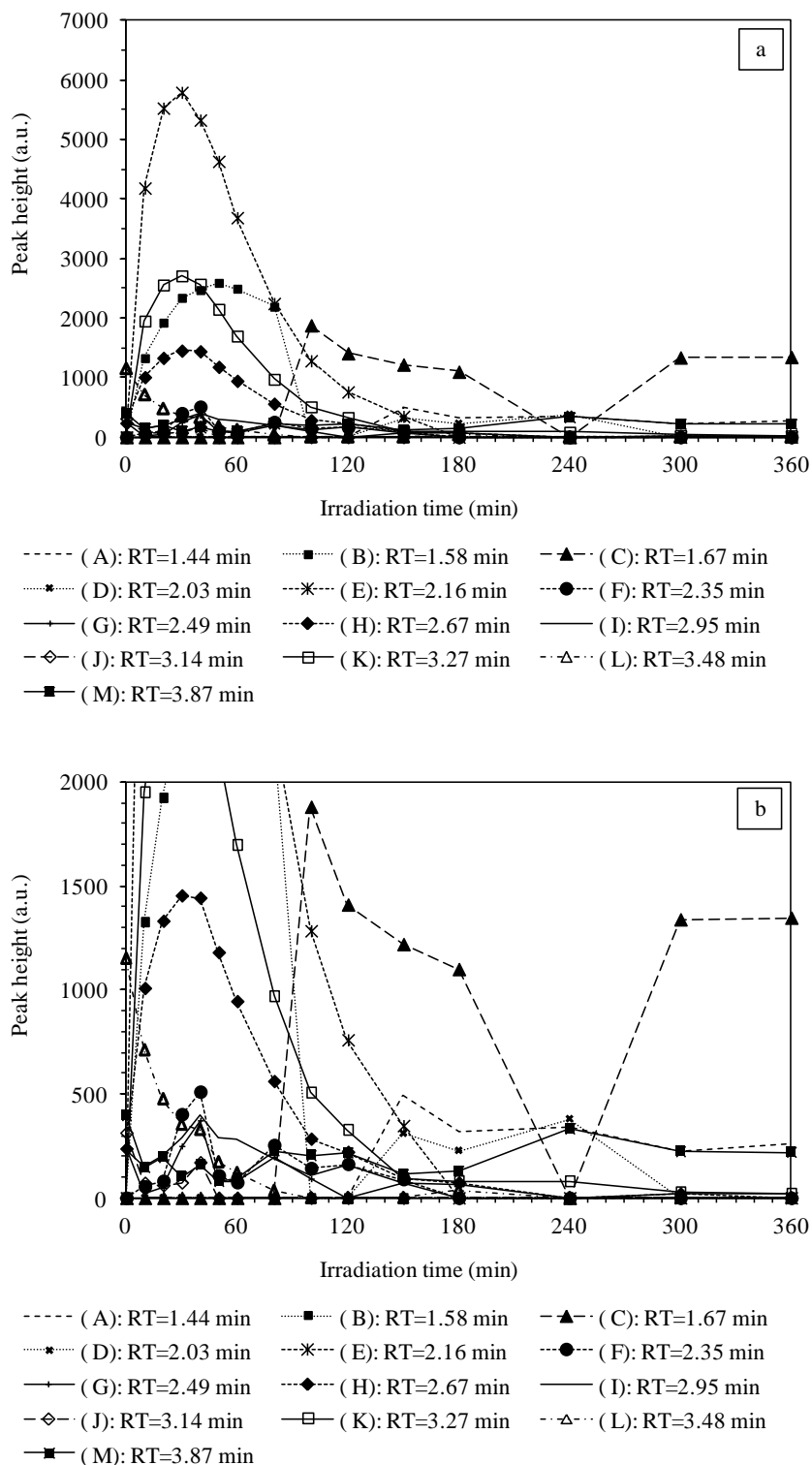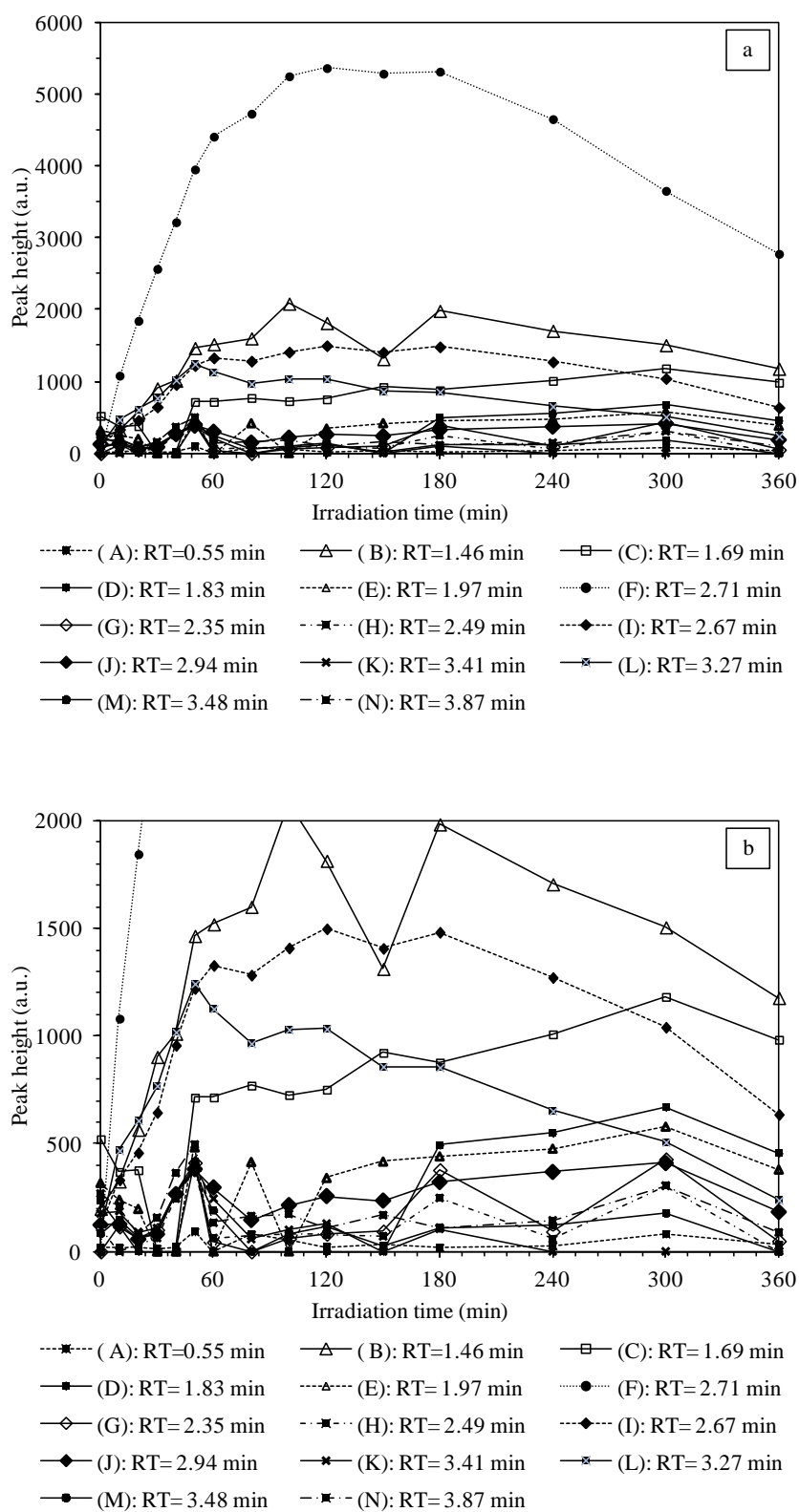
Figure 4.31 (a) HPLC peak height of intermediates generated during photocatalytic

degradation of linuron on commercial zinc oxide and (b) enlargement of (a)**.**

Figure 4.32 (a) HPLC peak height of intermediates generated during photocatalytic degradation of linuron on synthesized zinc oxide and (b) enlargement of (a)**.**

In Figure 4.29 and Figure 4.31, all intermediates are formed at the highest concentration within the first 30 min of reaction. Then subsequent degradation of the intermediates occurs. Some intermediates could not be detected after 150 min of irradiation time. However, some intermediates remain stable at low concentration even after 6 h of the reaction. For peak height of intermediates generated during photocatalytic degradation of linuron on the synthesized zinc oxide as shown in Figure 4.32, all intermediates are formed in the highest concentration within 150 min of reaction. Then concentrations of the intermediates decrease with the increase in irradiation time. On the other hand, the results of intermediates in Figure 4.30 reveal that the longer irradiation time would lead to the increase in concentration of the intermediates. So it shows that the degradation of linuron on the synthesized catalyst requires much longer time than 6 h to achieve complete mineralization.

The intermediates generated during the degradation process were further analyzed by LC/MS. The results from LC-MS comfirm that the degradation of linuron generates a lot of intermediate products complying to the results from HPLC analysis. The structures of intermediates were identified on the molecular ion and mass spectrometric fragmentation. Linuron peak was observed as a reported in literature at 247 m/z and 249 m/z in negative and positive detection mode respectively. The molecular ion and mass spectrometric fragmentation were identified structure of intermediate as shown in Table 4.10. The results confirm that, during the photocatalytic degradation, linuron was degraded into smaller compounds. While some intermediates were further degraded by the photocatalytic process, the formation and conjugation of intermediates into larger molecules was also observed. It also found that not all intermediates formed by the reaction on ZnO were found when the catalyst was changed to TiO_2. This might be the result of different interaction between linuron and surface of the catalyst.

Comparison of the intermediates formed, when different photocatalyst was used, revealed intermediates that were observed from both catalysts as well as intermediates that were specific to one particular catalyst. The difference in intermediate products may result from the difference in properties of the catalyst and the different mechanism of the reaction. It does not depend on degradation rate, which can be seen from the same irradiation time, which does not make the same intermediate. Although the detailed mechanism of linuron degraded on zinc oxide and on titania are different, the main photocatalytic degradation pathways remain the same. Nevertheless, the result suggested that the intermediate compounds are formed by dechlorination of the aromatic ring (resulting in compound 4, 10 and 14),

hydroxylation of the aromatic ring and the alkoxy alkyl urea group (resulting in compound 6, 7, 11, 16, 17, 19, 21 and 22), demethylation reaction (resulting in compound 3, 18, 8, 8, 14 and 15) and conjugation of intermediates (resulting in compound 24 and 25)

The formation of intermediate products and the possible degradation mechanism for linuron are described below in more detail. The OH radical attack may occur at different sites of linuron, namely the aromatic ring and the alkoxy alkyl urea group. The several routes of the photocatalytic degradation of linuron was suggested. The attack on the aromatic ring by OH radical without dechlorination [3, 41] is shown in Figure 4.33.
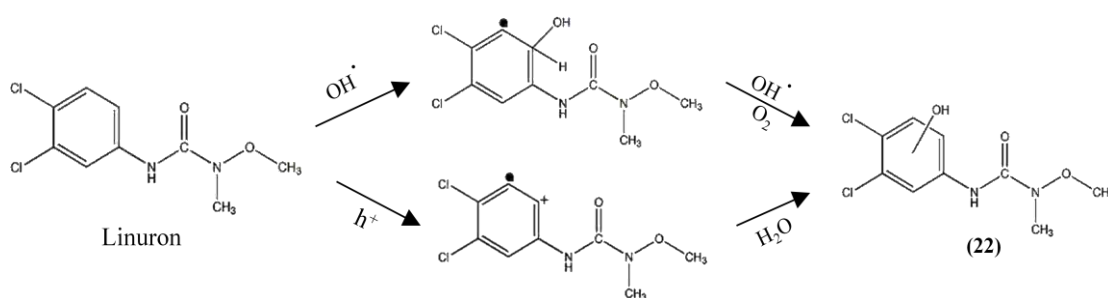
Figure 4.33 Hydroxylation of aromatic ring without dechlorination during photocatalytic degradation of linuron.

The degradation of linuron also includes a reductive mechanism, which results in the dechlorination as show in figure 4.34. Canle Lo′pez et al. [41] observed that this finding implies a competition between O_2 and linuron for the e^- that is transferred to the conduction band of semiconductor photocatalyst.
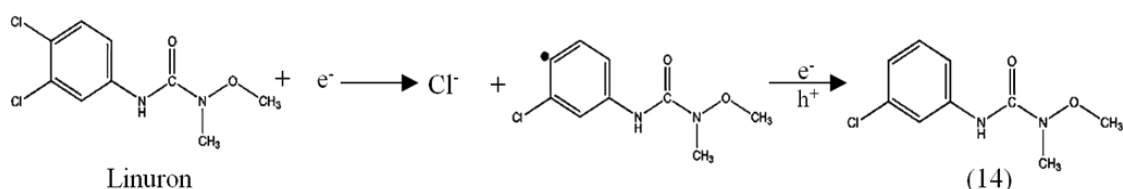
Figure 4.34 Dechlorination on aromatic ring during photocatalytic degradation of linuron.

Moreover, Figure 4.35 shows the substitution of Cl atom by the OH radical on aromatic ring. This mechanism of similar intermediates formation was reported by several authors in the other degradation [41-43]
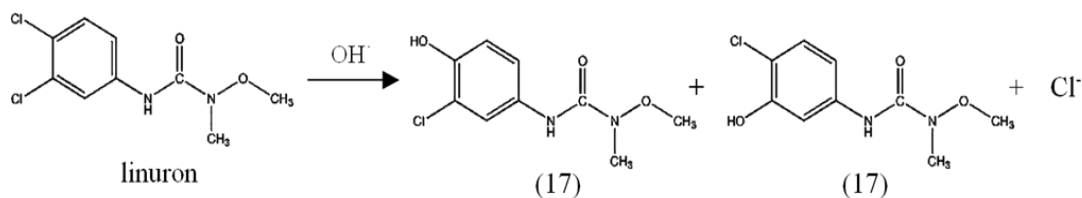
Figure 4.35 Dechlorination and hydroxylation on aromatic ring during photocatalytic degradation of linuron.

.

The main one being the oxidation of the methyl group on the alkoxy alkyl urea sites. The oxidation of the methyl group leading to alcohol. And then leading to aldehyde and acid, which then decarboxylation as shown in Figure 4.36.
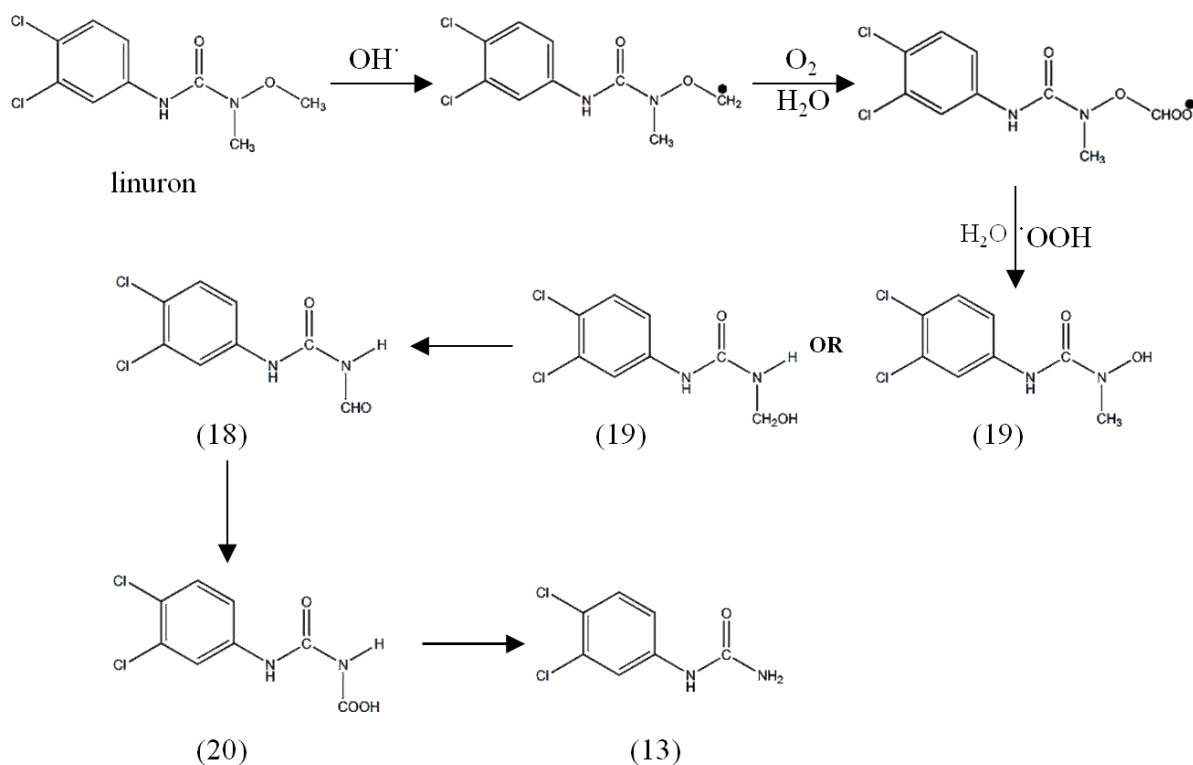
Figure 4.36 Decarboxylation on alkoxy alkyl urea sites during photocatalytic degradation of linuron.

Table 4.10 Possible intermediates generated from photodegradation of linuron on commercial titania, synthesized titania, commercial zinc oxide and synthesized titania.
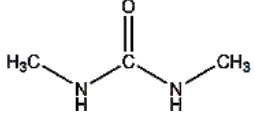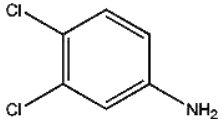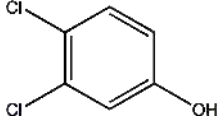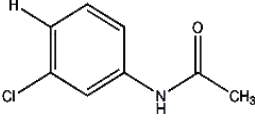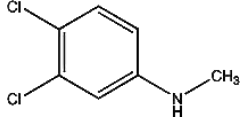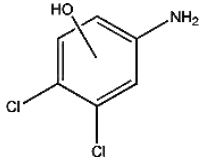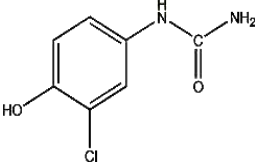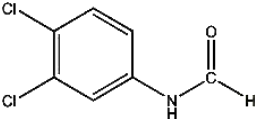
Compound	Proposed structure	commercial TiO$_2$	synthesized TiO$_2$	commercial ZnO	synthesized ZnO
1	(structure)				◆
2	(structure)	◆	◆	◆	◆
3 [30, 37, 38, 41-43]	(structure)	◆	◆		
4	(structure)		◆		◆
5	(structure)	◆			◆
6	(structure)	◆		◆	
7 [33]	(structure)			◆	◆
8	(structure)	◆			

Table 4.10 (continued).
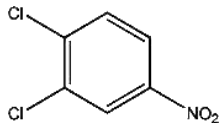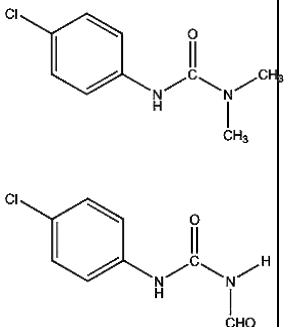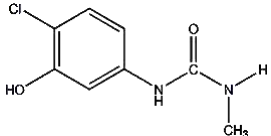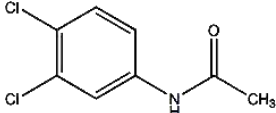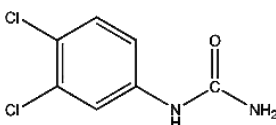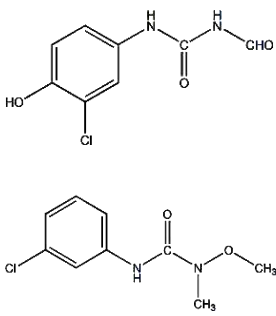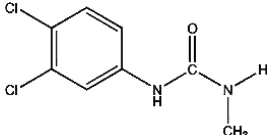
Compound	Proposed structure	commercial TiO$_2$	synthesized TiO$_2$	commercial ZnO	synthesized ZnO
9				◆	
10		◆		◆	
11 [42]			◆	◆	
12		◆	◆	◆	◆
13 [44]		◆	◆	◆	◆
14			◆	◆	◆
15 [37, 38, 42, 44]		◆	◆	◆	◆
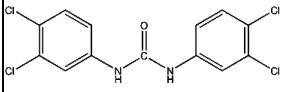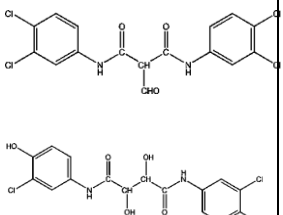
Table 4.10 (continued).

Compound	Proposed structure	commercial TiO$_2$	synthesized TiO$_2$	commercial ZnO	synthesized ZnO
16 [43]		◆			
17		◆	◆	◆	◆
18 [37, 44]		◆	◆	◆	
19 [41, 44]		◆	◆	◆	◆

Table 4.10 (continued).

Compound	Proposed structure	commercial TiO$_2$	synthesized TiO$_2$	commercial ZnO	synthesized ZnO
20 [41, 43, 44]		◆	◆	◆	◆
21 [37, 41]		◆	◆	◆	◆
22 [41, 43]		◆	◆	◆	◆
23 [33]		◆			◆

Table 4.10 (continued)

Compound	Proposed structure	commercial TiO$_2$	synthesized TiO$_2$	commercial ZnO	synthesized ZnO
24		◆	◆	◆	◆
25			◆		

For intermediate from the photocatalytic degradation of dichloroaniline, although the structures of the intermediates were not identified in this work, the result confirms that the degradation of dichloroaniline generates intermediates, as well, as analyzed by the detailed HPLC peaks of intermediates shown in Appendix D. In this study, the investigation of intermediates of dichloroaniline was inconclusive. It can be the result from that fact that the concentrations of intermediates are very low.

4.5.2 Effect of pH of Linuron Solution

The pH can be one of the most important factors affecting the photocatalytic process. The initial pH of the solution is an important factor determining the surface charge of the catalyst and affecting adsorption of the linuron on the surface of catalyst. So, the effects pH of the linuron solution on the photocatalytic degradation under UV irradiation were studied. The pH value of the linuron solution was adjusted by using 0.1 M HCl or NaOH to the value in the range of 5 to 10. For the study of this effect, the amount of photocatalyst added into the linuron solution was fixed at the ratio of 1 mg of photocatalyst to 10 ml of linuron solution. The intermediates during photocatalytic treatment on photocatalyst were detected by HPLC.

4.5.2.1 Photocatalytic degradation on titania

The effect of pH of the linuron solution on the degradation using titania as the catalyst was investigated for 6 hours of UV-A irradiation. Figure 4.37 shows the change of linuron concentration with respect to irradiation time at pH 5, 7 and 10. The degradation data were fitted with the Langmuir-Hinshelwood kinetic model. The fitted parameters, i.e. the reaction rate constants (k_r), and the adsorption constants (K), are shown in Table 4.11.
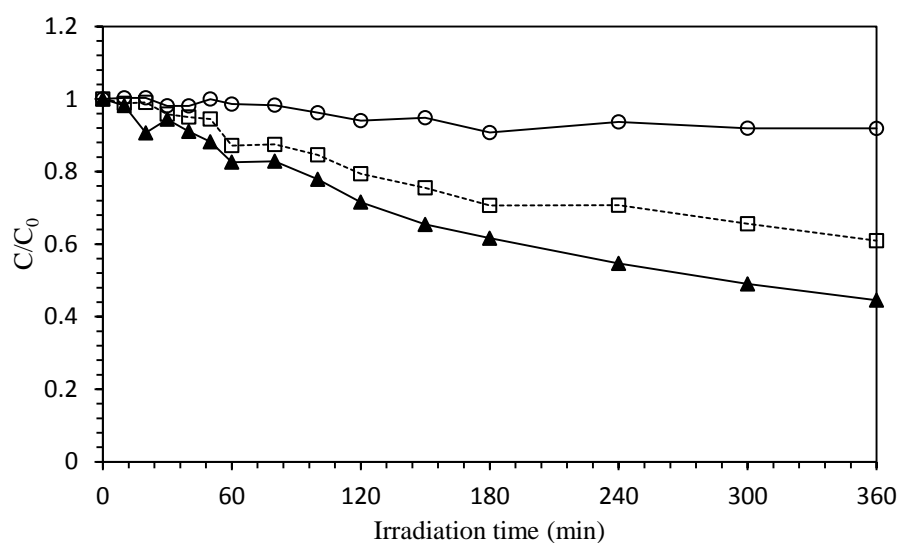

Figure 4.37 Effect of pH of the solution on photodegradation of linuron using synthesized titania as catalyst. (○) pH 5, (▲) pH 7 and (□) pH 10.

Table 4.11 The reaction rate constants (k_r), and the adsorption constant (K) for the photocatalytic degradation of linuron using synthesized titania as catalyst at various pH of linuron solution.

pH of solution	Langmuir-Hinshelwood model		
	k_r (ppm/min)	K (ppm^{-1})	R^2
5	0.6501	0.0053	0.9634
7	0.2405	0.0126	0.9757
10	0.1845	0.0095	0.9893

From the results presented in Table 4.11 and illustrated in Figure 4.37, it is observed that, at pH 7, the rate of degradation is faster compared to low and high pH. At pH 5, 7, and 10, it was found that linuron was degraded by about 8%, 55%, and 39 %, respectively. The pH at which the surface charge is zero is defined as the point of zero charge (pH_{pzc}). The point of zero charge for the synthesized titania was found to be 6.0. So, a low pH lower than the point of zero charge of titania (e.g. pH=5), the surface becomes positively charged. Whereas at the pH higher than the point zero charge, the surface becomes negative charged according to

$$Ti-OH + H^+ \quad \longleftrightarrow \quad TiOH^{2+} \qquad (pH < pHpzc)$$

$$Ti-OH + OH^- \quad \longleftrightarrow \quad TiO^- + H_2O \quad (pH > pHpzc)$$

where $TiOH^{2+}$, TiOH, and TiO^- are the positive, neutral, and negative surface hydroxyl groups, respectively. These characteristics affect the adsorption-desorption properties on the surface of TiO_2 because the charges of the reactant and/or intermediates are affected by pH (relating to their dissociation constants). When the pH of the solution is lower than pKa of the reactant, reactant is mainly present in neutral molecular form. On the contrary, at the pH of solution is higher than pKa the reactant is present in ionic form [45]. The point of zero charge of titania is 6.0 and the pKa of linuron is 2.97 [46]. For basic solution, the surface of TiO_2 is present as negative by charged in TiO^- form and linuron is primarily present in anionic form. Whereas, in acidic solution, the surface of TiO_2 is present as positive charged in $TiOH^{2+}$ form and linuron is primarily present in negative charged. So, the effect of pH on the photocatalytic performance of linuron cannot be solely in terms of electrostatic interaction between the TiO_2 surface and the linuron but also by other adsorption behaviors. The possible reason for this behavior is that basic pH range favours the formation of more OH radicals which will enhance the photocatalytic degradation of linuron significantly.

When TiO_2 was employed as the catalyst and the solution was adjusted to different pH, various kinds of intermediate were detected by HPLC analysis. The HPLC analysis shows 15 kinds of intermediate at all pH. According to Figure 4.38-Figure 4.40, it is found that the intermediate products are presented at very low concentration, but the data show some fluctuation. Generally, the concentration of the intermediates increase with irradiation time. However, some intermediates disappear after 6 hours, while some intermediates remain stable even after 6 hours of the reaction.
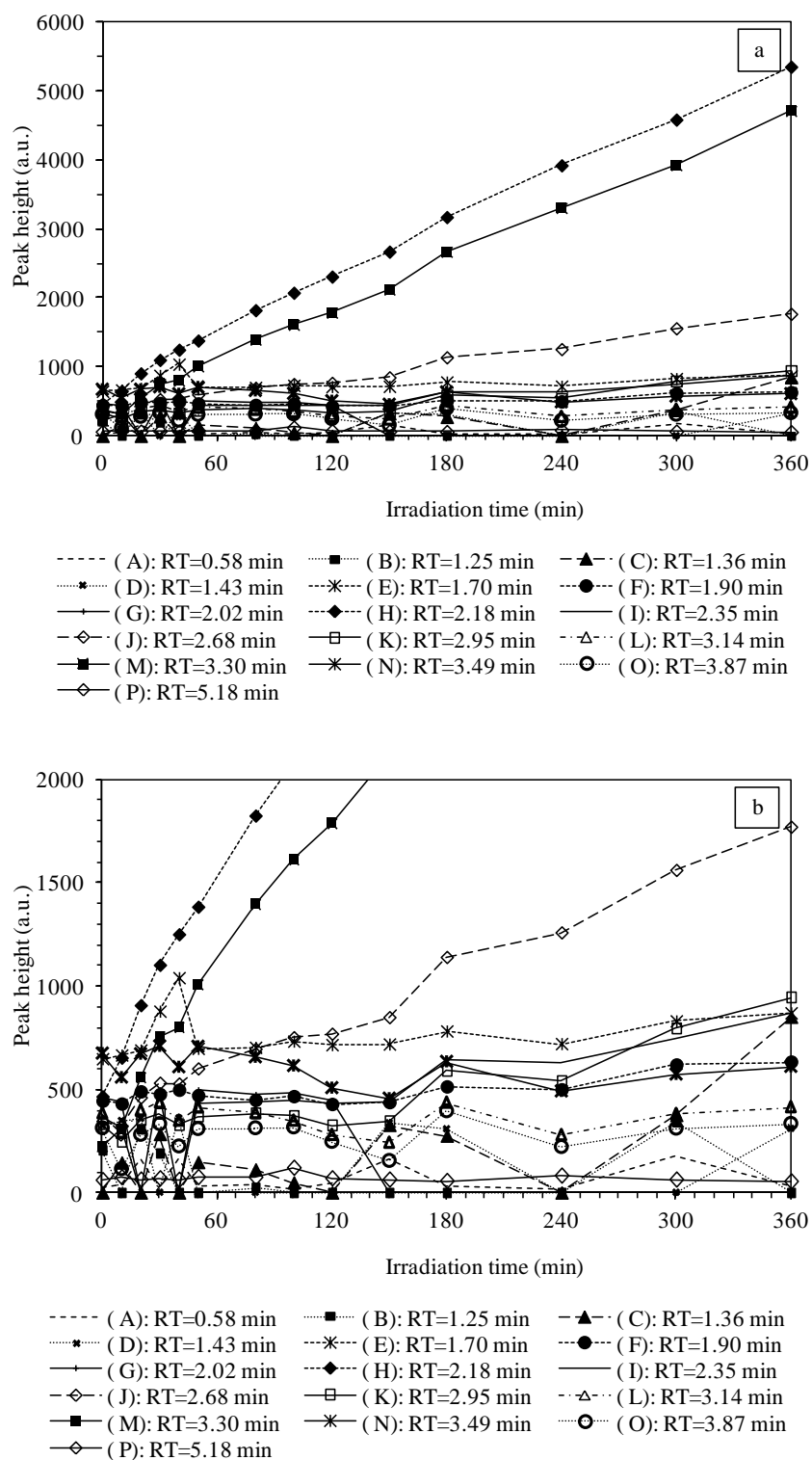
Figure 4.38 (a) HPLC peak height of intermediates generated during photocatalytic

degradation of linuron on titania. The initial pH of the solution was 5 and (b)
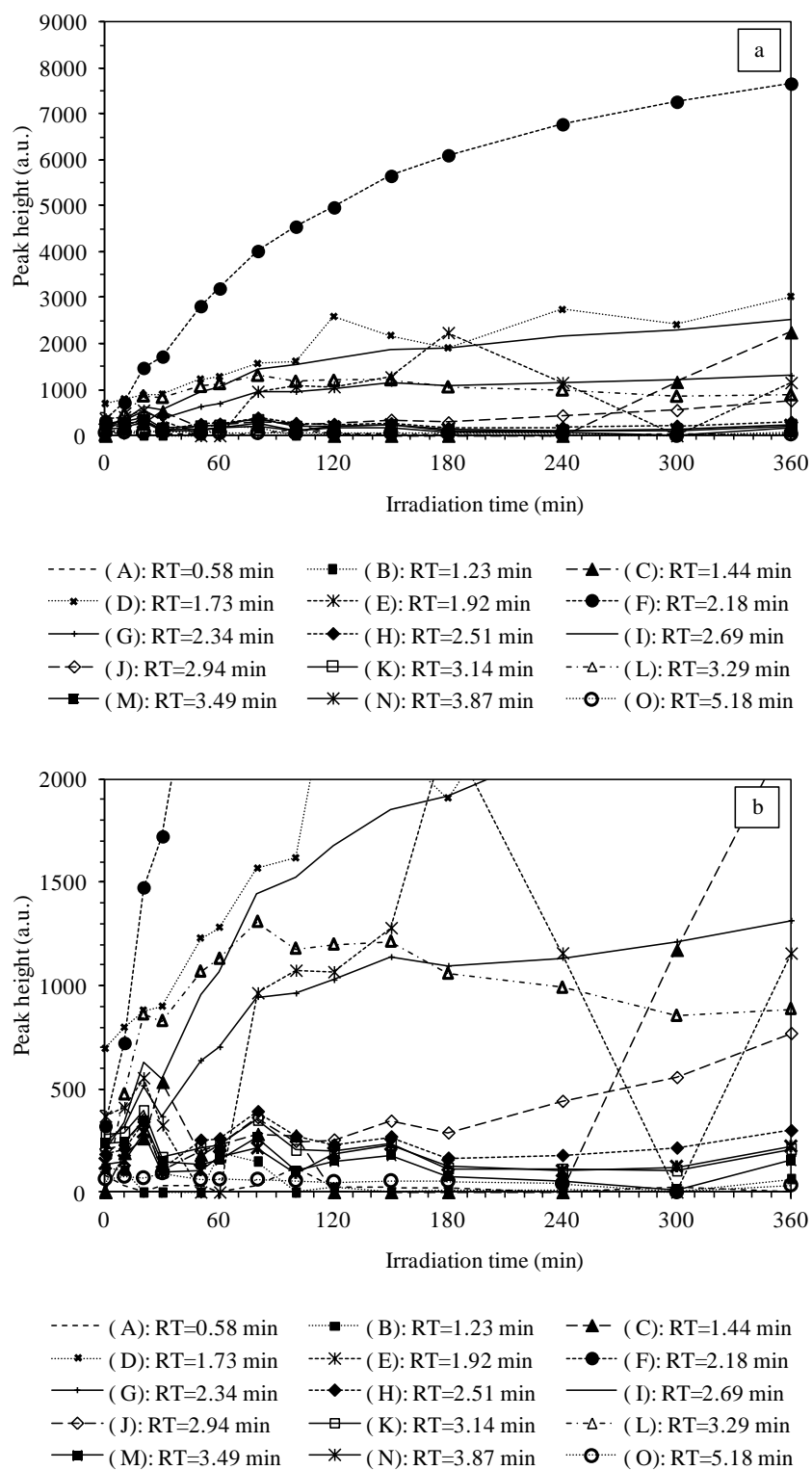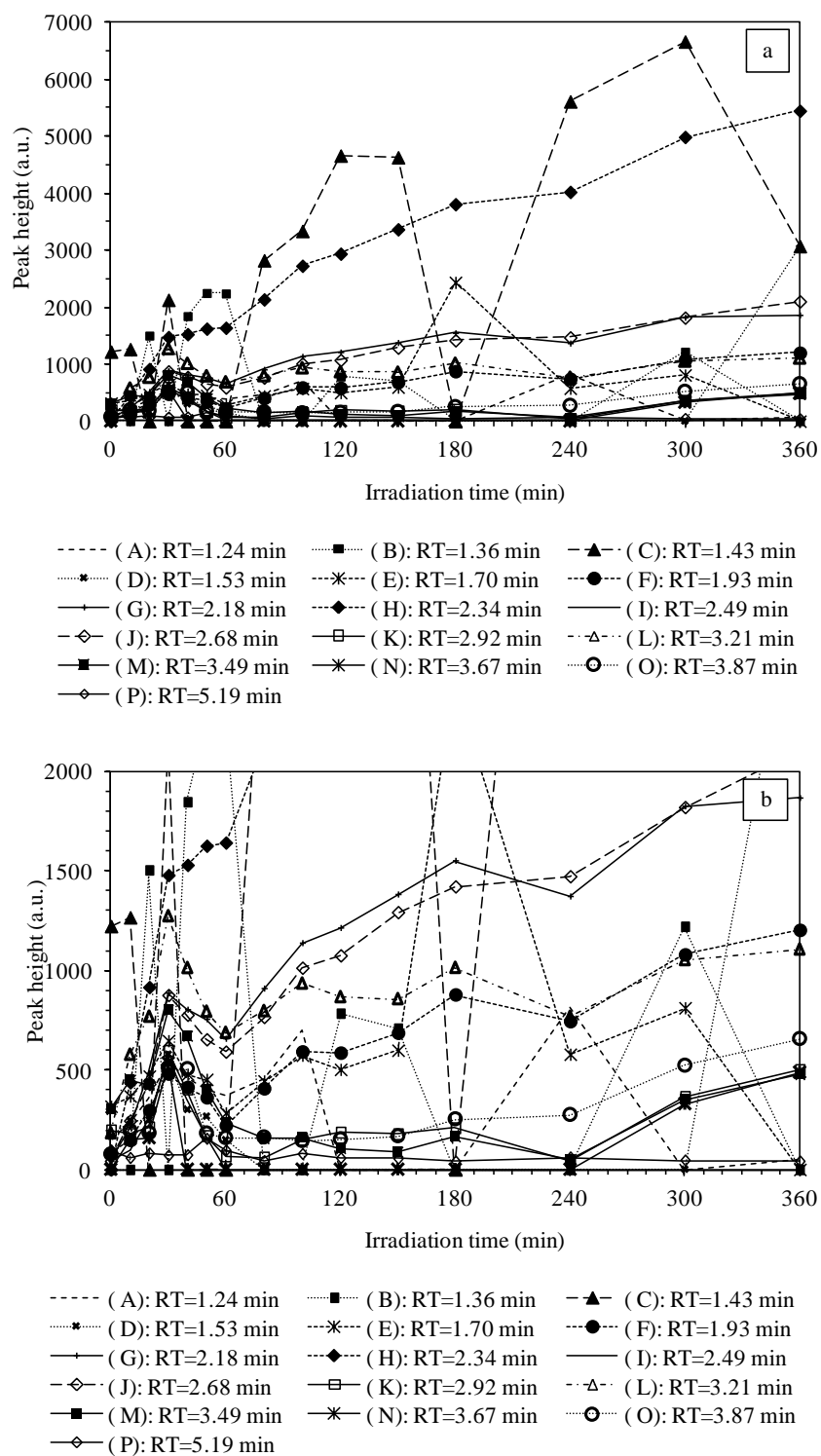
enlargement of (a)**.**

Figure 4.39 (a) HPLC peak height of intermediates generated during photocatalytic
degradation of linuron on titania. The initial pH of the solution was 7 and (b)
enlargement of (a)**.**

Figure 4.40 (a) HPLC peak height of intermediates generated during photocatalytic degradation of linuron on titania. The initial pH of the solution was 10 and (b) enlargement of (a).

Comparison of the intermediates formed from the reaction at various pH of solution, reveals intermediates that were observed from all pH conditions as well as intermediates that were specific to one particular pH. The intermediate were analyzed by LC-MS and the structures of all intermediates detected are proposed in Table 4.12.

Table 4.12 Possible intermediates generated from photodegradation of linuron on synthesized TiO_2 at various pH values.
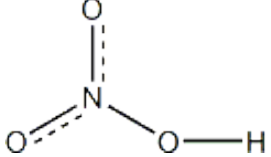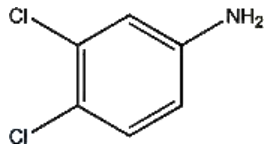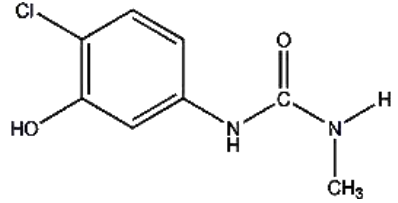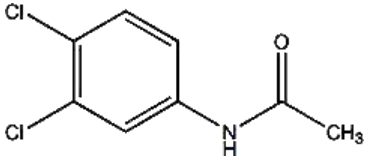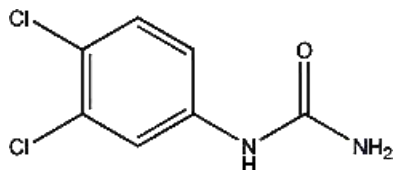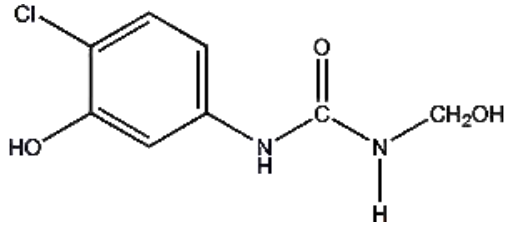
Compound	Proposed structure	pH 5	pH 7	pH 10
1		◆	◆	◆
2 [30, 37, 38, 41, 43]		◆		◆
3 [42]			◆	◆
4		◆	◆	◆
5 [37, 41, 42]		◆		◆
6				◆

Table 4.12 (continued).
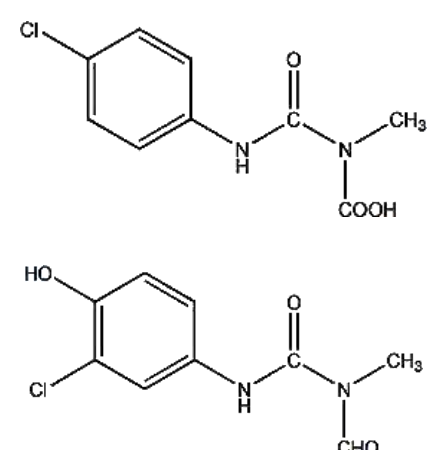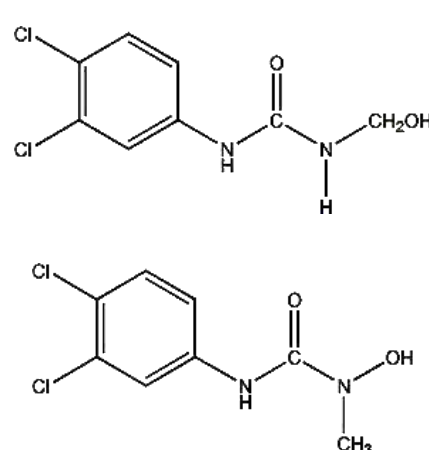
Compound	Proposed structure	pH 5	pH 7	pH 10
7				◆
8 [41, 44]		◆		

Table 4.12 (continued).
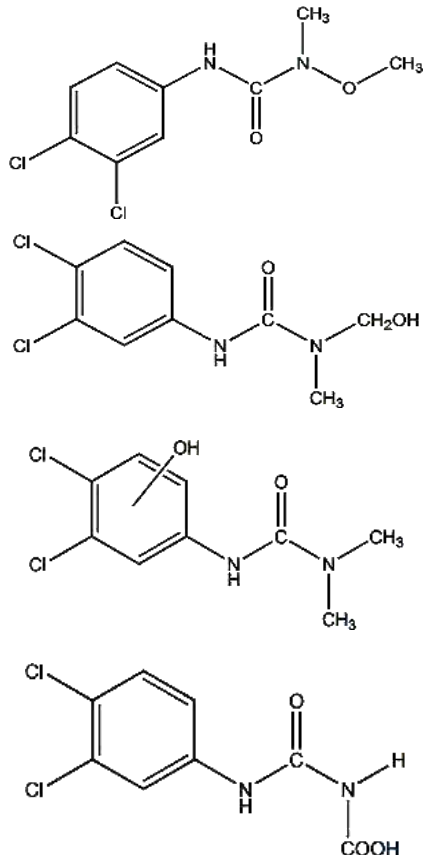
Compound	Proposed structure	pH 5	pH 7	pH 10
9 [37, 41-44]		◆	◆	◆

Table 4.12 (continued).
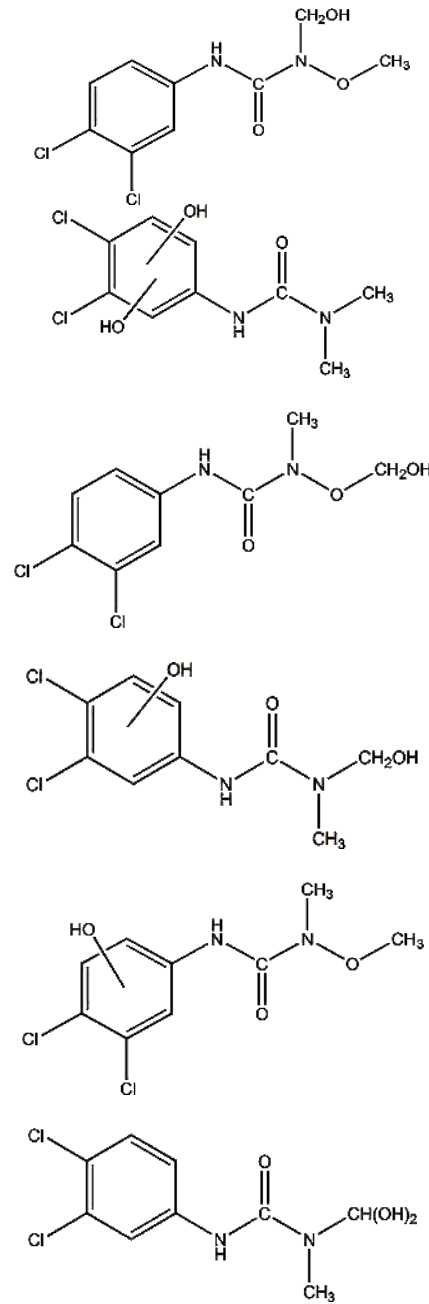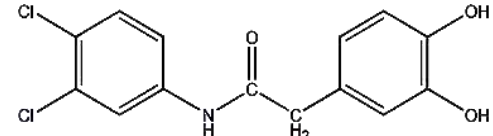
Compound	Proposed structure	pH 5	pH 7	pH 10
10 [41, 43]		◆	◆	◆
11			◆	◆

Table 4.12 (continued).

Compound	Proposed structure	pH 5	pH 7	pH 10
12		◆	◆	◆
13				◆
14		◆	◆	◆
15		◆		
16		◆	◆	◆
17				◆

Results obtained when titanium dioxide was used as photocatalyst show that the distribution of intermediate products depends on the pH of the solution. In neutral solution, the attack of the hydroxyl radicals is located both on the aromatic ring and on the methyl groups. In acidic solution, the main attack is located on methyl groups. Finally, in basic solution, the probability of the attack for hydroxylation increases compared to the acidic solution [47, 48].

4.5.2.2 Photocatalytic degradation on zinc oxide

When zinc oxide was used as the photocatalyst, intermediates were also detected by HPLC during the photocatalytic process. Figure 4.41 shows the changes of linuron concentration with irradiation time at pH 5, 7 and 10. The degradation data were fitted the Langmuir-Hinshelwood kinetic model. The results are shown in Table 4.13.
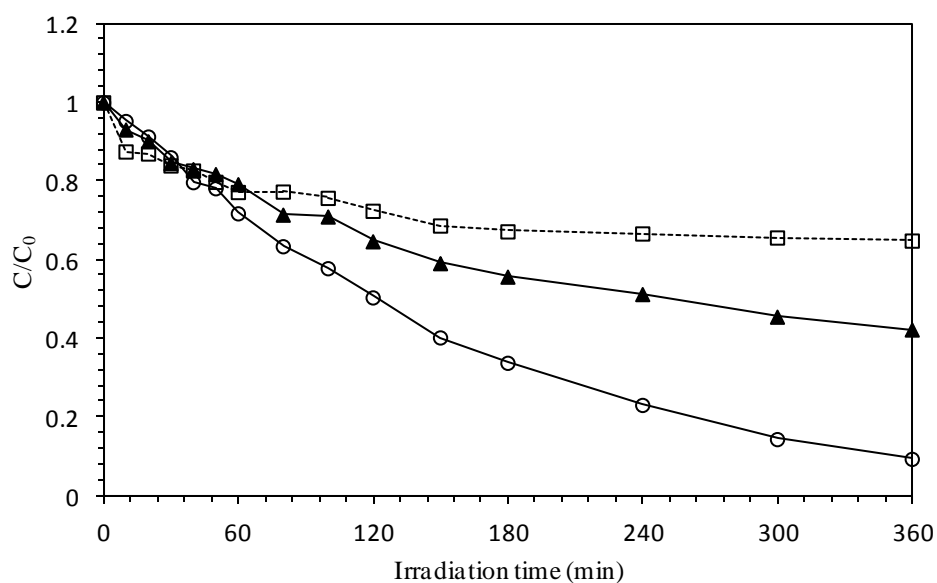

Figure 4.41 Effect of pH of the solution on photodegradation of linuron using synthesized zinc oxide as catalyst: (○) pH 5, (▲) pH 7 and (□) pH 10.

Table 4.13 The reaction rate constants (k_r), and the adsorption constant (K) for the photocatalytic degradation of linuron using synthesized zinc oxide as catalyst at various pH of linuron solution.

pH of solution	Langmuir-Hinshelwood model		
	k_r (ppm/min)	K (ppm^{-1})	R^2
5	0.6213	0.0127	0.9790
7	0.2373	0.0120	0.9893
10	0.1527	0.0115	0.9498

According to the results, the rate of degradation is increased when the pH is increased from 5 to 10. At pH 5, 7, and 10, linuron was degraded by about 90%, 57, and 30 %, respectively. Normally, the effect of pH on organic degradation assisted by the semiconductor oxides has been related to the establishment of acid-base equilibria governing the surface chemistry of metal oxides in water, as shown in the following reactions.

$$ZnOH_2^+ \longleftrightarrow ZnOH + H^+ \quad [pKa_1] \quad\quad\quad (4.9)$$

$$ZnOH + OH^- \longleftrightarrow ZnO^- + H_2O \quad [pKa_2] \quad\quad\quad (4.10)$$

For the pH at the point of zero charge, the surface of an oxide is unchared. The point of zero charge for synthesized zinc oxide was found to be 7.6. So, a low pH lower than the point of zero charge of zinc oxide (e.g. pH=5), the surface becomes positively charged. Whereas at the pH higher than the point zero charge, the surface becomes negative charged. When the pH of the solution is higher than pKa of the reactant, it presents in ionic form [45]. It has been reported that the pKa for linuron is 2.97 [46], whereas catalysts are positive by charged below pH 7.6. Optimal conditions were found at pKa < pH < pH$_{pzc}$ at which the positive by charged zinc oxide and negative by charged linuron should attract each other. The effect of pH on the photocatalytic performance can be explained in terms of electrostatic interaction between the catalyst surface and the target substrate [2]. It is expected that this interaction affects the encounter probability between hydroxyl radical and linuron. The reaction would be enhanced or hindered depending on whether attractive or repulsive forces prevail, respectively [49]. So, when the pH is increased, leading to function of electrostatic

repulsion between the increasing negative charge of ZnO surface and the anionic character of linuron, this may be the reason for lower degradation rate observed at basic pH of the solution linuron.

The characters of adsorption of linuron at various pH on ZnO surface and TiO_2 surface are different. It is observed that linuron can be adsorbed onto ZnO surface by electrostatic interaction. Whereas the adsorption of linuron onto TiO_2 surface is done by other mechanism of adsorption. However, the adsorption occurs not only by electrostatic attraction, but may be by van der Waals force as well.

Figure 4.42-4.44 show the intermediates generated during photocatalytic degradation of linuron on zinc oxide using different pH. The total number of intermediates are detected by HPLC during the reaction at pH 5, 7, and 10 are 15, 14, and 18 kinds of intermediate respectively. Concentrations of these intermediates are expected to be very low, since the intensities of the HPLC signals for the intermediate are much lower than that of linuron. The concentrations of the intermediates also change along the time of the photodegradation. The intermediates generated during the degradation process were further analyzed by LC/MS. The structures of all intermediates were identified on the molecular ion and mass spectrometric fragmentation as shown in Table 4.14.
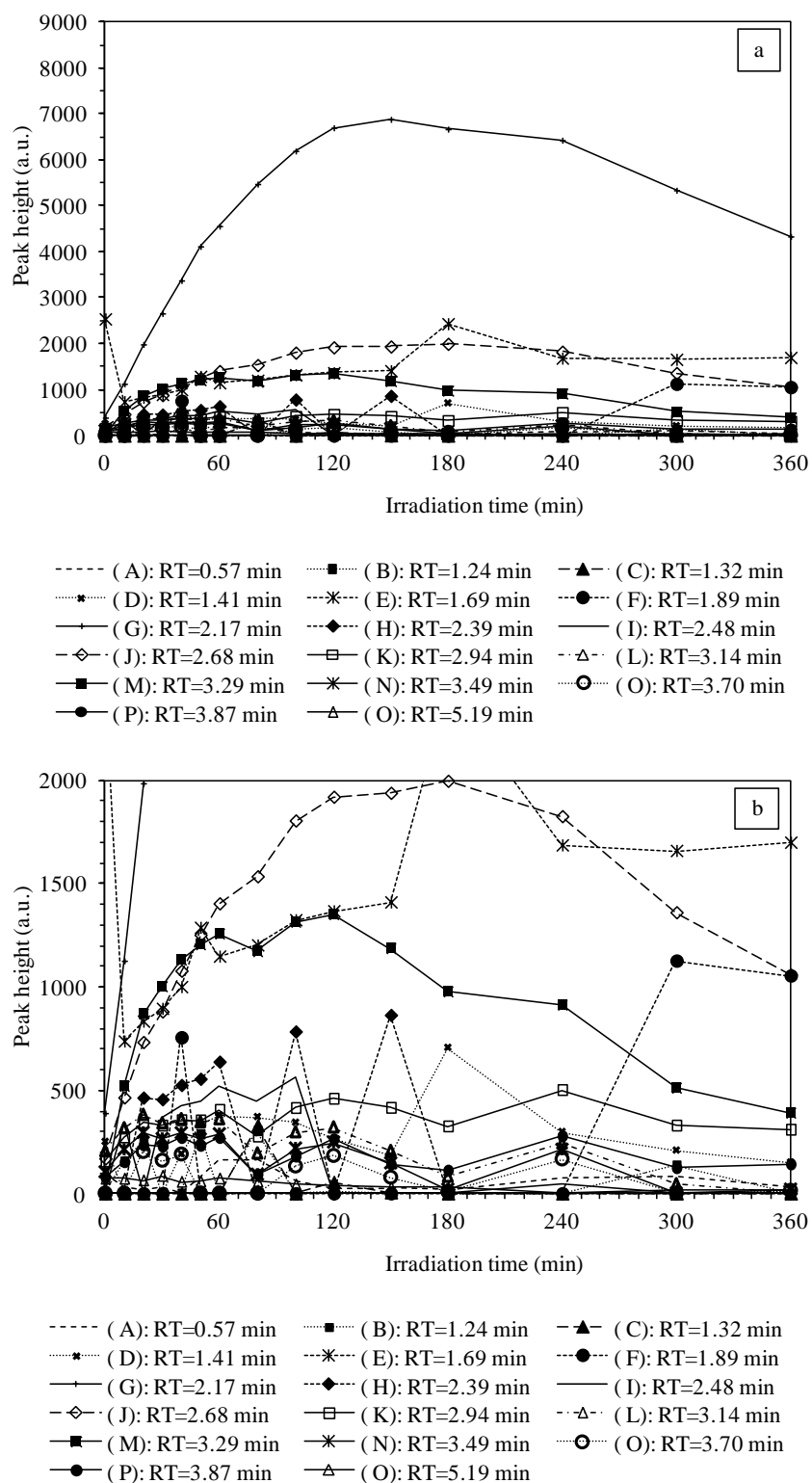
Figure 4.42 (a) HPLC peak height of intermediates generated during photocatalytic

degradation of linuron on zinc oxide. The initial pH of the solution was 5 and (b)
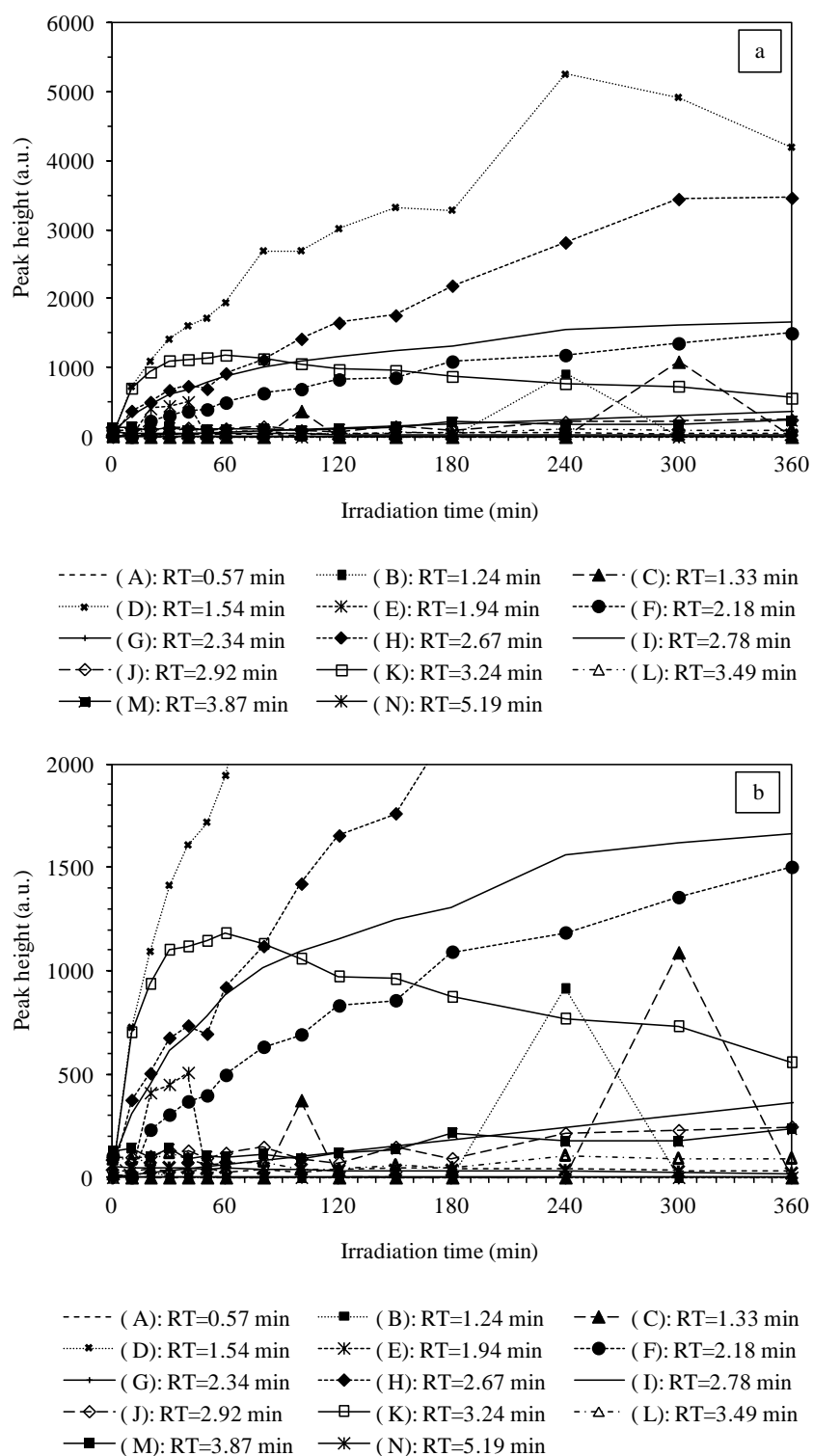
enlargement of (a)**.**

Figure 4.43 (a) HPLC peak height of intermediates generated during photocatalytic

degradation of linuron on zinc oxide. The initial pH of the solution was 7 and (b)
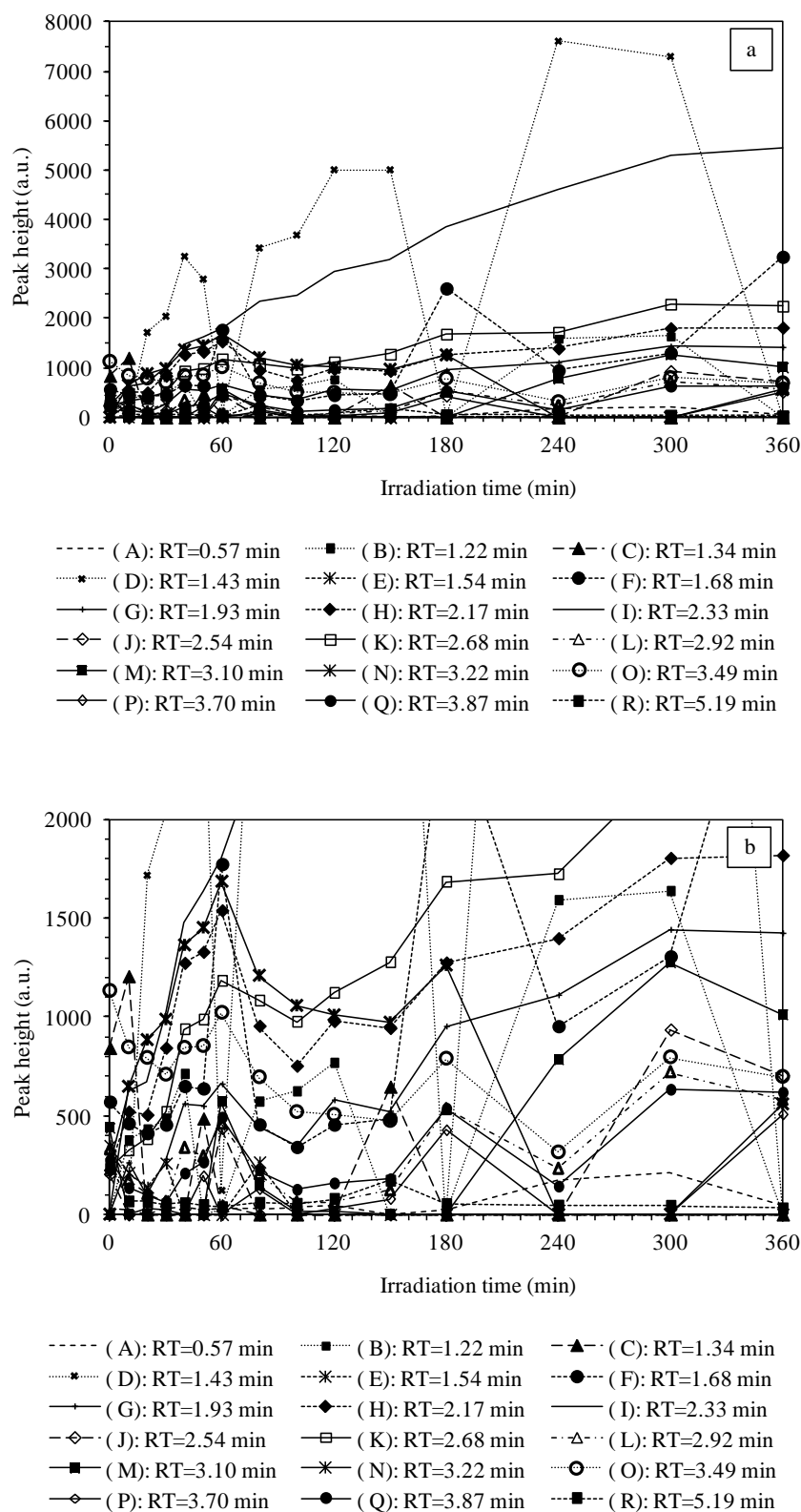
enlargement of (a)**.**

Figure 4.44 (a) HPLC peak height of intermediates generated during photocatalytic degradation on linuron on zinc oxide. The initial pH of the solution was 10 and (b) enlargement of (a).

Table 4.14 Possible intermediates generated from photodegradation of linuron on synthesized ZnO at various pH values.
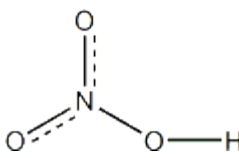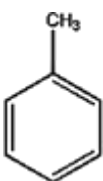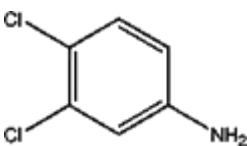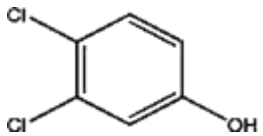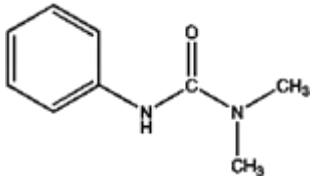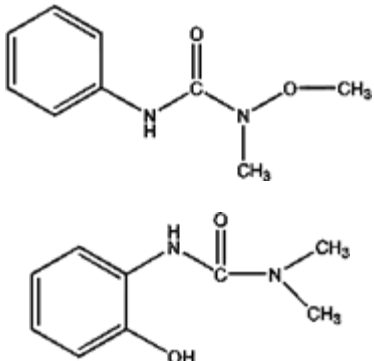
Compound	Proposed structure	pH 5	pH 7	pH 10
1		◆	◆	◆
2		◆		
3 [30, 37, 38, 41, 43]			◆	◆
4				◆
5				◆
6		◆		

Table 4.14 (continued).
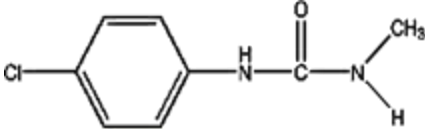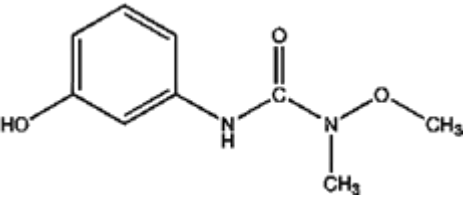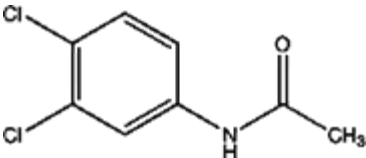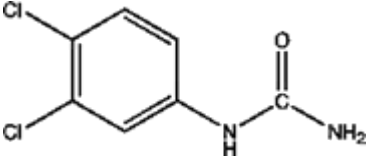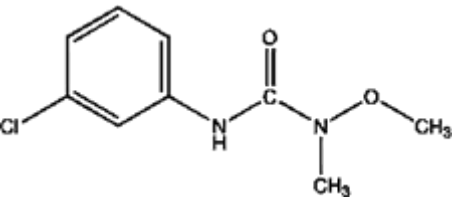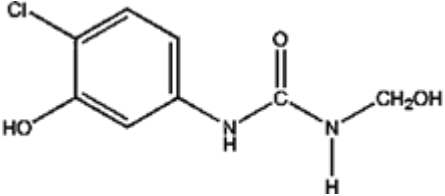
Compound	Proposed structure	pH 5	pH 7	pH 10
7				◆
8		◆		
9			◆	◆
10 [42, 44]				◆
11				◆
12				◆

Table 4.14 (continued).
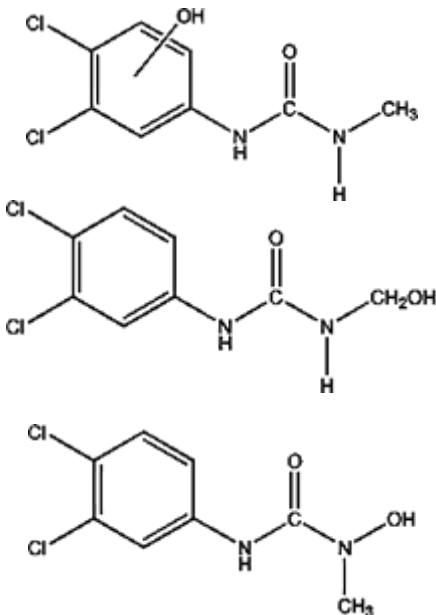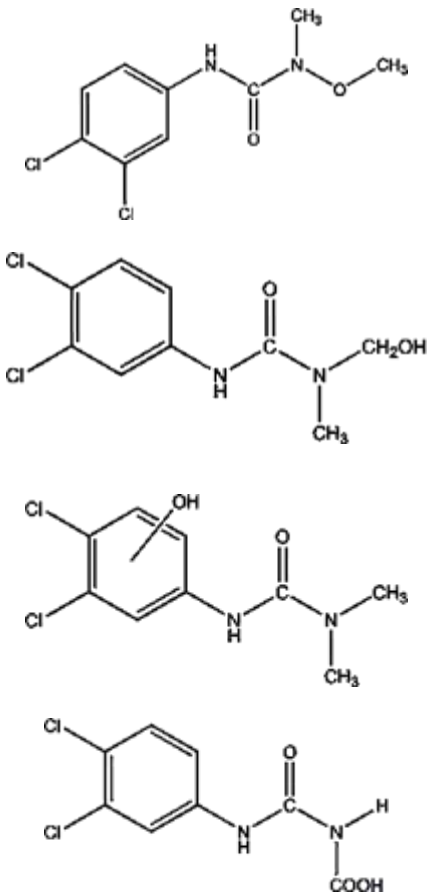
Compound	Proposed structure	pH 5	pH 7	pH 10
13 [37, 41-44]				◆
14 [3, 33, 41, 43, 44]		◆		◆

Table 4.14 (continued).
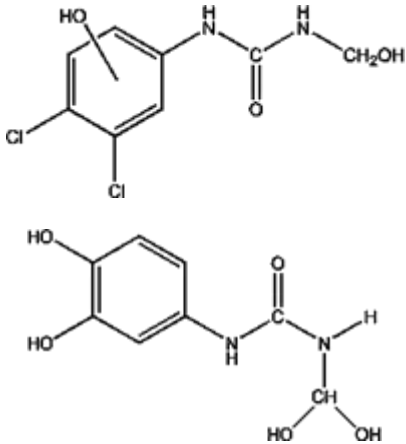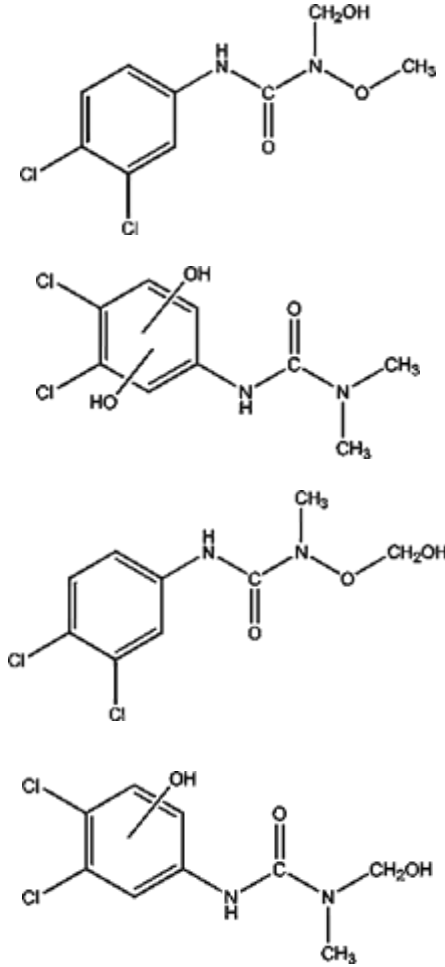
Compound	Proposed structure	pH 5	pH 7	pH 10
15 [33, 37, 41, 42]		◆	◆	
16 [3, 33, 41, 43]			◆	◆

Table 4.14 (continued).
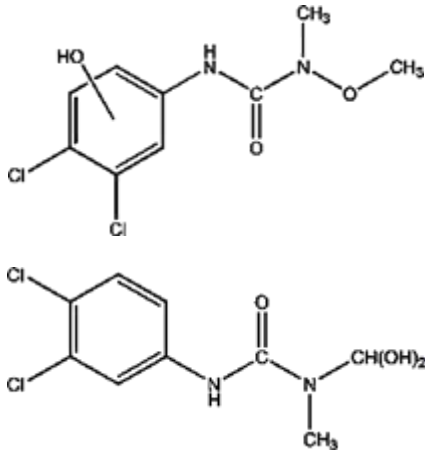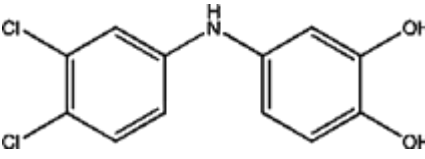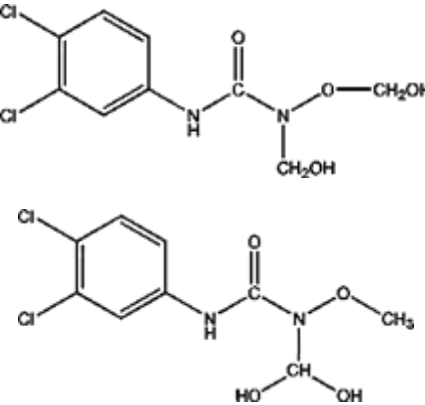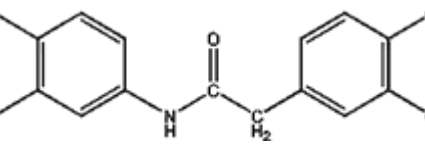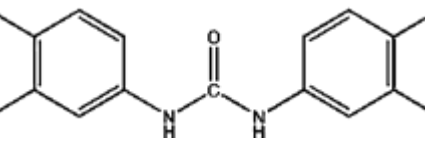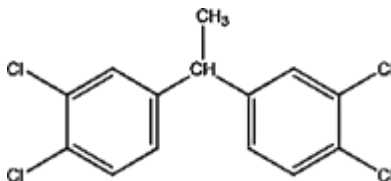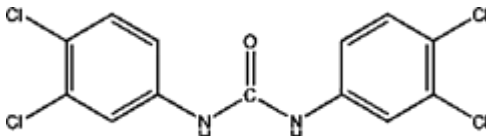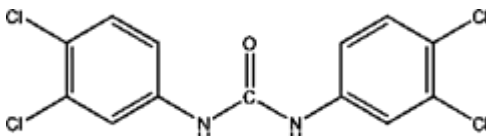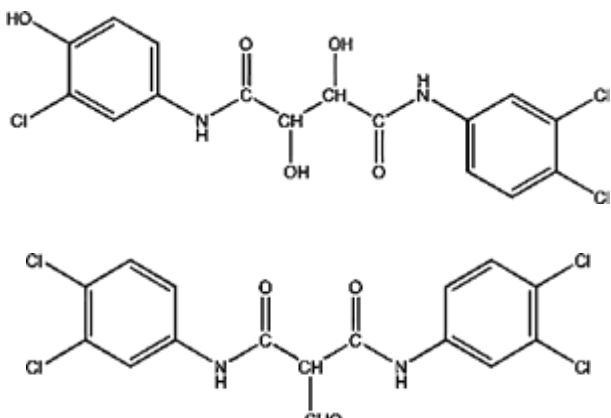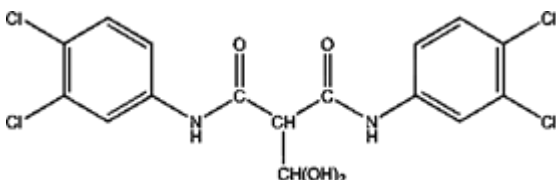
Compound	Proposed structure	pH 5	pH 7	pH 10
16 [3, 33, 41, 43]			◆	◆
17			◆	
18		◆		
19		◆		◆
20		◆		◆

Table 4.14 (continued).

Compound	Proposed structure	pH 5	pH 7	pH 10
21			◆	
22		◆	◆	◆
23				◆
24				◆
25				◆

Comparison of the intermediates formed from the reaction at different pH, reveals intermediates that were observed from both catalysts as well as intermediates that were specific to one particular catalyst. The fact that different pH of the solution produces different combination of reaction intermediates might be the result of charge on the surface of catalyst. Moreover, the conjugation of intermediates was found that at basic solution has conjugation more than at acidic solution.

CHAPTER V

CONCLUSIONS AND RECOMMENDATIONS

5.1 Summary of Findings

The summary of the results of the present research are the following:

1. The surface area of photocatalyst is not the major factor affecting the extent of decomposition.
2. Zinc oxide has higher performance in degrading and mineralization of linuron than titanium dioxide.
3. Intermediates of large molecular weight were detected, suggesting that conjugation of radicals during photodegradation occurs. Many intermediates are formed during the degradation of linuron.
4. The structure of intermediates generated during the photodegradation process is affected by photocatalyst and pH of linuron solution.
5. Photodegradation of linuron generates several intermediates. The degradation pathway mainly consist of oxidation, decarboxylation, hydroxylation and dechlorination at structure of linuron.

5.2 Conclusions

Photocatalytic degradation of linuron generates a lot of reaction intermediates. Several degradation intermediates are generated by reactions of hydroxyl radical attacking to several sites of linuron structure during the photocatalytic degradation process. The different photocatalysts and the different pH of linuron solution were used and revealed intermediates that were observed from both catalysts as well as intermediates that were specific to one particular catalyst, depending on the mechanism of the reaction. The difference in the degradation mechanism may result from the difference in interaction between the catalyst surface and the adsorbed linuron.

5.3 Recommendations

Recommendations for the future work, based on the results of this work, are following.

1. Further identification of the adsorption of linuron on the catalyst surface by using NMR analysis (solid).
2. Investigate long period of irradiation time for photocatalytic degradation of linuron, to achieve 100% conversion and 100% mineralization.
3. Identification of the intermediate generated during adsorption process.
4. Monitor the concentration of the radical such as $Cl^{\cdot}$, $OH^{\cdot}$ by ion-exchange chromatography.
5. Further identification of the degradation intermediate by using LC-MS-MS analysis.

REFERENCES

[1]   Rao, Y.F. and W. Chu. A new approach to quantify the degradation kinetics of linuron with UV, ozonation and UV/O_3 processes. Chemosphere 74,11 (2009): 1444-1449.

[2]   Daneshvar, N., S. Aber, M.S. Seyed Dorraji, A.R. Khataee., and M.H. Rasoulifard. Photocatalytic degradation of the insecticide diazinon in the presence of prepared nanocrystalline ZnO powders under irradiation of UV-C light. Separation and Purification Technology 58,1 (2007): 91-98.

[3]   Katsumata, H., S. Kaneco, T. Suzuki, K. Ohta., and Y. Yobiko. Degradation of linuron in aqueous solution by the photo-Fenton reaction. Chemical Engineering Journal 108,3 (2005): 269-276.

[4]   Phanikrishna Sharma, M.V., V. Durga Kumari., and M. Subrahmanyam. Photocatalytic degradation of isoproturon herbicide over TiO_2/Al-MCM-41 composite systems using solar light. Chemosphere 72,4 (2008): 644-651.

[5]   Burrows, H.D., M. Canle L, J.A. Santaballa., and S. Steenken. Reaction pathways and mechanisms of photodegradation of pesticides. Journal of Photochemistry and Photobiology B: Biology 67,2 (2002): 71-108.

[6]   Gomathi Devi, L.., and K. Mohan Reddy. Enhanced photocatalytic activity of silver metallized TiO_2 particles in the degradation of an azo dye methyl orange: Characterization and activity at different pH values. Applied Surface Science 256,10 (2010): 3116-3121.

[7]   Bianchi, C.L., G. Cappelletti, S. Ardizzone, S. Gialanella, A. Naldoni, C. Oliva., and C. Pirola. N-doped TiO_2 from $TiCl_3$ for photodegradation of air pollutants. Catalysis Today 144,1-2 (2009): 31-36.

[8]   Tian, J., J. Wang, J. Dai, X. Wang., and Y. Yin. N-doped TiO_2/ZnO composite powder and its photocatalytic performance for degradation of methyl orange. Surface and Coatings Technology 204,5 (2009): 723-730.

[9]   Lee, J., A.J. Easteal, U. Pal., and D. Bhattacharyya. Evolution of ZnO nanostructures in sol-gel synthesis. Current Applied Physics 9,4 (2009): 792-796.

[10]   Zeman, P.., and S. Takabayashi. Nano-scaled photocatalytic TiO_2 thin films prepared by magnetron sputtering. Thin Solid Films 433,1-2 (2003): 57-62.

[11]   Carp, O., C.L. Huisman., and A. Reller. Photoinduced reactivity of titanium dioxide. Progress in Solid State Chemistry 32,1-2 (2004): 33-177.

[12]   Depero, L.E., Bonzi, P. and Zocchi, M Study of the anatase-rutile transformation in TiO_2 powders obtained by laser-induced synthesis. Journal of Materials Research 8,10 (1993).

[13] Cheng, P., C. Deng, M. Gu., and X. Dai. Effect of urea on the photoactivity of titania powder prepared by sol-gel method. Materials Chemistry and Physics 107,1 (2008): 77-81.

[14] Lizama, C., J. Freer, J. Baeza., and H.D. Mansilla. Optimized photodegradation of Reactive Blue 19 on TiO2 and ZnO suspensions. Catalysis Today 76,2-4 (2002): 235-246.

[15] Chen, S.-J., L.-H. Li, X.-T. Chen, Z. Xue, J.-M. Hong., and X.-Z. You. Preparation and characterization of nanocrystalline zinc oxide by a novel solvothermal oxidation route. Journal of Crystal Growth 252,1-3 (2003): 184-189.

[16] Yang, L., G. Wang, C. Tang, H. Wang., and L. Zhang. Synthesis and photoluminescence of corn-like ZnO nanostructures under solvothermal-assisted heat treatment. Chemical Physics Letters 409,4-6 (2005): 337-341.

[17] J.E Rodríguez-Paéza, A.C Caballerob, M Villegasb, C Moureb, P Duránb., and J.F. Fernándezb. Controlled precipitation methods: formation mechanism of ZnO nanoparticles. Journal of the European Ceramic Society 21,7 (2001): 925-930.

[18] Su, C., B.Y. Hong., and C.M. Tseng. Sol-gel preparation and photocatalysis of titanium dioxide. Catalysis Today 96,3 (2004): 119-126.

[19] Zou, L., Y. Luo, M. Hooper., and E. Hu. Removal of VOCs by photocatalysis process using adsorption enhanced TiO_2-SiO_2 catalyst. Chemical Engineering and Processing 45,11 (2006): 959-964.

[20] Shao, M., J. Han, M. Wei, D.G. Evans., and X. Duan. The synthesis of hierarchical Zn-Ti layered double hydroxide for efficient visible-light photocatalysis. Chemical Engineering Journal 168,2 (2011): 519-524.

[21] Houas, A., H. Lachheb, M. Ksibi, E. Elaloui, C. Guillard., and J.-M. Herrmann. Photocatalytic degradation pathway of methylene blue in water. Applied Catalysis B: Environmental 31,2 (2001): 145-157.

[22] Konstantinou, I.K.., and T.A. Albanis. TiO_2-assisted photocatalytic degradation of azo dyes in aqueous solution: kinetic and mechanistic investigations: A review. Applied Catalysis B: Environmental 49,1 (2004): 1-14.

[23] Daneshvar, N., D. Salari., and A.R. Khataee. Photocatalytic degradation of azo dye acid red 14 in water on ZnO as an alternative catalyst to TiO_2. Journal of Photochemistry and Photobiology A: Chemistry 162,2-3 (2004): 317-322.

[24] Djebbar, K.E., A. Zertal, N. Debbache., and T. Sehili. Comparison of Diuron degradation by direct UV photolysis and advanced oxidation processes. Journal of Environmental Management 88,4 (2008): 1505-1512.

[25] Madani, M.E., C. Guillard, N. Perol, J.M. Chovelon, M.E. Azzouzi, A. Zrineh., and J.M. Herrmann. Photocatalytic degradation of diuron in aqueous solution in presence of two industrial titania catalysts, either as suspended powders or deposited on flexible industrial photoresistant papers. Applied Catalysis B: Environmental 65,1-2 (2006): 70-76.

[26] Klongdee, J., W. Petchkroh, K. Phuempoonsathaporn, P. Praserthdam, A.S. Vangnai., and V. Pavarajarn. Activity of nanosized titania synthesized from thermal decomposition of titanium (IV) n-butoxide for the photocatalytic degradation of diuron. Science and Technology of Advanced Materials 6,3-4 (2005): 290-295.

[27] Lapertot, M., S. Ebrahimi, S. Dazio, A. Rubinelli., and C. Pulgarin. Photo-Fenton and biological integrated process for degradation of a mixture of pesticides. Journal of Photochemistry and Photobiology A: Chemistry 186,1 (2007): 34-40.

[28] Vasanth Kumar, K., K. Porkodi., and A. Selvaganapathi. Constrain in solving Langmuir-Hinshelwood kinetic expression for the photocatalytic degradation of Auramine O aqueous solutions by ZnO catalyst. Dyes and Pigments 75,1 (2007): 246-249.

[29] Liu, Y., Z. Xu, X. Wu, W. Gui., and G. Zhu. Adsorption and desorption behavior of herbicide diuron on various Chinese cultivated soils. Journal of Hazardous Materials 178,1-3 (2010): 462-468.

[30] Salvestrini, S., P. Di Cerbo., and S. Capasso. Kinetics of the chemical degradation of diuron. Chemosphere 48,1 (2002): 69-73.

[31] Matsushita, Y., N. Ohba, S. Kumada, K. Sakeda, T. Suzuki., and T. Ichimura. Photocatalytic reactions in microreactors. Chemical Engineering Journal 135, Supplement 12008): 303-308.

[32] Naeem, K., P. Weiqian., and F. Ouyang. Thermodynamic parameters of activation for photodegradation of phenolics. Chemical Engineering Journal 156,2 (2010): 505-509.

[33] Rao, Y.F.., and W. Chu. Linuron decomposition in aqueous semiconductor suspension under visible light irradiation with and without H_2O_2. Chemical Engineering Journal 158,2 (2010): 181-187.

[34] Mittal, A., L. Kurup., and J. Mittal. Freundlich and Langmuir adsorption isotherms and kinetics for the removal of Tartrazine from aqueous solutions using hen feathers. Journal of Hazardous Materials 146,1-2 (2007): 243-248.

[35] Valente, J.P.S., P.M. Padilha., and A.O. Florentino. Studies on the adsorption and kinetics of photodegradation of a model compound for heterogeneous photocatalysis onto TiO_2. Chemosphere 64,7 (2006): 1128-1133.

[36] Bulut, Y.., and H. Aydarn. A kinetics and thermodynamics study of methylene blue adsorption on wheat shells. Desalination 194,1-3 (2006): 259-267.

[37] Katsumata, H., M. Sada, Y. Nakaoka, S. Kaneco, T. Suzuki., and K. Ohta. Photocatalytic degradation of diuron in aqueous solution by platinized TiO_2. Journal of Hazardous Materials 171,1-3 (2009): 1081-1087.

[38] Carrier, M., M. Besson, C. Guillard., and E. Gonze. Removal of herbicide diuron and thermal degradation products under Catalytic Wet Air Oxidation conditions. Applied Catalysis B: Environmental 91,1-2 (2009): 275-283.

[39] Wannipa Pradittakan, E.S., Alisa S. Vangnai, Varong Pavarajarn. <u>Comparative Study on Mechanism of Photocatalytic Degradation of Diuron on Titanium Dioxide and Zinc Oxide.</u> Master' s Thesis, Department of Chemical Engineering, Faculty of Engineering, Chulalongkorn, 2011.

[40] Kansal, S.K., M. Singh., and D. Sud. Studies on photodegradation of two commercial dyes in aqueous phase using different photocatalysts. <u>Journal of Hazardous Materials</u> 141,3 (2007): 581-590.

[41] Canle López, M., M.I. Fernández, S. Rodríguez, J.A. Santaballa, S. Steenken., and E. Vulliet. Mechanisms of Direct and TiO_2-Photocatalysed UV Degradation of Phenylurea Herbicides. <u>ChemPhysChem</u> 6,10 (2005): 2064-2074.

[42] Oturan, M.A., M.C. Edelahi, N. Oturan, K. El kacemi., and J.-J. Aaron. Kinetics of oxidative degradation/mineralization pathways of the phenylurea herbicides diuron, monuron and fenuron in water during application of the electro-Fenton process. <u>Applied Catalysis B: Environmental</u> 97,1–2 (2010): 82-89.

[43] Farré, M.J., S. Brosillon, X. Domènech., and J. Peral. Evaluation of the intermediates generated during the degradation of Diuron and Linuron herbicides by the photo-Fenton reaction. <u>Journal of Photochemistry and Photobiology A: Chemistry</u> 189,2–3 (2007): 364-373.

[44] Macounovи, K., H. Krsovи, J. Ludvиk., and J. Jirkovsk. Kinetics of photocatalytic degradation of diuron in aqueous colloidal solutions of Q-TiO_2 particles. <u>Journal of Photochemistry and Photobiology A: Chemistry</u> 156,1-3 (2003): 273-282.

[45] Lin, S.-H., C.-H. Chiou, C.-K. Chang., and R.-S. Juang. Photocatalytic degradation of phenol on different phases of TiO_2 particles in aqueous suspensions under UV irradiation. <u>Journal of Environmental Management</u> 92,12 (2011): 3098-3104.

[46] Jeevan L. KHURANA, C.J.J., Colin SCOTT, Gunjan PANDEY, Irene HORNE, Robyn J. RUSSELL, Anthony HERLT, Christopher J. EASTON and John G. OAKESHOTT. Characterization of the phenylurea hydrolases A and B: founding members of a novel amidohydrolase subgroup. <u>Biochemical Journal</u> 4182009): 431-441.

[47] Richard, C., and S. Bengana. PH effect in the photocatalytic transformation of a phenyi-urea herbicide. <u>Chemosphere</u> 33,4 (1996): 635-641.

[48] Sharma, M.V.P., K. Lalitha, V. Durgakumari., and M. Subrahmanyam. Solar photocatalytic mineralization of isoproturon over TiO_2/HY composite systems. <u>Solar Energy Materials and Solar Cells</u> 92,3 (2008): 332-342.

[49] Huang, L., Y. Sun, W. Wang, Q. Yue., and T. Yang. Comparative study on characterization of activated carbons prepared by microwave and conventional heating methods and application in removal of oxytetracycline (OTC). <u>Chemical Engineering Journal</u> 171,3 (2011): 1446-1453.
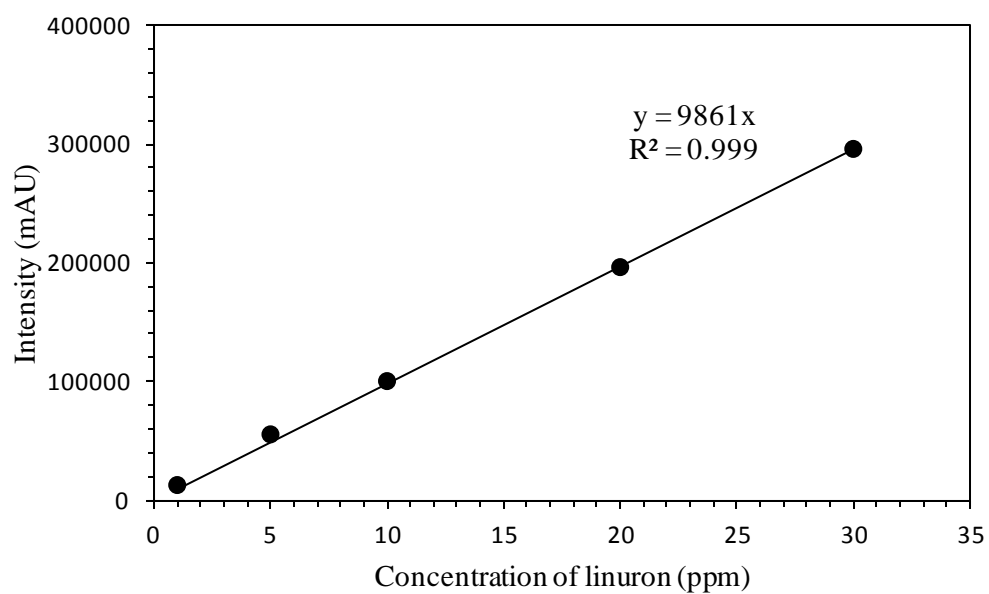
APPENDICES

APPENDIX A

LINURON CALIBRATION CURVE

$$y = 9861x$$
$$R^2 = 0.999$$

Figure A.1 The calibration curve of linuron.

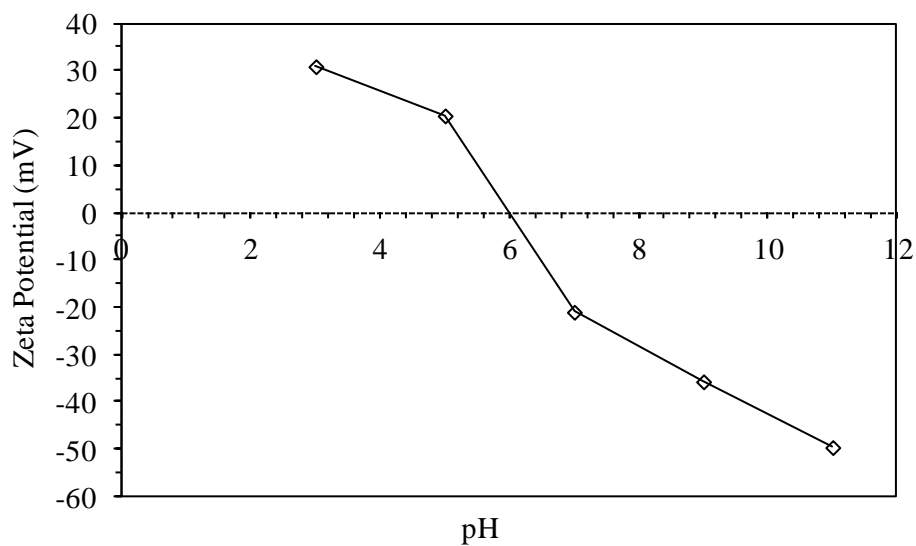# APPENDIX B

POINT OF ZERO CHARGE DETERMINATION

Figure B.1 Determination of the point of zero charge of synthesized titamia.
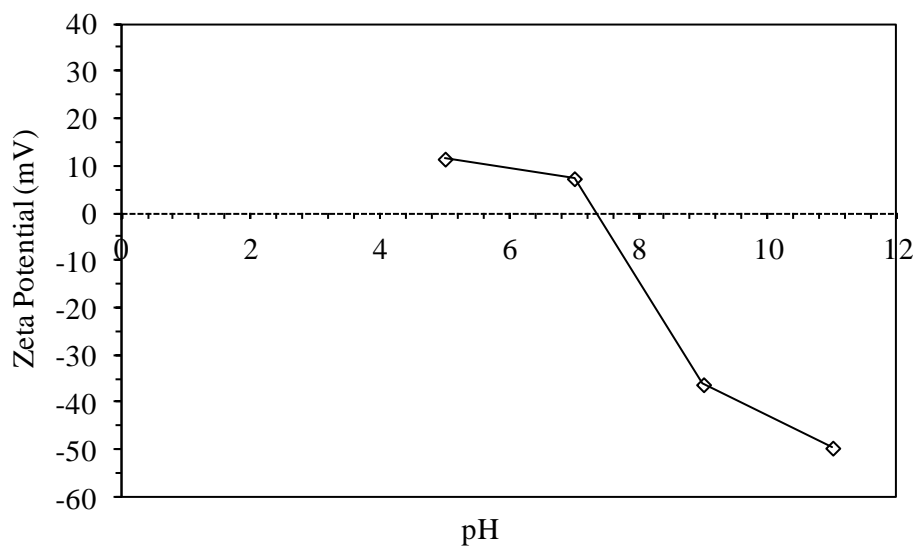

Figure B.2 Determination of the point of zero charge of synthesized zinc oxide.

APPENDIX C

LC/MS MASS SPECTRUM

All samples were sent for analysis at Central Laboratory (Thailand) Ltd. Co. During a sample inject, three types of diagrams were obtained: chromatogram from UV detector, chromatogram from mass detector, and mass spectrum. Chromatogram from UV and mass detector spanned the LC runtime. The mass spectrum is obtained at a specific retention time.

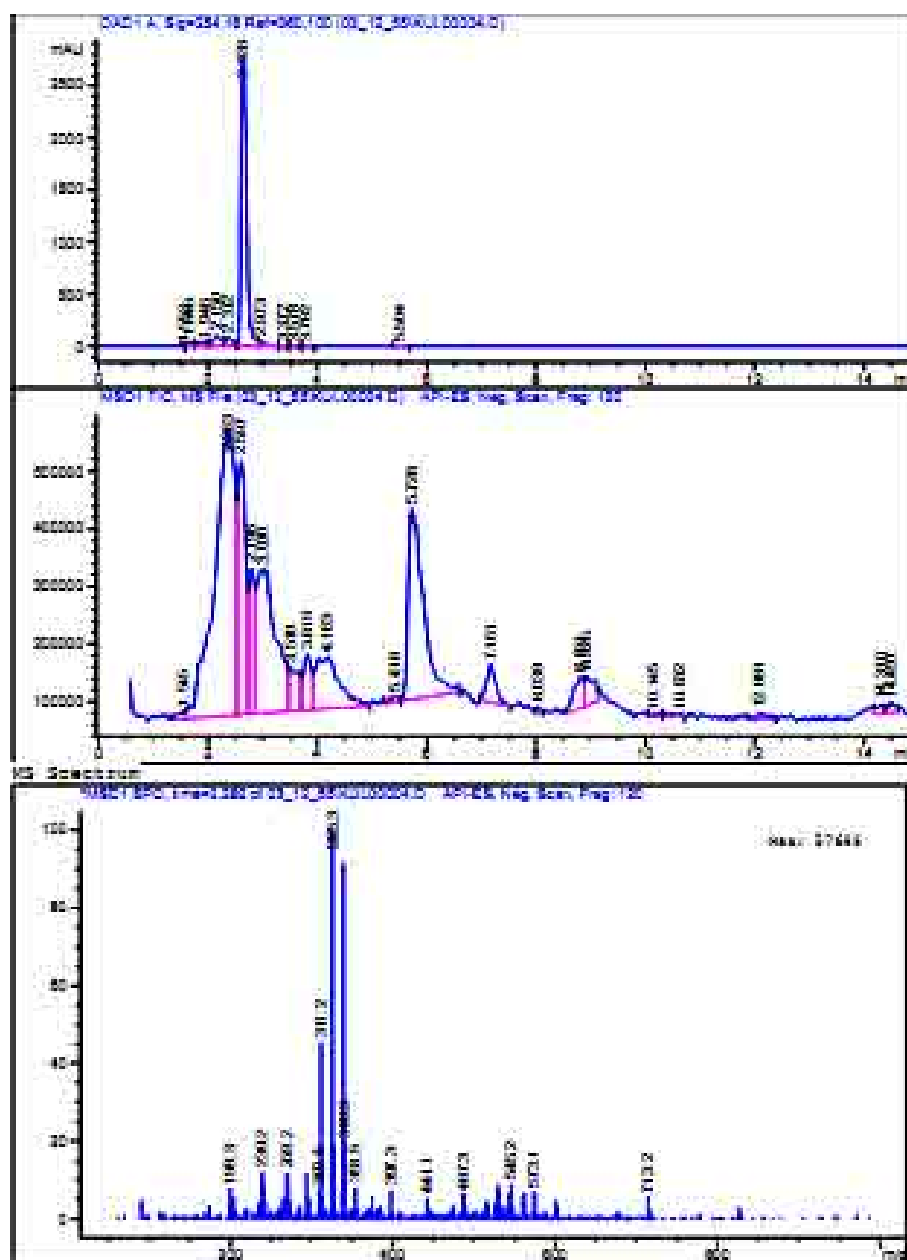**C.1 Mass spectrum of linuron solution from photodegradation by synthesized titania.**
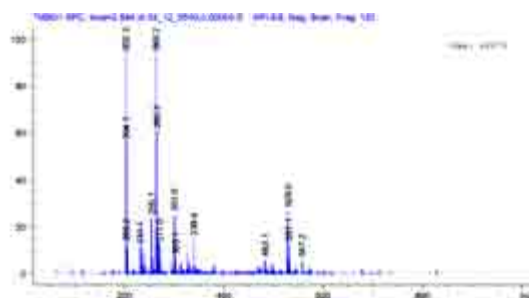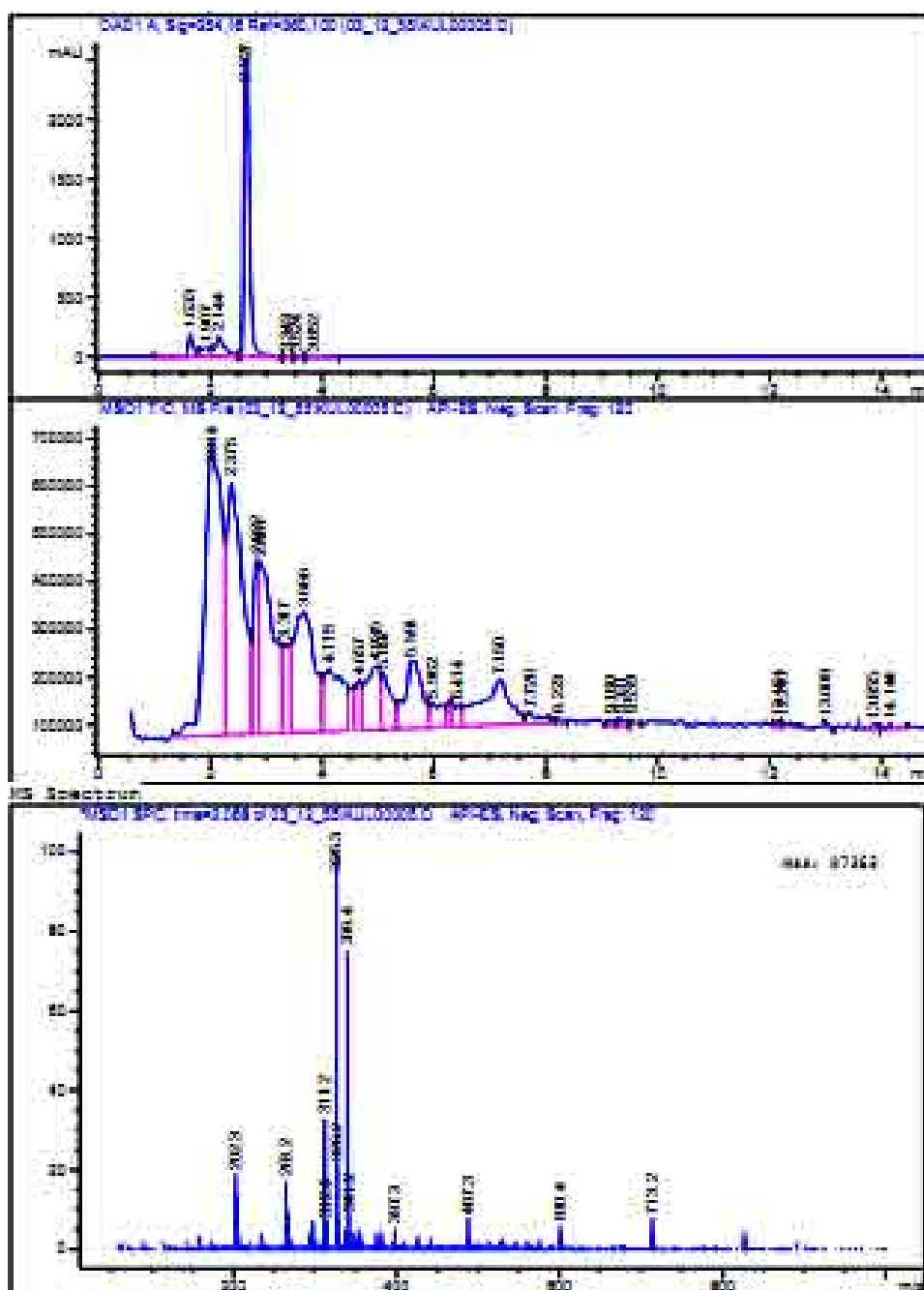
C.1.1 pH 5
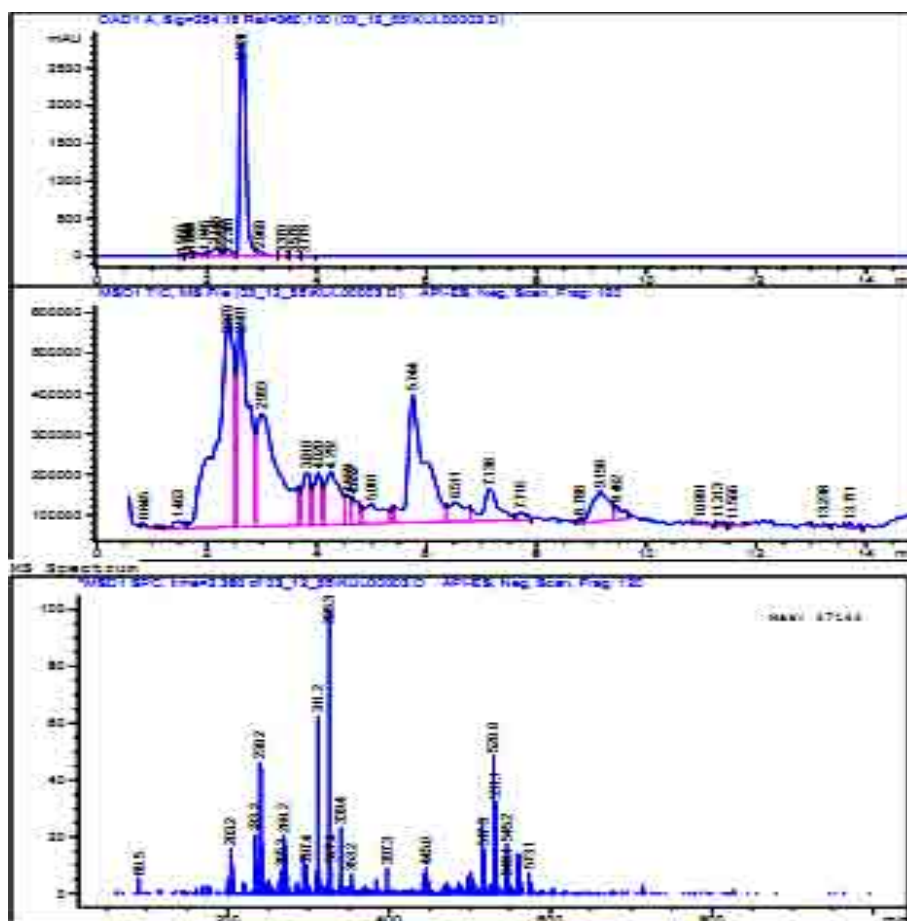
(a)

Figure C.1 Chromatogram of linuron solution photodegradation at pH5 obtained from UV detector and mass detector are displayed in (a). Mass spectrums were obtained using fragmentator of 120 V at various retention times as sown in (a)-(i).

(b)

(c)

(d)

(e)

(f)

(g)

(h)

(i)

Figure C.1 (continued)

C.1.2 pH 7

(a)

Figure C.2 Chromatogram of linuron solution photodegradation at pH7 obtained from UV detector and mass detector are displayed in (a). Mass spectrums were obtained using fragmentator of 120 V at various retention times as sown in (a)-(i).

(b)

(c)

(d)

(e)

(f)

(g)

(h)

(i)

Figure C.2 (continued)

C.1.3 pH 10

(a)

Figure C.3 Chromatogram of linuron solution photodegradation at pH10 obtained from UV detector and mass detector are displayed in (a). Mass spectrums were obtained using fragmentator of 120 V at various retention times as sown in (a)-(i).
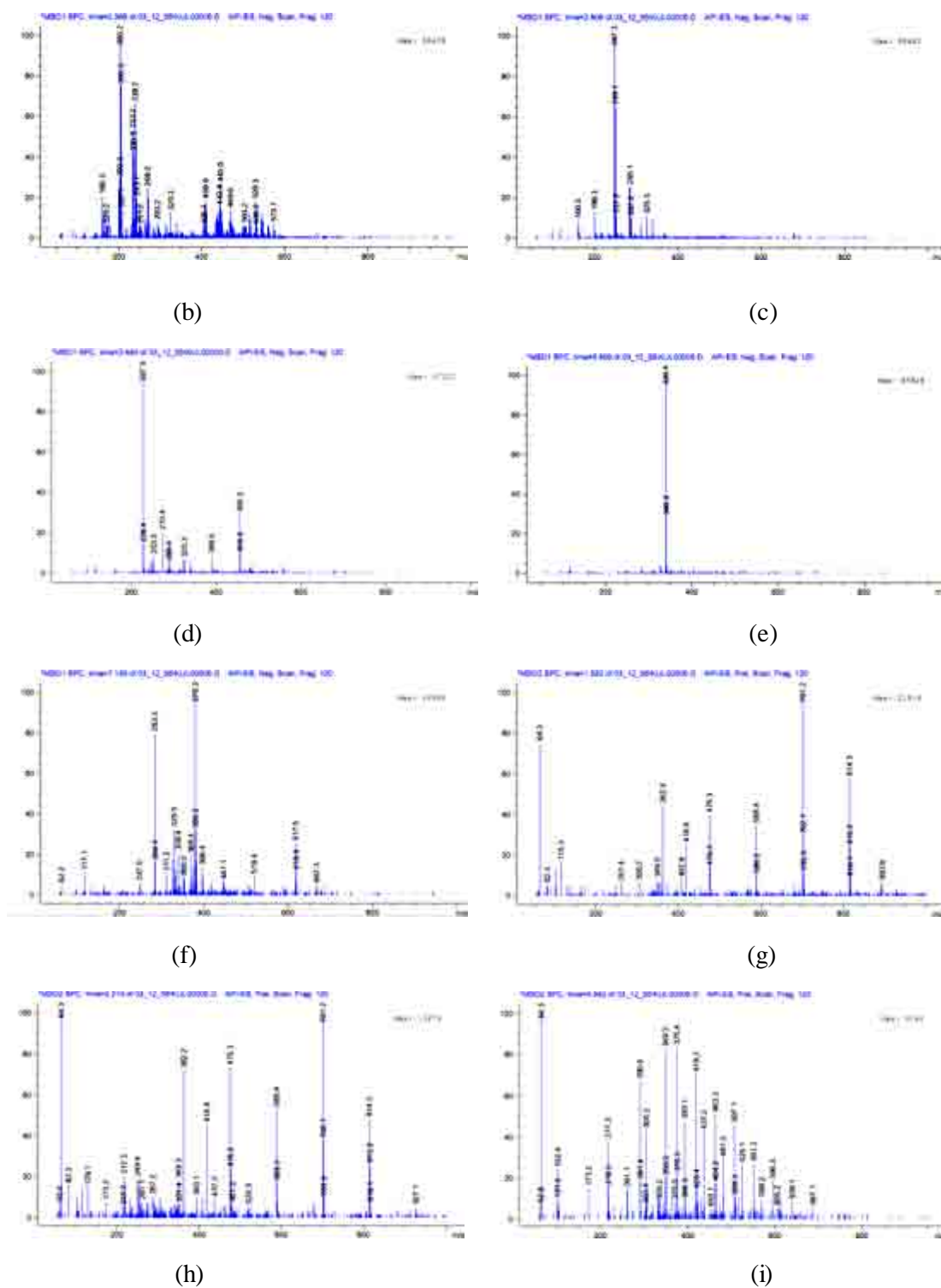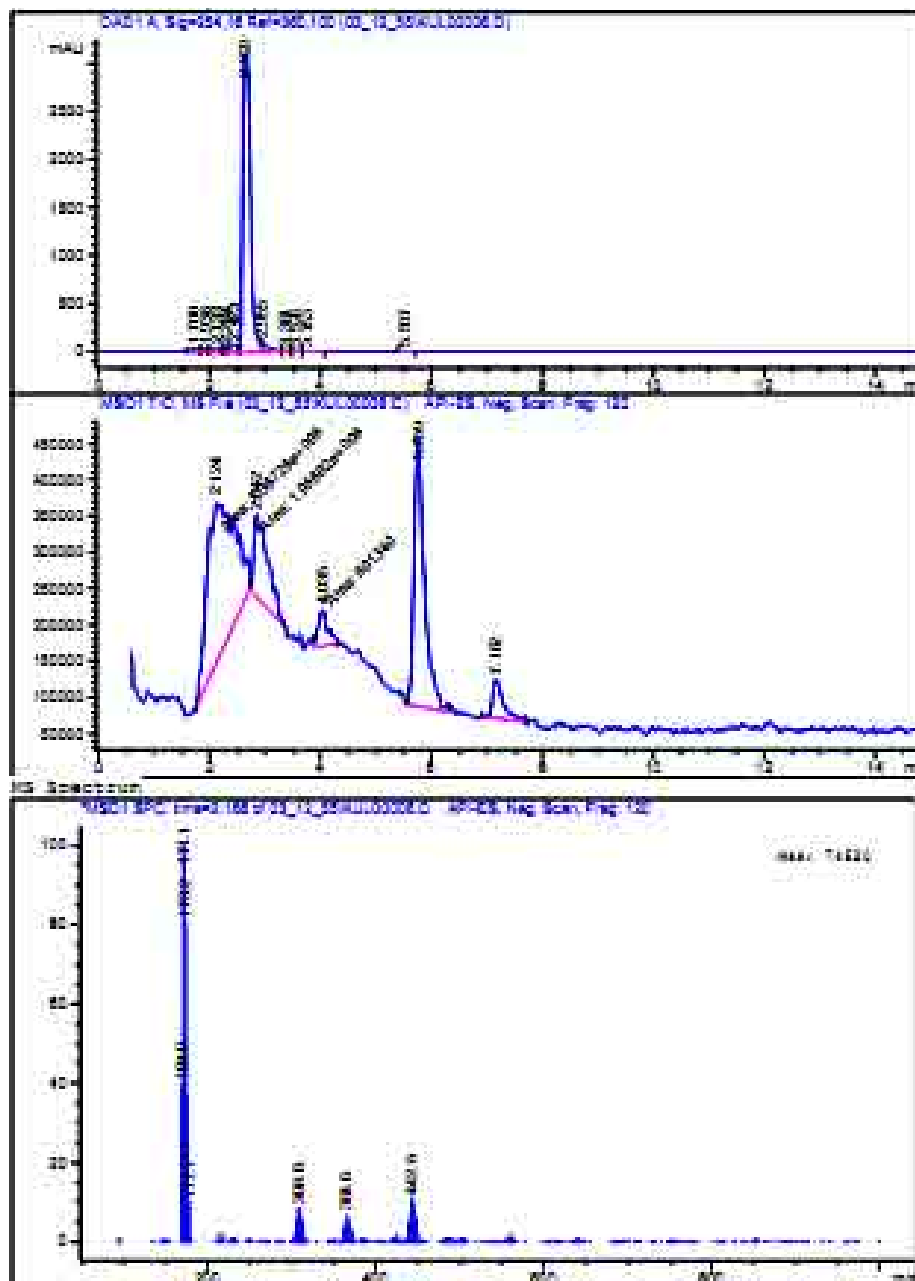
(b)

(c)

(d)

(e)

(f)

(g)

(h)

(i)

Figure C.3 (continued)

C.2 Mass spectrum of linuron solution from photodegradation by synthesized zinc oxide.

C.2.1 pH 5

(a)

Figure C.4 Chromatogram of linuron solution photodegradation at pH5 obtained from UV
detector and mass detector are displayed in (a). Mass spectrums were obtained
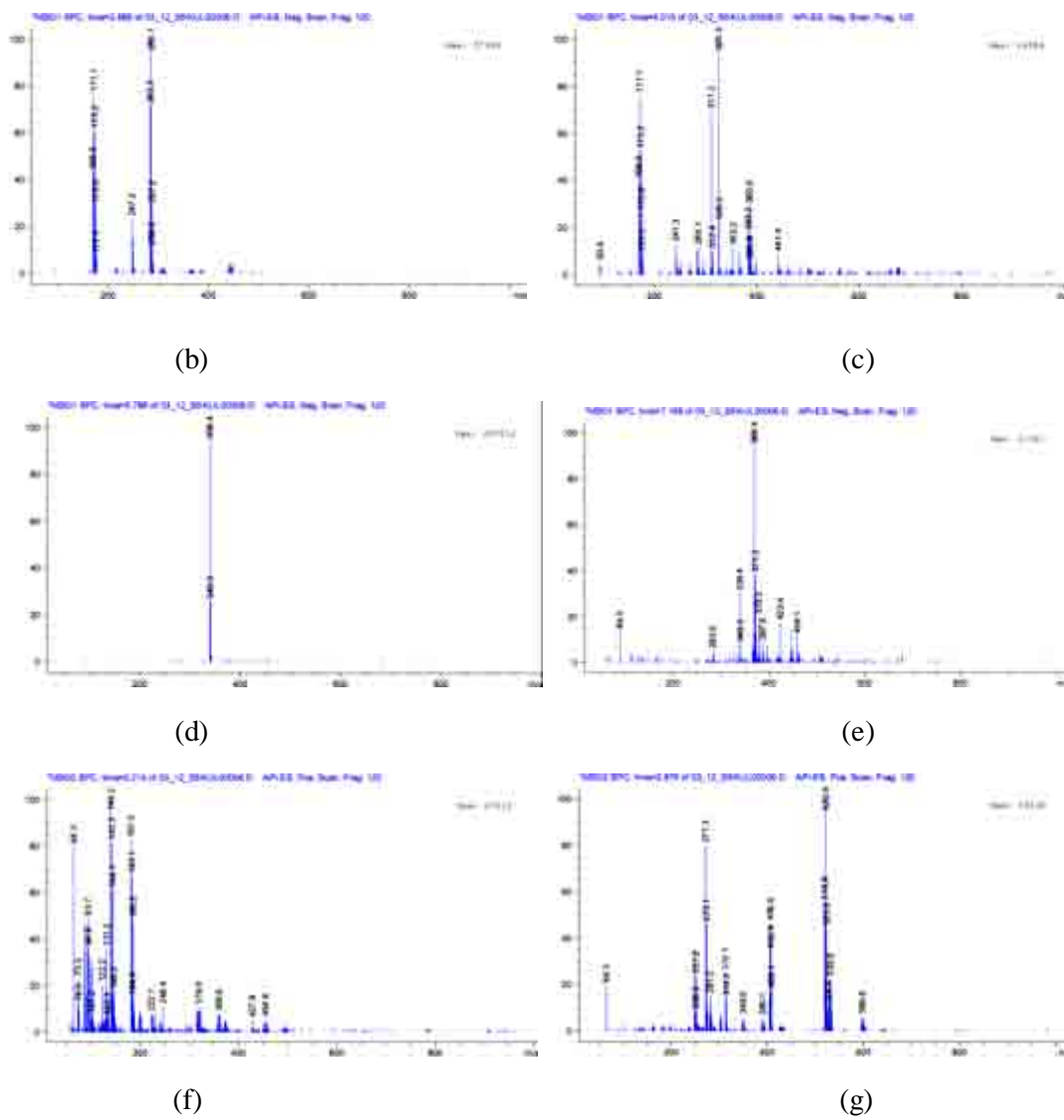using fragmentator of 120 V at various retention times as sown in (a)-(g).

(b)

(c)

(d)

(e)

(f)
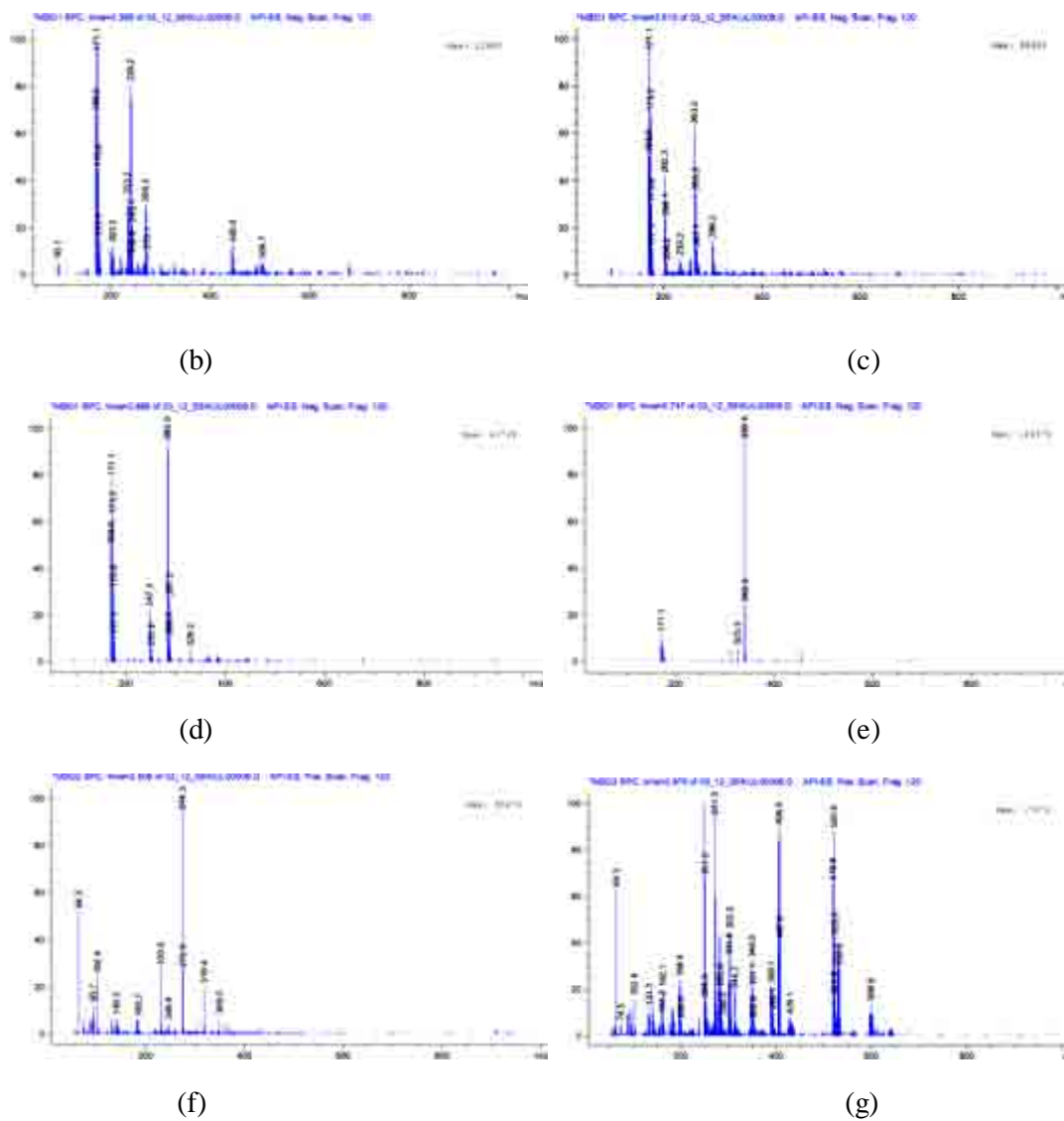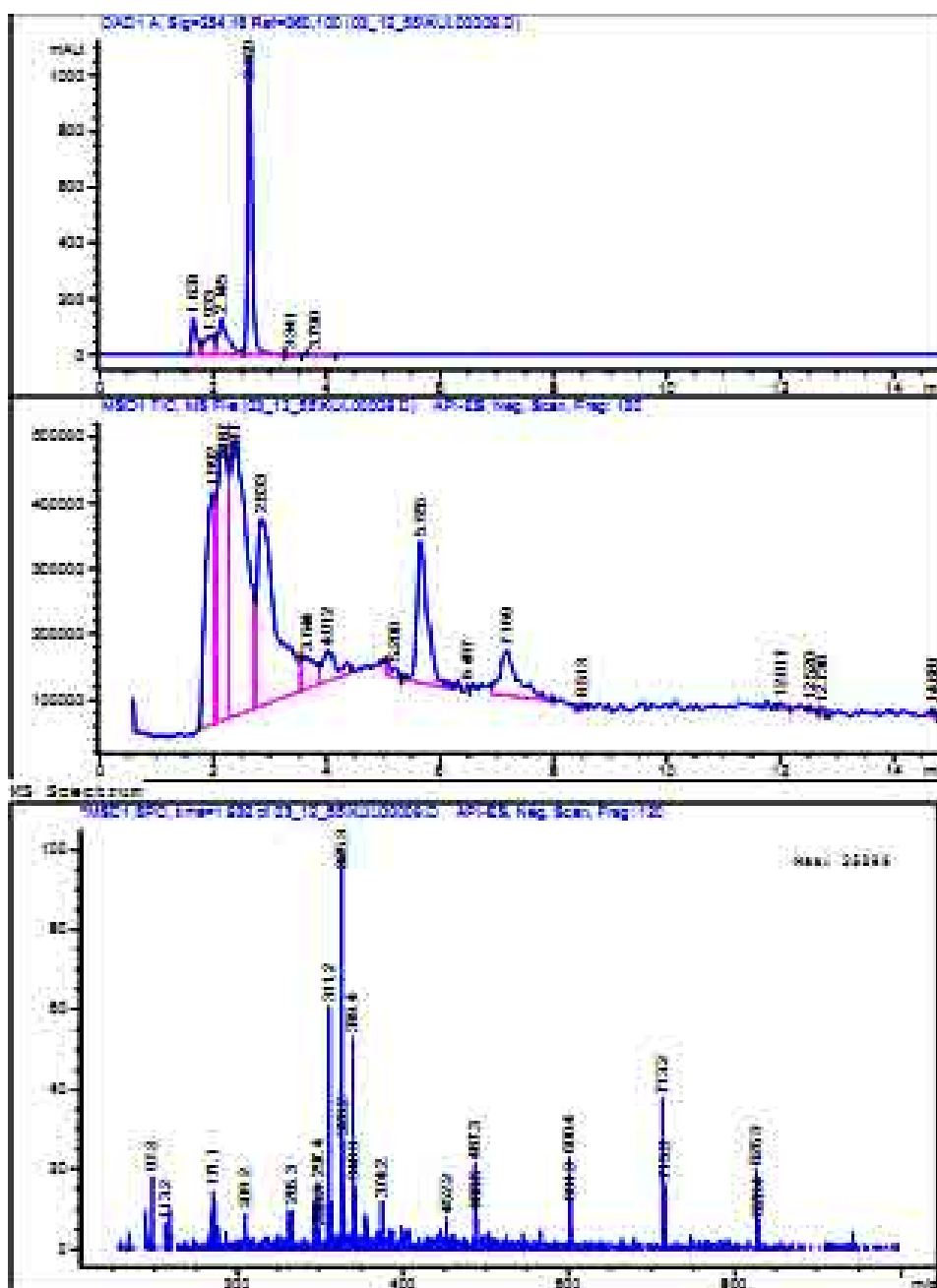
(g)

Figure C.4 (continued)

C.2.2 pH 7

(a)

Figure C.5 Chromatogram of linuron solution photodegradation at pH7 obtained from UV detector and mass detector are displayed in (a). Mass spectrums were obtained using fragmentator of 120 V at various retention times as sown in (a)-(g).
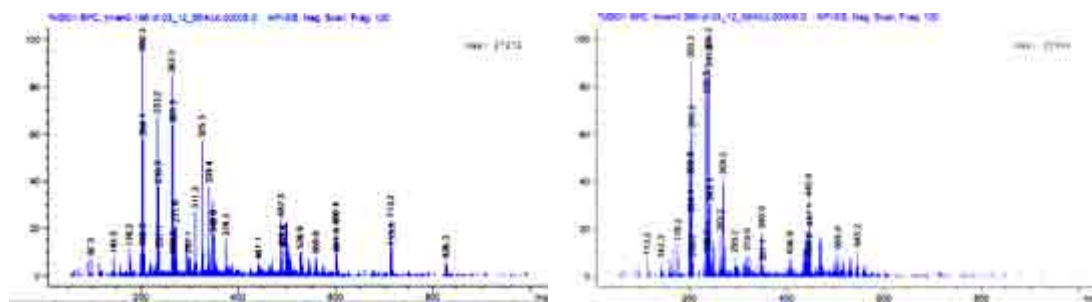
(b)

(c)

(d)

(e)

(f)

(g)

Figure C.5 (continued)

C.2.3 pH 10

(a)

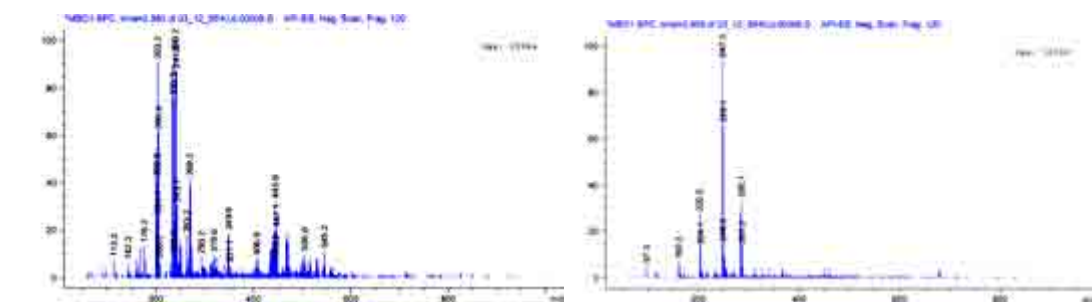**Figure C.6** Chromatogram of linuron solution photodegradation at pH10 obtained from UV detector and mass detector are displayed in (a). Mass spectrums were obtained using fragmentator of 120 V at various retention times as sown in (a)-(i).
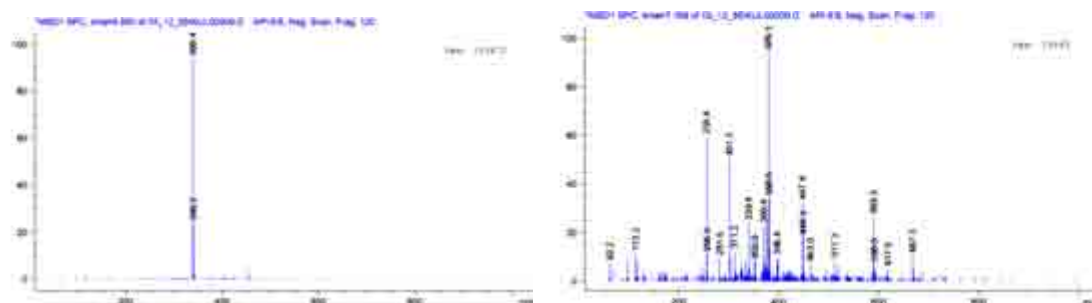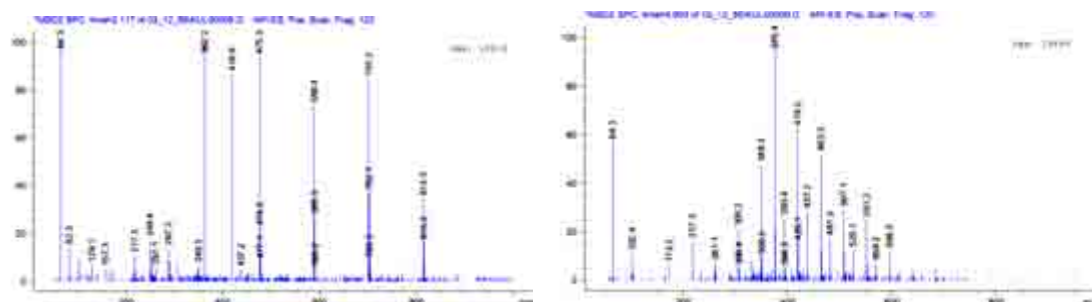
(b)

(c)

(d)

(e)

(f)

(g)

(h)

(i)

Figure C.6 (continued)

APPENDIX D

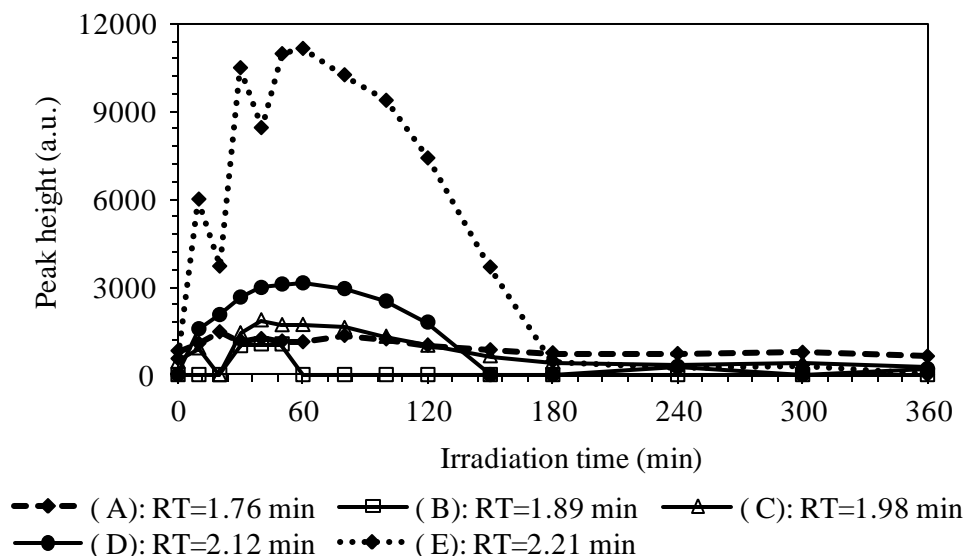# INTERMEDIATES OF DCA FROM HPLC ANALYSIS

Figure D.1 HPLC peak height of intermediates generated during photocatalytic degradation of DCA on commercial titania.
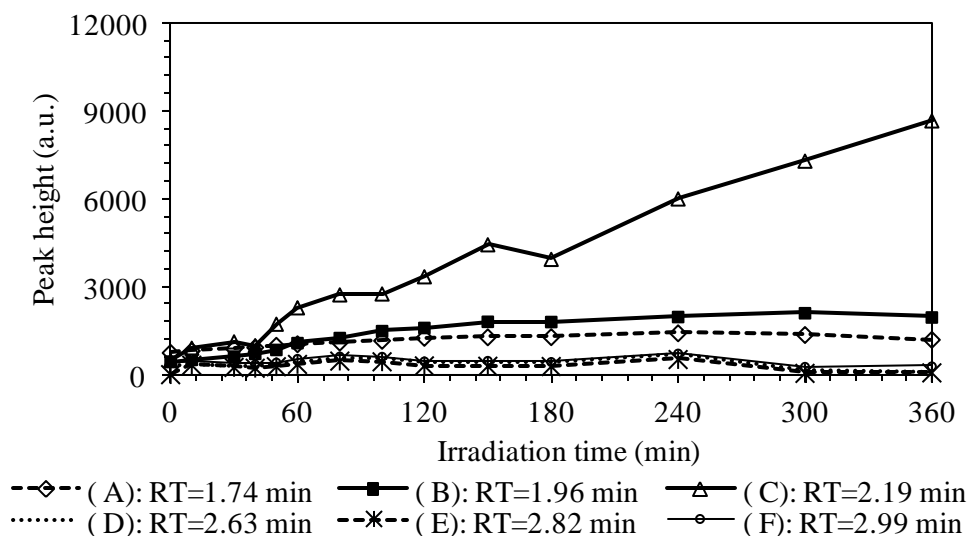

Figure D.2 HPLC peak height of intermediates generated during photocatalytic degradation of DCA on synthesized titania.
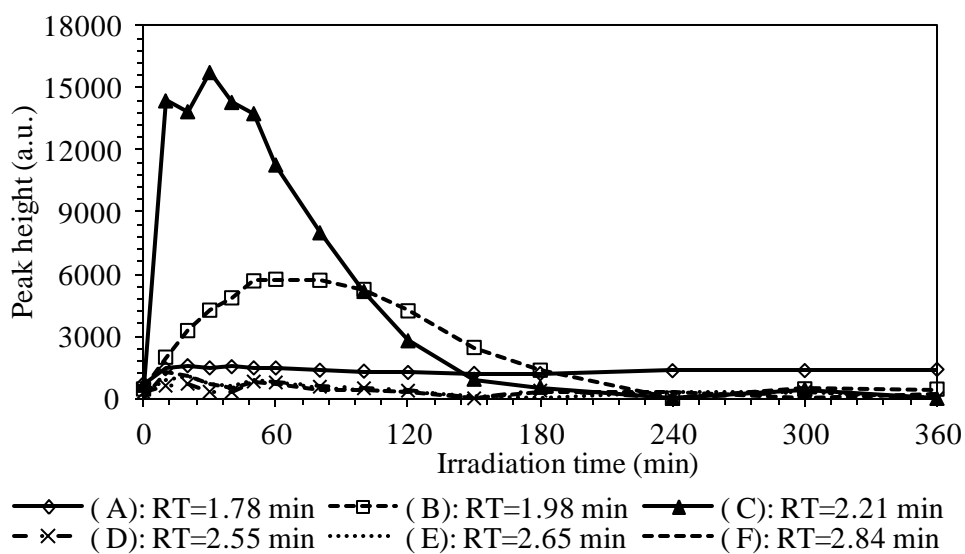
Figure D.3 HPLC peak height of intermediates generated during photocatalytic degradation of DCA on commercial zinc oxide.
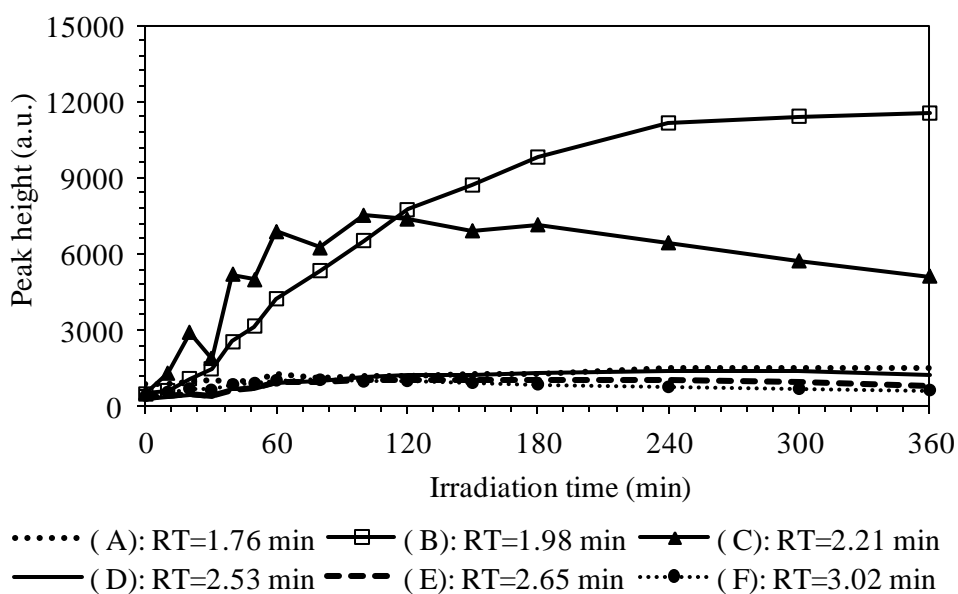

Figure D.4 HPLC peak height of intermediates generated during photocatalytic degradation of DCA on synthesized zinc oxide.

APPENDIX E

THE LANGMUIR-HINSHELWOOD MODEL

In this model, it is assumed that the reaction occurs on the heterogeneous catalyst surface and the rate of reaction (r) is proportional to the fraction of surface covered by the substrate (Θ):

$$r = -\frac{dC}{dt} = k_r\theta = k_r\frac{KC}{1+KC} \qquad \text{(E1)}$$

where C = the concentration of the substance being degraded

     t = the irradiation time

     k = the rate constant

     K = the adsorption constant

Integration of (E1) for boundary condition $t = 0$ to $t = t$ and $C_t = C_0$ to $C_t = C$ gives the form:

$$\ln\left(\frac{C_0}{C}\right) + K(C_0 - C) = k_r Kt \qquad \text{(E2)}$$

$$\ln\left(\frac{C_0}{C}\right) = -K(C_0 - C) + k_r Kt \qquad \text{(E3)}$$

$$\ln\left(\frac{C_0}{C}\right) = -KC_0 + KC + k_r Kt \qquad \text{(E4)}$$

From non-linear equation form:

$$y = m_1 x_1 + m_2 x_2 + b \qquad \text{(E5)}$$

The equation (E4) can be rearranged into non-linear equation form (E5) as shown in equation (E6)

$$\ln\left(\frac{C_0}{C}\right) = k_r Kt + KC - KC_0 \qquad \text{(E6)}$$

Where,
$$y = \ln\left(\frac{C_0}{C}\right)$$

$$x_1 = t$$

$$x_2 = C$$

Thus, the constants k_r and K can be identified from:

$$m_1 = k_r K$$

$$m_2 = K$$

$$b = -KC_0$$

The constant kinetic data for the photodegradation of linuron were analysed using Langmuir-Hinshelwood kinetic model as described here and as shown in Table E1.

Table E1. The reaction rate constants (k_r), and the adsorption constant (K) for the photocatalytic degradation of linuron using synthesized titania, commercial titania, synthesized zinc oxide and commercial zinc oxide as catalyst.

catalyst	Langmuir-Hinshelwood model		
	k_r (ppm/min)	K (ppm^{-1})	R^2
Commercial titania	0.6086	0.0534	0.9676
Synthesized titania	0.2333	0.0126	0.9553
Commercial zinc oxide	0.7118	0.0454	0.9394
Synthesized zinc oxide	0.5955	0.0132	0.9974

APPENDIX F

LIST OF PUBLICATION

1. Saowalux Sittichoktum and Varong Pavarajarn (2012) "Photocatalytic Degradation of Linuron on Titania and Zinc Oxide." Proceedings of the Pure and Applied Chemistry International 2012, Changmai, Thailand, Jan. 11 – Jan. 13, 2012.

VITA

Miss Saowalux Sittichoktum was born on February 14, 1987 in Phetchaburi Province, Thailand. She received the Bachelor Degree of Chemical Engineering from Faculty of Engineer, Thammasat University in 2010. She continued her Master's study at Chulalongkorn University in June, 2010.